$^{40}Ar/^{39}Ar$ AGES OF MUSCOVITE FROM THE WESTERN BLUE RIDGE AND TALLADEGA BELT, GEORGIA AND NORTH CAROLINA

Except where reference is made to the work of others, the work described in this thesis is my own or was done in collaboration with my advisory committee. This thesis does not include proprietary or classified information.

_____

Wayne M. McDonald

Certificate of Approval:

_____	_____
Luke J. Marzen Associate Professor Geology and Geography	Willis E. Hames, Chair Professor Geology and Geography
_____	_____
Mark G. Steltenpohl Professor Geology and Geography	George T. Flowers Interim Dean Graduate School

$^{40}Ar/^{39}Ar$ AGES OF MUSCOVITE FROM THE WESTERN BLUE RIDGE AND TALLADEGA BELT, GEORGIA AND NORTH CAROLINA

Wayne M. McDonald

A thesis

Submitted to

the graduate faculty of

Auburn University

in partial fulfillment of the

Requirements for the

Degree of

Master of Science

Auburn, Alabama
May 10, 2008

$^{40}Ar/^{39}Ar$ AGES OF MUSCOVITE FROM THE WESTERN BLUE RIDGE AND TALLADEGA BELT, GEORGIA AND NORTH CAROLINA

Wayne M. McDonald

_____
Signature of Author

_____
Date of Graduation

VITAE

Wayne M. McDonald, son of Dr. William J. McDonald and Virginia M. Leritz, was born January 25, 1974, in West Palm Beach, Florida. He graduated from Cardinal Newman High School in 1992. Subsequently, he attended Auburn University, Alabama, and graduated in December, 1998 with a Bachelor of Science degree in Geology. He worked as an environmental consultant for a few years and then entered Graduate School, Auburn University, in August, 2003.

THESIS ABSTRACT

$^{40}Ar/^{39}Ar$ AGES OF MUSCOVITE FROM THE WESTERN BLUE RIDGE AND TALLADEGA BELT, GEORGIA AND NORTH CAROLINA

Wayne M. McDonald

Masters of Science, May 10, 2008
(B.S., Auburn University, 1998)

114 Typed Pages

Directed by Willis E. Hames

Radiometric age constraints regarding the timing of metamorphism in the western Blue Ridge province of the southern Appalachians have been too limited or uncertain to enable broader correlation and understanding of Taconian, Acadian, and Alleghanian events in the region between western North Carolina and Alabama. Moreover, various fossil, stratigraphic and radiometric data for the timing of metamorphism in the Talladega belt of Alabama are difficult to reconcile with radiometric ages of comparable tectonic units in the western Blue Ridge of North Carolina. New $^{40}Ar/^{39}Ar$ radiometric data for single-muscovite crystals have been collected, utilizing the Auburn Noble Isotope Mass Analysis Laboratory (ANIMAL), to help constrain the timing of metamorphism in the western Blue Ridge of Georgia and North Carolina. The mean ages of muscovite in

phyllites collected from the Cartersville transverse zone record crystallization and cooling in the interval from 321.4±0.3 - 335.5±0.8 Ma (corresponding to Serpukhovian and Visean stages of the Mississippian). The mean ages of muscovite in three phyllites from a sampling transect along U.S. Hwy. 64 (between Murphy, North Carolina and Ducktown, Tennessee) are similar to those of the Cartersville transverse zone. However, the age distributions of single-crystal muscovite in six other schists and phyllites from this Murphy-Ducktown transect are complex, with ages ranging up to ca. 465 Ma. The mean ages of muscovite in metasiltstones and phyllites collected within or near the Great Smoky fault (between the Murphy-Ducktown transect and the Cartersville transverse zone) also tend to be Visean. However, several samples from this tectonic setting also yield very complex age distributions. The complex age distributions determined in this study seem mainly due to effects of polymetamorphism in some rocks, but are also influenced by the presence of relict-detrital muscovite and incorporation of unsupported-extraneous ('excess') ^{40}Ar in some samples. The single-crystal $^{40}Ar/^{39}Ar$ ages determined in this study are interpreted to indicate that Mississippian tectonic events dominated metamorphic and structural evolution in the Talladega belt and in the Mineral Bluff Group of the western Blue Ridge. For Ocoee Supergroup rocks, in the western Blue Ridge, the muscovite in phyllites and schists record a history of pre-Carboniferous (Acadian or Taconian) events partially overprinted by Mississippian deformation. The Mississippian ages are interpreted to represent Alleghanian events recorded in the muscovite of Talladega belt-western Blue Ridge rocks that pre-date final emplacement of the Blue Ridge thrust sheet, as the youngest deformed strata of the Valley and Ridge (Pottsville Formation; 316-303 Ma) indicates Pennsylvanian deposition. This combined

with Tournaisian fossil control (*Periastron* plant fossil; 360-350 Ma) indicates Alleghanian metamorphism and deformation in the Talladega belt-western Blue Ridge is constrained to ~ 360-300 Ma, older and longer in duration than the classic view of the Alleghanian as Pennsylvanian to Permian.

ACKNOWLEDGEMENTS

The National Science Foundation funded this study and provided financial assistance to the author for one year. Special thanks to Dr. Willis Hames for the opportunity to work on this study and his effort to see it through. Thanks are also due to committee members Dr. Luke Marzen, for assistance with the GIS, and Dr. Mark Steltenpohl, for help with understanding structural aspects of this study. Also worth noting are Dr. Ashraf Uddin and Dr. Charles Savrda for their moral support and general guidance, John Simms for his almost daily assistance with various things, and Dr. Mehmet Billor for many helpful discussions. Thanks are mostly due to family members William and Virginia whose financial support made working on this study a possibility.

Style manual or journal used: Geology

Computer software used: Adobe® EasySVG, Adobe® Photoshop®, ESRI® ARCGIS® 9.1, Microsoft® Excel® 2003, Microsoft® FrontPage® 2003, Microsoft® Word® 2003, Microsoft® PowerPoint® 2003

TABLE OF CONTENTS

LIST OF FIGURES

LIST OF TABLES

INTRODUCTION

The western Blue Ridge and Talladega belt (Figure 1) together represent the leading thrust belt of the southern Appalachian metamorphic core and consist primarily of low-grade metasedimentary rocks. These rocks were deposited as shallow marine sediment along the eastern-coastal margin of Late Proterozoic to Paleozoic Laurentia. Subsequently, these sediments were metamorphosed and thrusted cratonward over younger sedimentary rocks through several orogenic events of Paleozoic Appalachian evolution (Williams and Hatcher, 1982; Thomas, 1983; Hatcher, 1987; Hatcher, 1989; Horton et al., 1989; Tull and Holm, 2005).

The tectonic history of the western Blue Ridge in northwest Georgia is unclear, and its relationship to well constrained southern Appalachian events elsewhere is uncertain. Research in the Smoky Mountain region of the western Blue Ridge indicates a Taconian and Acadian dominated tectonic history (Connelly and Dallmeyer, 1993; Kunk et al., 2006). Geologic studies in the Talladega belt of Alabama indicate an Alleghanian dominated tectonic history (Gastaldo et al., 1993; Steltenpohl and Kunk, 1993; McClellan et al., 2005; Steltenpohl, et al., 2005; McClellan et al., 2007). This thesis focuses on constraining timing limits of metamorphism and cooling in the western Blue Ridge of Georgia by $^{40}Ar/^{39}Ar$ radiometric dating of muscovite and how it relates to the tectonic history known for adjacent regions.

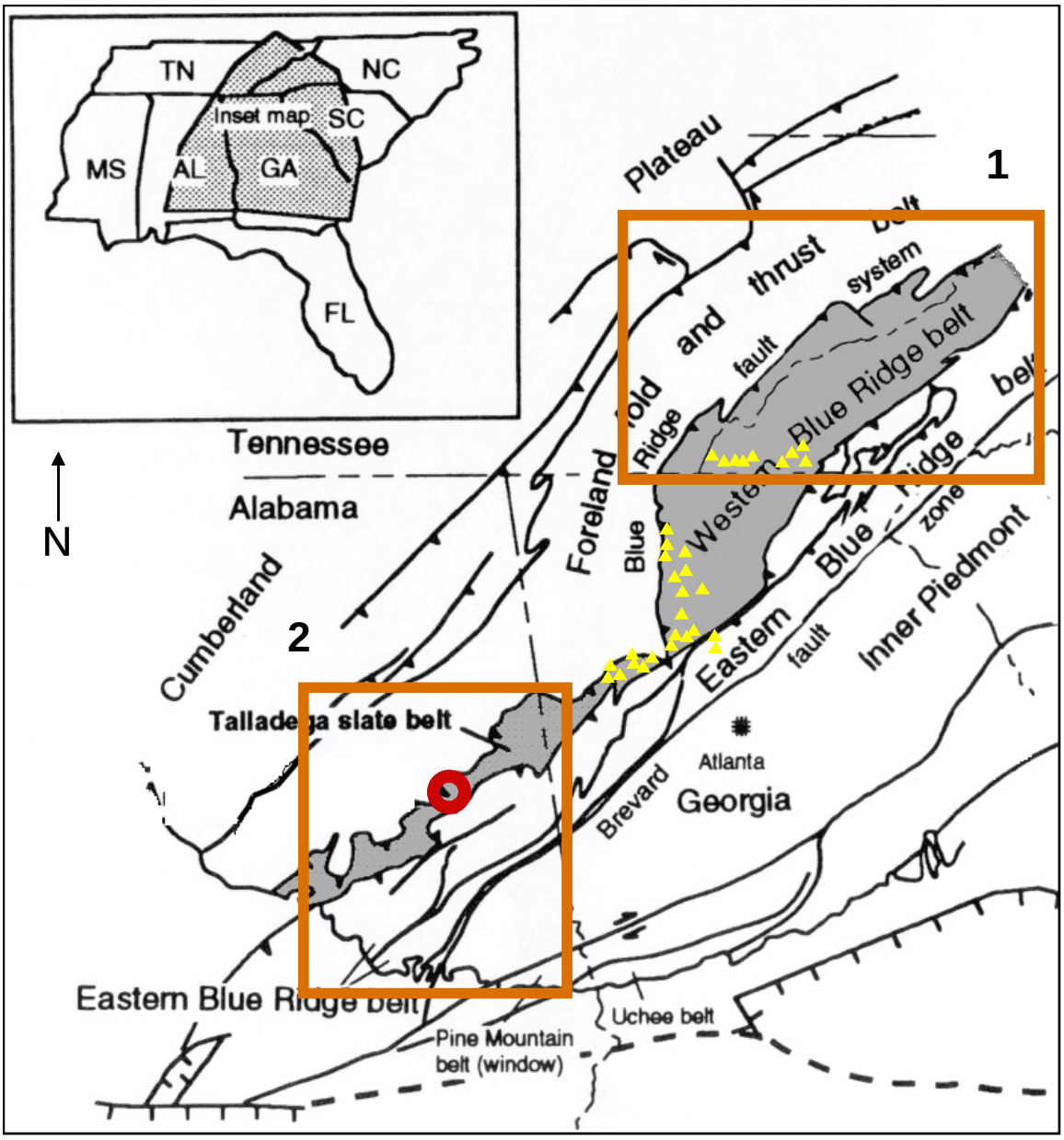

Figure 1: The southern Appalachians depicting the Talladega belt-western Blue Ridge and other tectonic units as labeled (modified from Gastaldo et al., 1993). The inset boxes indicate areas of previous geochronologic research: 1) Connelly and Dallmeyer (1993), Ordovician-Silurian (Taconian) and Late Devonian (Acadian) tectonics; 2) Steltenpohl and Kunk (1993), McClellan et al. (2005) and Steltenpohl et al. (2005), Carboniferous (Alleghanian) tectonics. Yellow triangles indicate approximate sampling locations for this thesis. Red circle indicates location of an Early Mississippian (Tournaisian) *Periastron* plant fossil reported by Gastaldo et al. (1993).

Muscovite is a relatively plentiful mineral in the metasedimentary and meta-igneous rocks of the western Blue Ridge. Furthermore, it is amenable to $^{40}Ar/^{39}Ar$ dating, as the growth of this mineral can usually be placed in the context of a sample's structural evolution, has a closure temperature conducive for dating low to moderate temperature events, and is relatively insensitive to problems associated with extraneous argon (McDougall and Harrison, 1999). Radiometric ages for muscovite could represent the timing of metamorphism, the timing of cooling to a temperature at which radiogenic argon accumulates ("closure temperature;" see Dodson, 1973), or the timing of deformation at low metamorphic grade (e.g., Dunlap, 1991). The cooling history has important implications for the accumulation of radiogenic argon. A rapid cooling history for a rock sample gives similar age dates for different minerals with relatively high closure temperatures. Slow cooling rates give a range of age dates due to different mineral closure temperatures.

Thirty-two samples of lower-greenschist facies rocks were collected, based on regional setting and petrography, from the Talladega belt-western Blue Ridge (Georgia, North Carolina, and Tennessee; Figure 1). The study areas include 1) the Cartersville Transverse Zone, 2) the Blue Ridge thrust front in northwest Georgia, and 3) a sampling transect from Ducktown-Tennessee east through the Murphy synclinorium in North Carolina. The samples were analyzed petrographically to verify whether the rocks have a simple metamorphic history or evidence of polymetamorphism. A web-enabled GIS was constructed for use as a database for sample and research locations, and to make the radiometric data readily available to other researchers.

GEOLOGIC SETTING OF THE SOUTHERN BLUE RIDGE PROVINCE

The southern Appalachian orogen culminated in the Paleozoic from a series of contractional events (Figure 2) along the eastern margin of Laurentia (Thomas, 1983; Hatcher, 1987). These orogenic events follow the processes of a complete Wilson cycle (Wilson, 1966). The evolution of the southern Appalachians (Figure 3) began with Late Proterozoic continental rifting and formation of a subsiding passive continental margin into the Early Paleozoic, followed by later Paleozoic plate convergence and accretion of rifted-terrane fragments and island-arc terranes, finalized by continent-continent collision (Hatcher, 1989).

REGIONAL GEOLOGY

The Cumberland Plateau and the Valley and Ridge represent the Appalachian foreland. The Appalachian metamorphic core comprises, from west to east, the western Blue Ridge and correlative Talladega belt, the eastern Blue Ridge, the Inner Piedmont, and peri-Gondwanaland arcs of the Carolina terrane (Figures 1 & 3).

The Cumberland Plateau represents the westernmost Appalachian deformation belt and consists of gently folded, Paleozoic sedimentary rocks (Rodgers, 1970). To the southeast the Valley and Ridge (foreland fold and thrust belt) overlies the Cumberland Plateau and consists of intensely folded and faulted Paleozoic-sedimentary rocks (Weaver, 1970).

		Ma	Orogeny	Events
Jurassic		144		Rifting and opening of Atlantic
Triassic		208		
Permian		245 286	ALLEGHANIAN	Collision with Africa
Carboniferous	Pa	320		
	Miss	360		
Devonian		408	ACADIAN	Terrane Accretion
Silurian		438		
Ordovician		505	TACONIC ---------- PENOBSCOT	A-Subduction Obduction Arc Collision / Accretion
Cambrian		570		
Precambrian		1000-1200	AVALONIAN	Subduction Volcanic Arc Generation
			GRENVILLE	Rifting and Opening of Iapetos

Figure 2: Timing of major events in the tectonic evolution of the southern Appalachians (modified from Hatcher, 1987).

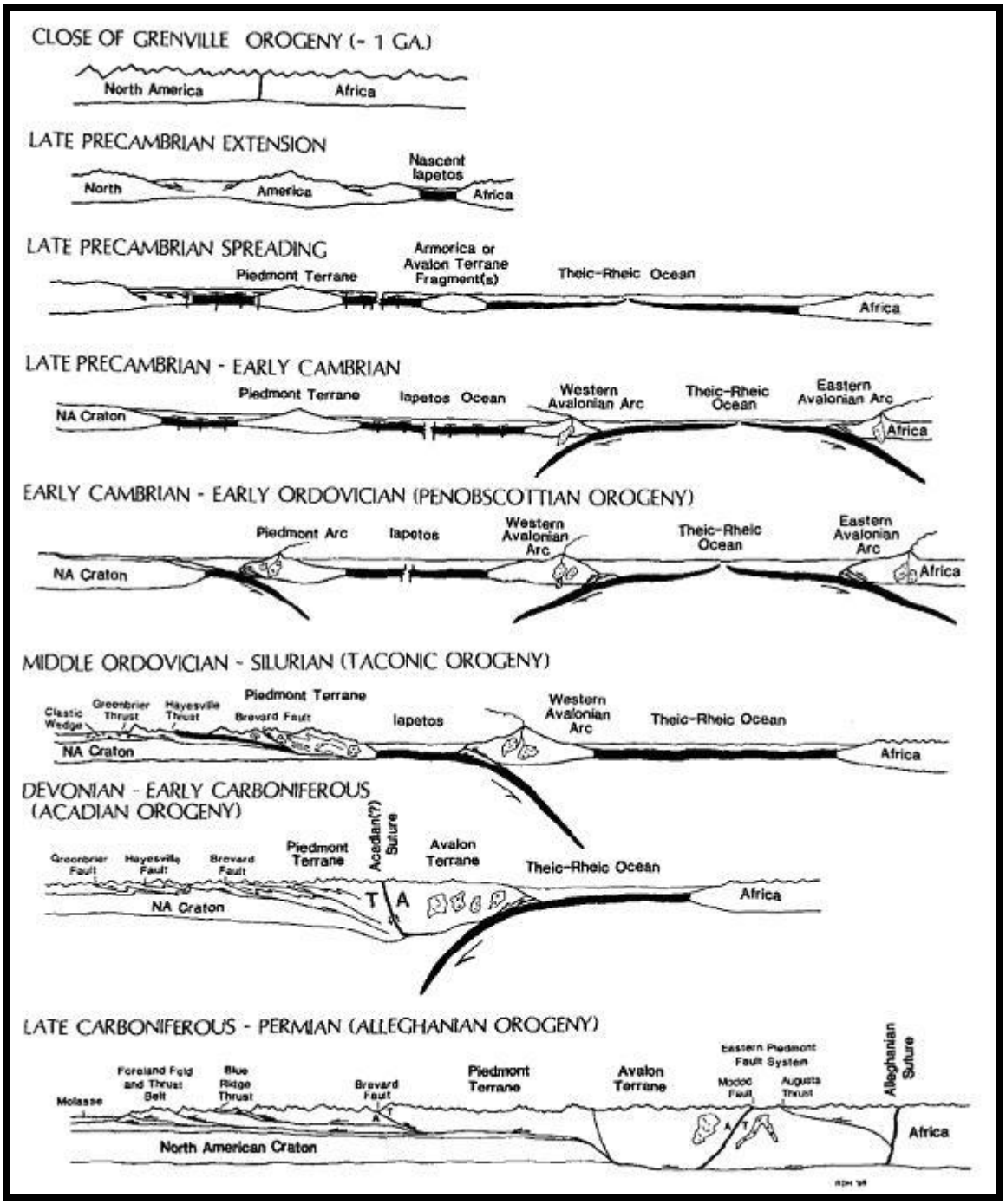

Figure 3: Main tectonic events in schematic cross-sections depicting evolution of the southern Appalachians (from Hatcher, 1987).

The Valley and Ridge was thrust cratonward by thin-skinned decollement, foreland thrusting (Hatcher and Odom, 1980).

The westernmost metamorphic belt of the southern Appalachians and easternmost occurrence of Laurentian rocks is represented by the western Blue Ridge, in northwest Georgia and western North Carolina, and the Talladega Belt, in west-central Georgia and east-central Alabama (Tull and Holm, 2005). The western Blue Ridge and Talladega belt were originally deposited on the Late Proterozoic to Paleozoic, rifted to passive margin along the eastern margin of Laurentia and western shoreline of the Iapetos Ocean (Williams and Hatcher, 1982). These terranes consist primarily of lower-greenschist facies metasedimentary rocks and Grenville basement that were thrust upon Paleozoic sedimentary rocks of the foreland fold and thrust belt along the Talladega – Cartersville – Great Smoky fault (Horton et al., 1989). The western Blue Ridge and Talladega belt preserve the initial and subsequent metamorphic history of the southern Appalachians.

To the east, amphibolite-facies crystalline rocks of the eastern Blue Ridge were thrust upon western Blue Ridge and Talladega belt rocks along the Hollins Line – Hayesville fault (Horton et al., 1989; McClellan et al., 2005). The eastern Blue Ridge is interpreted as the accretionary wedge that resulted from accretion of the Piedmont Arc to Laurentia (Hatcher, 1987). The eastern Blue Ridge consists primarily of metamorphosed distal-clastic rocks deposited off the eastern Laurentian margin as slope-rise sediments, fragments of oceanic crust, mafic bodies, felsic intrusives, and Grenville basement (Hopson, 1989). The major Paleozoic phases of the southern Appalachian Orogen (Hatcher, 1987, and discussed below) include the Taconian, Acadian, and Alleghanian orogenies.

TACONIAN OROGENY

Middle Ordovician to Early Silurian (ca. 480-430 Ma) plate convergence resulted in the initial closing of the Iapetos Ocean and production of a system of thrust faults (Drake et al., 1989; Horton et al., 1989). This included partial subduction of the Laurentian margin and minor obduction of oceanic crust. Accretion of an Early Ordovician arc terrane (Piedmont Terrane) to the Laurentian margin resulted in thrusting of Late Proterozoic to Cambrian Laurentian-margin terrane cratonward over Laurentia. An Appalachian foreland basin formed due to tectonic loading and eroded sediment was deposited as a clastic wedge over the Cambrian, Appalachian platformal margin (Thomas, 1977; Drake et al., 1989). The Taconic clastic wedge is represented by the Blount and Martinsburg formations in the central-northern Appalachian foreland basin and the Sevier-Paperville formation in the southern Appalachian foreland basin (Stevens and Wright, 1981; Thomas 1991). The Taconian orogeny is considered the principal Paleozoic event that metamorphosed Laurentian rocks of the central and northern Appalachians.

ACADIAN OROGENY

Early to Late Devonian (ca. 420-340 Ma) plate convergence resulted in closure of the Iapetos Ocean and the corresponding accretion of a Middle Ordovician arc terrane (Carolina terrane) to the Laurentian margin (Horton et al., 1989; Osberg et al., 1989). The timing of Carolina terrane deformation has been confirmed by $^{40}Ar/^{39}Ar$ analysis of pseudotachylite from the Gold Hill shear zone (muscovite ca. 377 ±4 Ma; Lavallee, 2003). Emplacement of the Carolina terrane resulted in thrusting of the Piedmont terrane, further thrusting of elements of the Late Proterozoic to Cambrian Laurentian margin

cratonward over Laurentia, and additional clastic wedge deposition primarily onto the central Appalachian platform margin (Thomas, 1977; Osberg et al., 1989). The Acadian clastic wedge is represented by the Chattanooga Shale (Early Devonian) in the central Appalachian foreland basin and the Catskill delta (Middle to Late Devonian) in the northern Appalachian foreland basin (Thomas, 1991). The Acadian orogeny is not known to have metamorphosed Laurentian rocks of the southern Appalachians (Osberg et al., 1989; Tull, 2002), though it may have been a time of local deformation and magmatism.

ALLEGHANIAN OROGENY

Early Carboniferous to Permian (ca. 340-270 Ma) plate convergence resulted in closure of the Theic-Rheic Ocean and corresponding oblique-dextral collision of Gondwanaland with Laurentia (Secor et al., 1986; Hatcher et al., 1989). It has been suggested that the Uchee terrane, a rifted fragment similar to the Carolina terrane, was also accreted to the Laurentian margin before collision with Gondwanaland (Mueller et al., 2005). Collision with Gondwanaland resulted in thrusting of the Late Proterozoic to Permian Laurentian margin and Piedmont terranes as a composite thrust sheet cratonward over Laurentia (Secor et al., 1986; Hatcher et al., 1989; Hatcher, 2002). This resulted in significant deposition and subsequent deformation of clastic-wedge sediment in the Appalachian foreland basin that prograded cratonward onto the platform from the southern and central Appalachians (Thomas, 1977; Hatcher et al., 1989; Hatcher, 2002). The Alleghanian clastic wedge is represented by the Pottsville Formation (Pennsylvanian) in the southern Appalachian foreland basin (Hatcher et al., 1989; Thomas, 1991). Alleghanian metamorphic effects are pervasive in the eastern Blue Ridge and Piedmont, and have been thoroughly documented in the Talladega Belt.

TIMING OF EVENTS

The record of Ordovician (Taconian) and Devonian (Acadian) tectonics in the Smoky Mountain region of North Carolina and Tennessee and how its extension to the south fits with the Late Devonian-Permian (Acadian-Alleghanian) tectonic history in Alabama and west-central Georgia is important for a more complete understanding of southern Appalachian evolution. There is no consensus among current researchers concerning the timing of western Blue Ridge metamorphism between its southernmost extension and the Great Smoky Mountain region farther to the north.

STRATIGRAPHIC CONSTRAINTS

In the Talladega belt of Alabama, the youngest metamorphosed fossils are Early Mississippian (Tournaisian) *Periastron* plant fossils from the Erin Slate (Gastaldo et al., 1993). The presence of these fossils constrains the age of metamorphism in the Talladega belt-western Blue Ridge to be no older than ~360-350 Ma, Early Mississippian (Tournaisian; based on the time scale of Gradstein et al., 2004).

The foreland-sedimentary sequence (Valley and Ridge) is isoclinally folded and cut by faults related to thrust emplacement of the Talladega belt and western Blue Ridge (Tull and Holm, 2005). The youngest deformed sediments of this sequence are the Pottsville Formation (Hatcher et al., 1989). The Pottsville clastic wedge was deposited in the Appalachian foreland basin during the Alleghanian tectonic event. The Pottsville

Formation stratigraphically constrains the youngest age of deformation for the Talladega belt-western Blue Ridge to ~ 316-303 Ma.

RADIOMETRIC CONSTRAINTS

Kish (1983; 1990) made some conventional K/Ar age determinations for whole rock and mineral samples from the western Blue Ridge in the Tennessee-North Carolina region southwest of the Smoky Mountains. However, these data are generally difficult to interpret due to effects of extraneous argon and heterogeneous-mineral assemblages inherent to whole-rock ages (Kish, 1991).

In the western Blue Ridge of North Carolina and Tennessee, $^{40}Ar/^{39}Ar$ age data for low-grade metamorphic rocks indicate Taconian and Acadian metamorphism (Figure 4). Chlorite-grade rocks record Middle to Late Ordovician metamorphism at 460-440 Ma and biotite-grade rocks record Late Devonian metamorphism at 380-360 Ma (e.g., Connelly and Dallmeyer, 1993). Muscovite from mylonitic rocks record Early Mississippian cooling at 355-330 Ma (e.g., Kunk et al., 2006). Taconian metamorphism in the garnet and staurolite zones of the Smoky Mountains has been confirmed by recent U/Pb TIMS ages of ca. 445-455 Ma for garnet-hosted monazite inclusions (Corrie and Kohn, 2007).

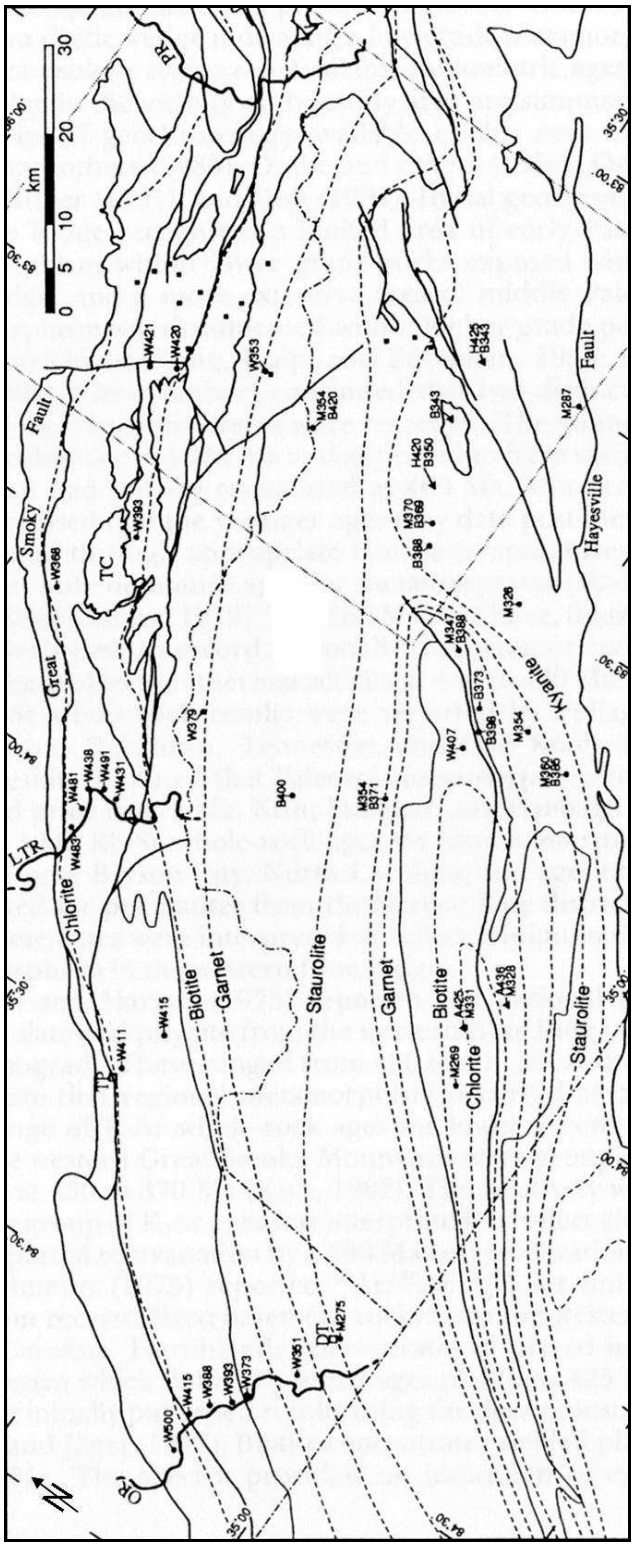

Figure 4: Map from the Smoky Mountain region southwest to the Cohuttas of North Georgia, with isograds and a combination of $^{40}Ar/^{39}Ar$ and K/Ar ages (from Connelly and Dallmeyer, 1993).

In the Talladega belt of Alabama, $^{40}Ar/^{39}Ar$ age data indicate Alleghanian metamorphism. The oldest $^{40}Ar/^{39}Ar$ ages for metamorphic muscovite are Middle Mississippian, ca. 329-327 Ma, and for hornblende are also Middle Mississippian, ca. 334-330 Ma (Figures 5; McClellan et al., 2007; Steltenpohl et al., 2005). The oldest $^{40}Ar/^{39}Ar$ ages for white mica are Middle to Late Mississippian, ca. 334-320 Ma (Figure 6; McClellan et al., 2005; McClellan et al., 2007). These radiometric ages imply rapid cooling and constrain the timing of the earliest metamorphism to be no younger than ca. 334-320 Ma, Middle to Late Mississippian. In the Piedmont of Alabama and southwest Georgia, Steltenpohl and Kunk (1993) made some $^{40}Ar/^{39}Ar$ age determinations for hornblende (ca. 347-320 Ma; Mississippian), muscovite (ca. 296-283 Ma; Early Permian), and biotite (ca. 293-276; Early Permian) indicating Alleghanian metamorphism. This combined with stratigraphic constraints clearly indicates Mississippian to Pennsylvanian tectonics dominated the history of this region.

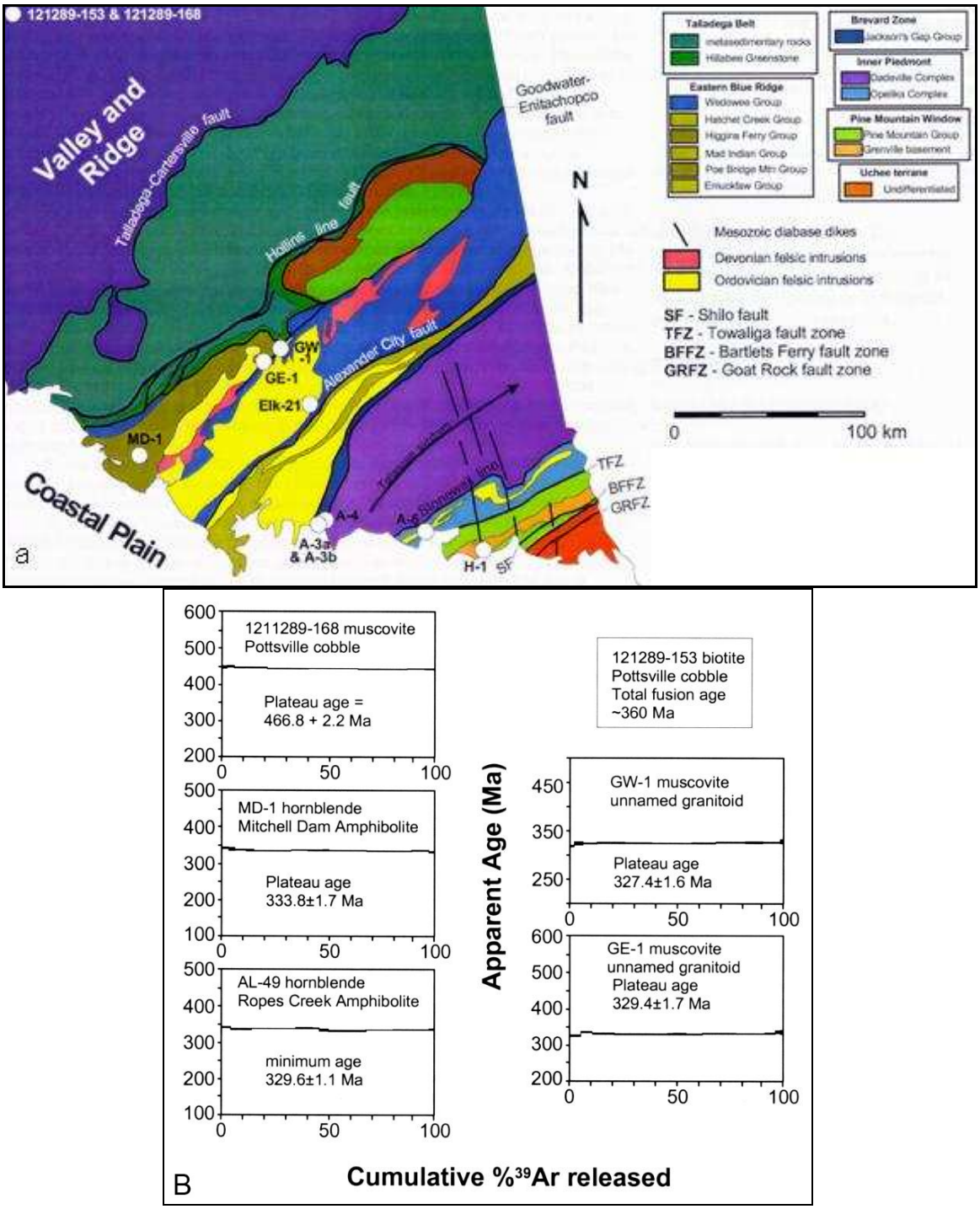

Figure 5: a) Map of the southern Appalachians in Alabama with locations for samples as studied by Steltenpohl et al. (2005). b) Incremental heating spectra and $^{40}Ar/^{39}Ar$ ages for samples reported by Steltenpohl et al. (2005).

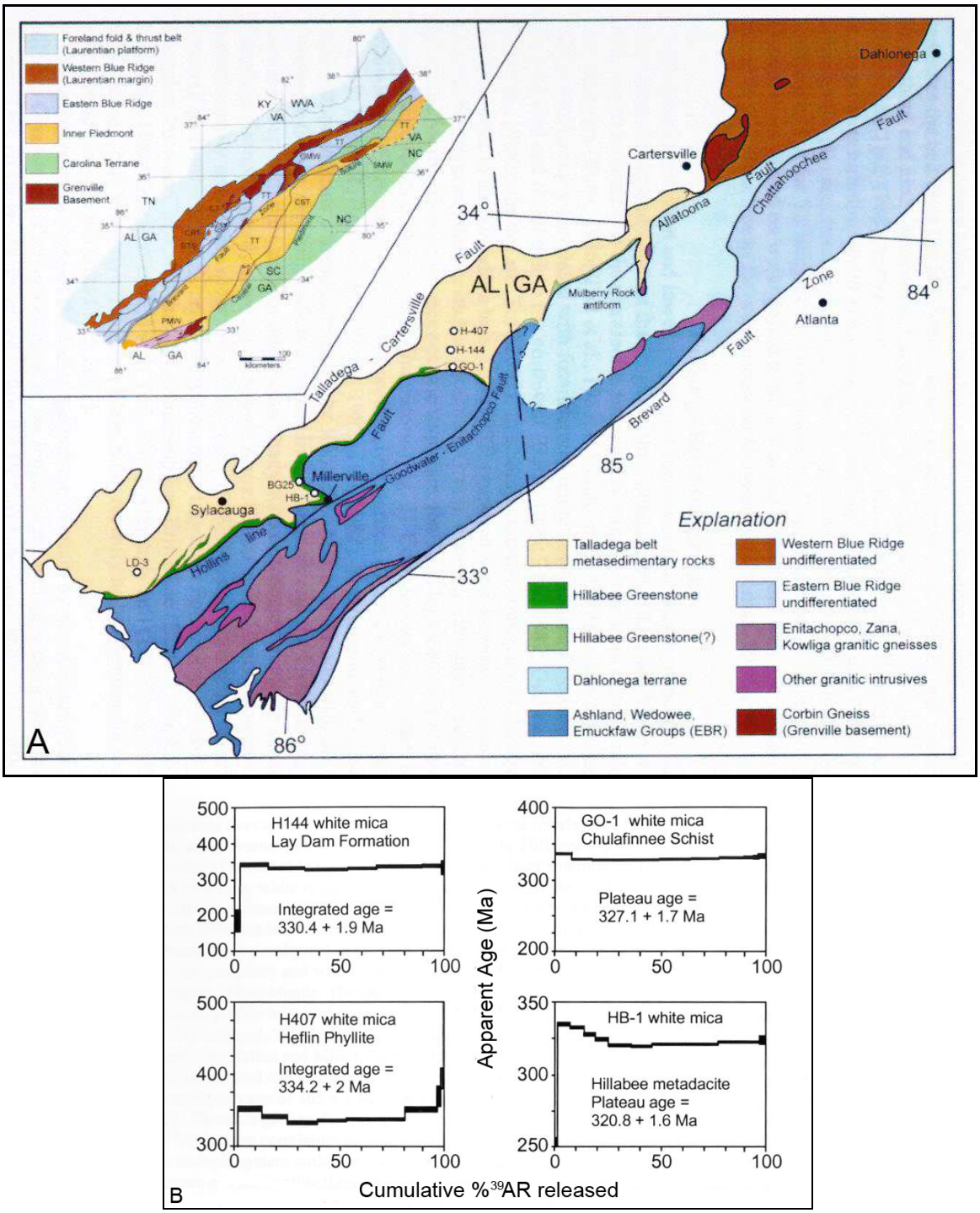

Figure 6: a) Map of the southern Appalachians in Alabama with locations for samples as studied by McClellan et al. (2005). b) Incremental-heating spectra and $^{40}Ar/^{39}Ar$ ages for samples reported by McClellan et al. (2005). Note that the main area for sampling in the present study (see Figure 7) begins in the vicinity of Cartersville, where the Talladega belt tectonic stratigraphy has been correlated with the Blue Ridge stratigraphy by the mapping of Tull and Holm (2005).

GIS DATABASE

A GIS database was constructed in order to manage, interpret, and present the radiometric data generated in this thesis. This database includes sample locations, regional and mesoscopic geologic information, and as much sample characterization (petrography, chemical data, etc.) as is practical. The database is web-enabled, and can potentially be utilized by other researchers (Figure 7).

The web-enabled GIS database was constructed using a desktop computer, Auburn University server space, ARCMAP (ARCGIS 9.1 desktop by ESRI) GIS software, the EasySVG (by Adobe) plug-in for ARCMAP, and FrontPage (by Microsoft) web authoring software. A geologic map of the southern Appalachians was scanned and imported into ARCMAP as the raster basemap of the study area and then geo-referenced to the WGS 1984, geographic-coordinate system. The x-y data, attributes, and hyperlinks for each sample location were entered into ARCMAP in spreadsheet form, added as layers to the basemap, and then converted into shapefiles. HTML webpages were constructed for each sample location using FrontPage. The geo-referenced raster basemap and shapefiles were converted, using the EasySVG plugin, into Scalable Vector Graphics (SVG) format. The SVG map files and hyperlinked HTML webpages were published, using FrontPage, onto Auburn University server space. Installation of the SVGViewer (by Adobe), a web browser plug-in, is needed to access the GIS map on the World Wide Web.

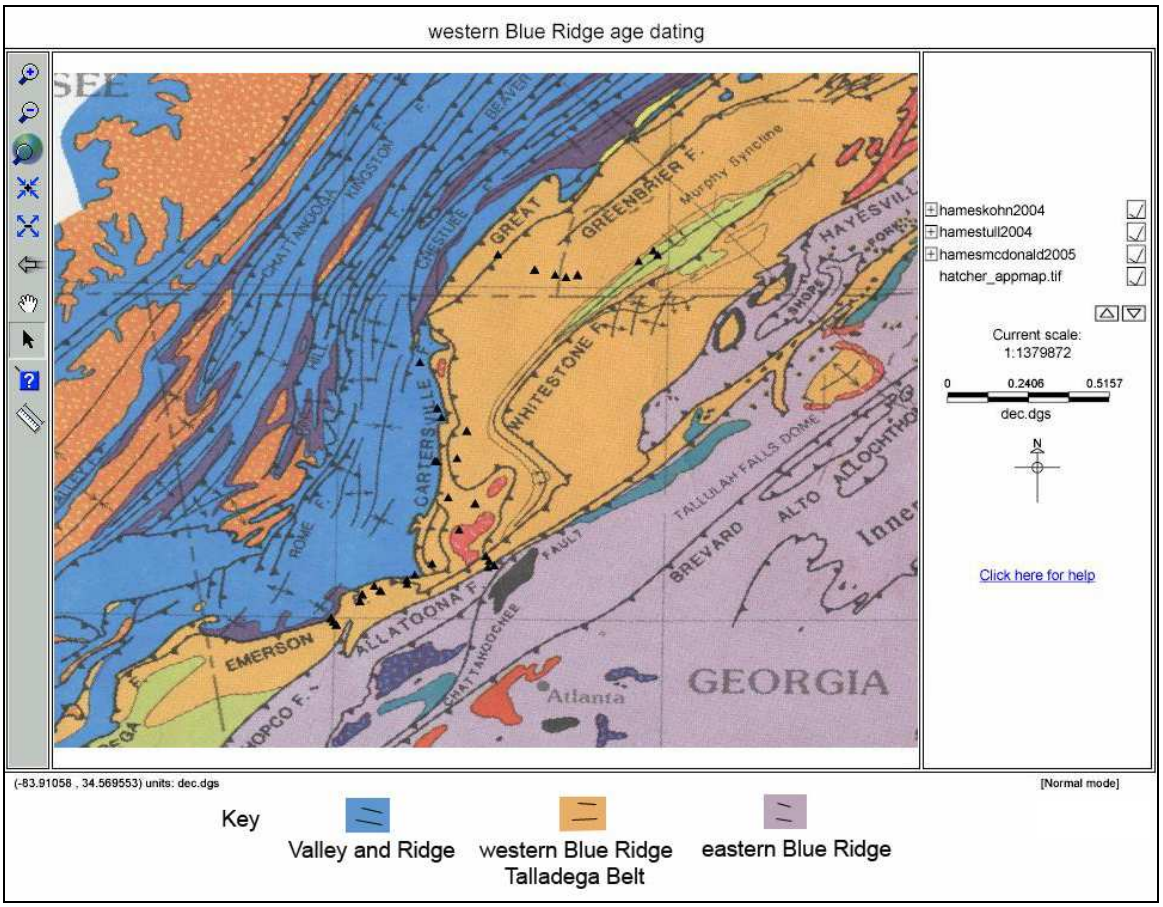

Figure 7: Screen capture of the web-enabled GIS map of study area. The particular basemap used is that of Hatcher et al. (1990). The sampling locations (n=24) shown as black triangles.

Scalable Vector Graphics (SVG) is showing promise as a new XML based graphics standard for internet applications and is the best choice for internet mapping (Duce et al., 2002; Herman & Dardailler, 2002; Ruffle & Richens, 2004). SVG is the W3C (World Wide Web Consortium) mark-up language for vector graphics on the internet and also specifies interactive mechanisms and behavior tools (Carrarat et al., 2003). The high retention of resolution by vector graphics at high zoom levels is an inherent advantage of SVG as well as the facilities to interact with the graphics and assign resolution levels to specific map features or zoom levels (Cecconi & Galanda, 2002). The raster image format has been the standard for mainstream internet mapping, however the image quality of raster graphics is marginal for internet mapping (Cecconi & Galanda, 2002) and the raster format requires large server capacities and lacks interactive abilities (Duce, et al, 2002).

The web-enabled GIS constructed for this thesis can be classified as a "single-source GIS," meaning it has a single website or server, and sub-classified as dynamic due to the interactive nature of SVG (Shaig, 2001). The functionality of this web-enabled GIS can be classified as a "map server," defined by Rinner (1998) as being able to provide graphics on the internet as well as interactive tools, or alternatively as a "dynamic map browser" by Plewe (1997).

DESCRIPTION OF TECTONIC UNITS STUDIED

Muscovite-bearing rocks were collected from several tectonic units of the Talladega belt (Figure 8a) and western Blue Ridge (Figure 8b). Refer to Table 1 for tectonostratigraphy of the formations sampled.

Rocks of the Talladega belt have been biostratigraphically correlated with the Laurentian Ocoee Supergroup and Chilhowee Group of the western Blue Ridge and the Shady Dolomite of the Valley and Ridge (Tull et al., 1988). The Talladega belt includes a lower clastic sequence (1.5 km thick; Kahatchee Mountain Group), conformably overlain by a middle carbonate sequence (1.5 km thick; Sylacauga Marble Group), unconformably overlain by an upper clastic sequence (2-5 km thick; Talladega Group), which is tectonically overlain by a Middle Ordovician volcanic terrane (Hillabee Greenstone; Tull et al., 1982; McClellan et al., 2007). Seven samples were collected from the Lay Dam Formation of the Talladega Group (Table 1). The Lay Dam Formation is a clastic sequence of slates and metasiltstones unconformably overlying the Sylacauga Marble Group (Carrington, 1973). The Lay Dam Formation is stratigraphically equivalent to the Mineral Bluff Group in the western Blue Ridge (Tull, 2002; Tull et al., 1988).

The Ocoee Supergroup is the primary rift-basin sequence (300 km long, 75 km wide, and 12 km thick; Hadley, 1970) of the western Blue Ridge and occurs in at least six thrust sheets (Hadley, 1970; Rankin, 1975). The units were originally deposited in a continental rift basin along the eastern Laurentian margin during the Late Proterozoic

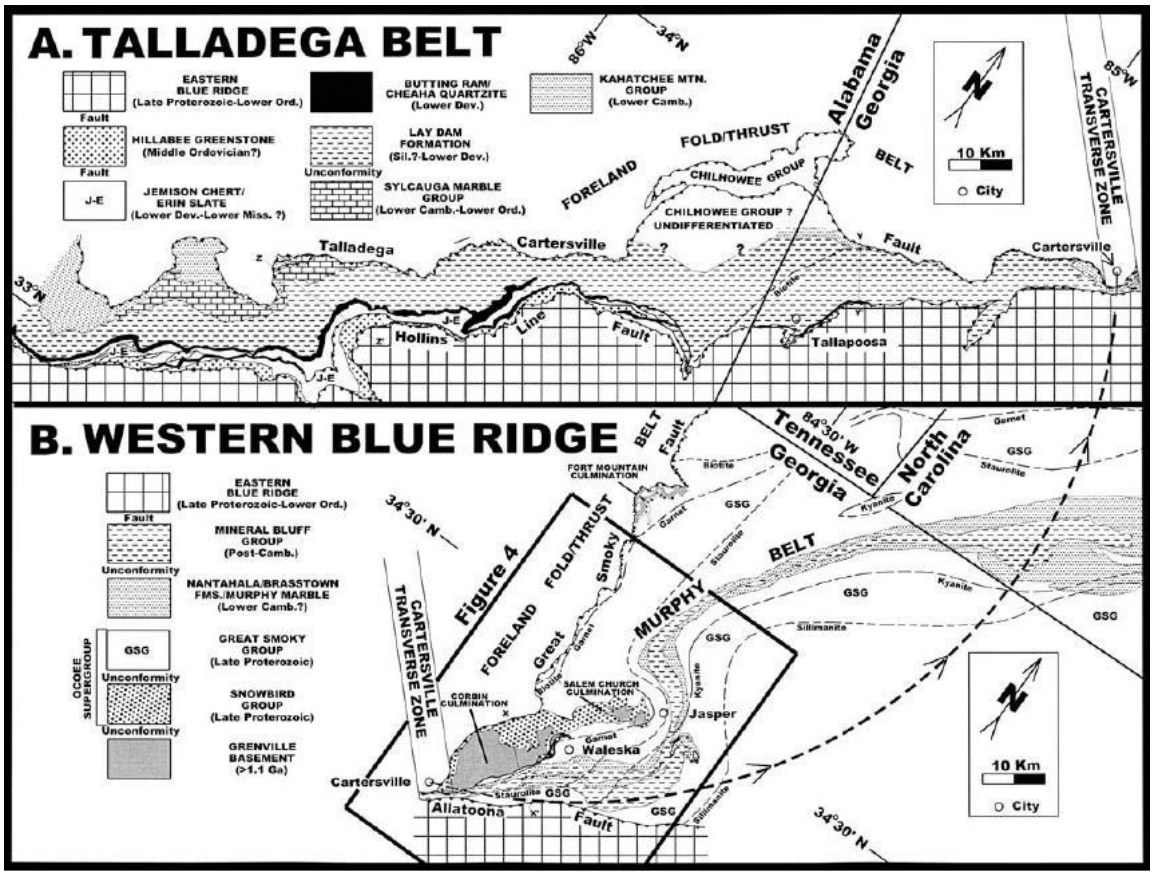

Figure 8: Tectonostratigraphic map of the study region: a) Talladega belt of Alabama and Georgia; and b) western Blue Ridge of Georgia and adjacent North Carolina (from Tull and Holm, 2005, their Figure 3b).

(Hatcher, 1989; Tull and Holm, 2005). The Ocoee Supergroup includes the Great Smoky Group overlying the Snowbird Group along the pre-metamorphic Greenbrier fault (King, 1958; Tull et al., 1993). The Snowbird Group consists primarily of highly feldspathic alluvial, fluvial, and shallow marine clastic rocks deposited over Grenville basement (Hatcher, 1989; Tull and Holm, 2005) during a limited cycle of extension associated with continental rifting (Li and Tull, 1998). The Snowbird Group is 4-km thick and had a source area to the east and southeast (King, 1964; Rodgers, 1972). Four samples were collected from the Pinelog Formation of the Snowbird Group (see Table 1). The Great Smoky Group is a thick unit of relatively deep marine sandstone and shale (Hatcher, 1989; Tull and Holm, 2005) and was deposited during a more aggressive cycle of extension (Li and Tull, 1998). The Great Smoky Group is 7-km thick and had a source area to the northeast (King, 1958; Rodgers, 1972). Thirteen samples were collected from several formations of the Great Smoky Group (see Table 1). The Walden Creek Group overlies the Great Smoky Group on the footwall side of the Greenbrier fault (King, 1958; Tull et al., 1993) and is a unit of unstable shelf deposits that could be facies equivalent to the Great Smoky Group or an unrelated sequence of a separate basin (Rankin, 1975). The Walden Creek Group is 2-km thick and had a source area to the northwest (King, 1964; Rodgers, 1972). Three samples were collected from the Wilhite Formation of the Walden Creek Group. The Chilhowee Group, a drift-facies sequence, conformably overlies the Ocoee Supergroup and is relatively widespread (Rankin 1975; Tull et al., 1993). The Chilhowee Group consists of shallow-marine sandstones and shales originally deposited post-rift over the Ocoee Supergroup and Grenville basement highs, during the Early Cambrian (King, 1958; Hatcher, 1989; Tull and Holm, 2005).

Rocks of the Murphy belt lies within the core of a regional isoclinal fold (170 km long, 1300-2000 m thick; Hurst, 1955) and gradationally overlie the Ocoee Supergroup southeast of the Greenbrier fault (Tull et al., 1993). Lithologies of the Murphy belt consist primarily of the drift-facies Hiawassee River Group (Tull et al., 1991) or alternatively the Murphy Belt Group (Thigpen and Hatcher, 2006). The Murphy Belt Group includes the Nantahala and Brasstown Formations and the Murphy Marble (Tull and Holm, 2005) unconformably overlain by the Mineral Bluff Group. The Nantahala and Brasstown Formations conformably overlie the Ocoee Supergroup (Tull and Holm, 2005) and are considered to be outer margin equivalents of the Chilhowee Group (Aylor, 1994). The Murphy Marble conformably overlies the Nantahala and Brasstown Formations (Tull and Holm, 2005) and represents the base of the Cambrian-Ordovician carbonate shelf along the Laurentian margin (Keith, 1907). The Mineral Bluff Group is a clastic sequence of metaconglomerates, metasandstones, and metasiltstones that are interbedded with metavolcanic units (Tull et al., 1991). Four samples were collected from the Mineral Bluff Group (see Table 1).

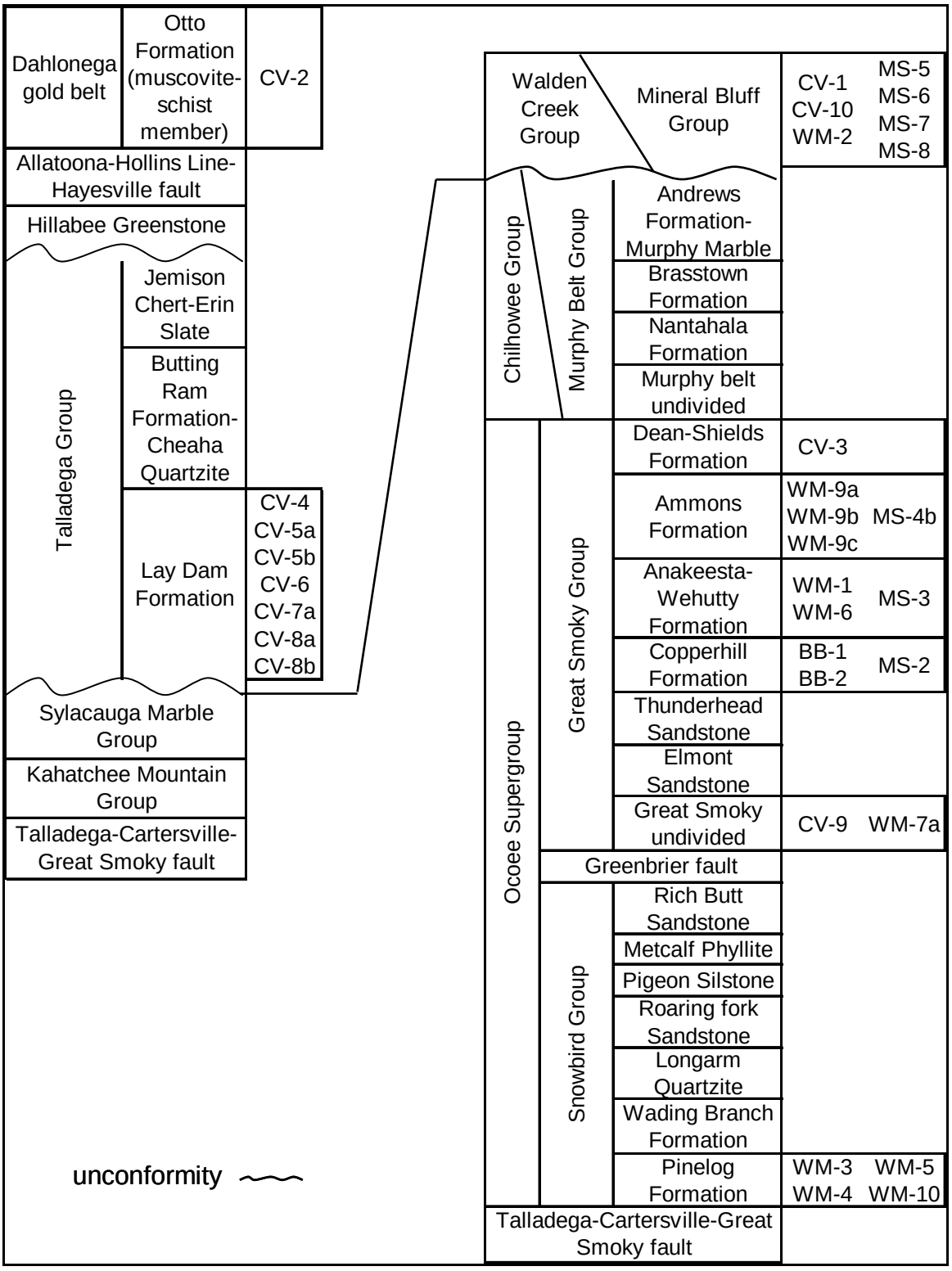

Table 1: Schematic tectonostratigraphy of units sampled in this study, based on the regional compilations of Tull and Holm (2005) and Thigpen and Hatcher (2006).

SAMPLE PETROGRAPHY

The petrography of minerals - a study of their characteristics including habit, strain state, grain size, and associations in rock assemblages - provides a foundation for interpreting their history. Thus, efforts to date minerals by radioactive decay are best carried out with a characterization that focuses on the phase(s) of interest. Muscovite is a very powerful mineral for the radiometric dating of orogenic events through the K-Ar and $^{40}Ar/^{39}Ar$ method. The bulk closure temperature of muscovite for argon retention (350 ± 50°C; e.g., Purdy and Jager, 1976) is such that ages from sub-greenschist and lower greenschist facies rocks can approximate the timing of muscovite growth, whereas ages for higher-grade rocks tend to record the timing of cooling. Muscovite is common in metamorphic rocks from a wide range of protoliths. Furthermore, the growth of muscovite can usually be placed in the context of a sample's deformational history and its crystal structure efficiently retains radiogenic gases. The relationship of muscovite grains to fabric development within a rock sample has important implications for interpreting the radiometric data. Muscovite from a rock that has a simple metamorphic history would be expected to yield a single age. Muscovite from a rock that has experienced multiple generations of fabric development would be expected to yield a range of ages, assuming those fabrics developed near the closure interval (Dodson, 1973) for Ar in muscovite. However, if the muscovite was thoroughly recrystallized, thereby overprinting the older fabrics, the radiometric data pertains to the latest metamorphic generation.

Rock samples for this thesis are from four distinct structural settings within the western Blue Ridge. These are the Cartersville transverse zone, the Great Smoky fault, the Ducktown anticlinorium, and the Murphy synclinorium. The four sample groups have unique metamorphic grades, muscovite characters, strain features, and metamorphic fabrics. Petrography for representative samples will first be discussed for the southernmost extent of the western Blue Ridge and then west to east according to structural setting from the thrust front into the center of the belt.

CARTERSVILLE TRANSVERSE ZONE

The Cartersville transverse zone (see Figure 8; as defined by Tull and Holm, 2005) marks stratigraphic and structural contrasts between the Talladega and western Blue Ridge belts. The western Blue Ridge is a thick rift-facies sequence metamorphosed mostly to biotite grade or higher (indicating relatively deep burial) with regional isoclinal folds. The Talladega belt is a relatively thin terrane metamorphosed mostly to biotite grade or lower (indicating relatively shallow burial), with no rift-facies rocks or isoclinal folds. Samples CV-7a, CV-8a, CV-8b, and CV-5a (Figure 9) were collected from the northeast extension of the Talladega belt. Samples CV-3 and CV-2 (Figure 10) were collected from the zone where the Talladega belt trends into the western Blue Ridge. Samples CV-1 and CV-10 (Figure 11) were collected from the southwestern extension of the western Blue Ridge. Refer to Table 2 (Analytical Results chapter) for geographic coordinates.

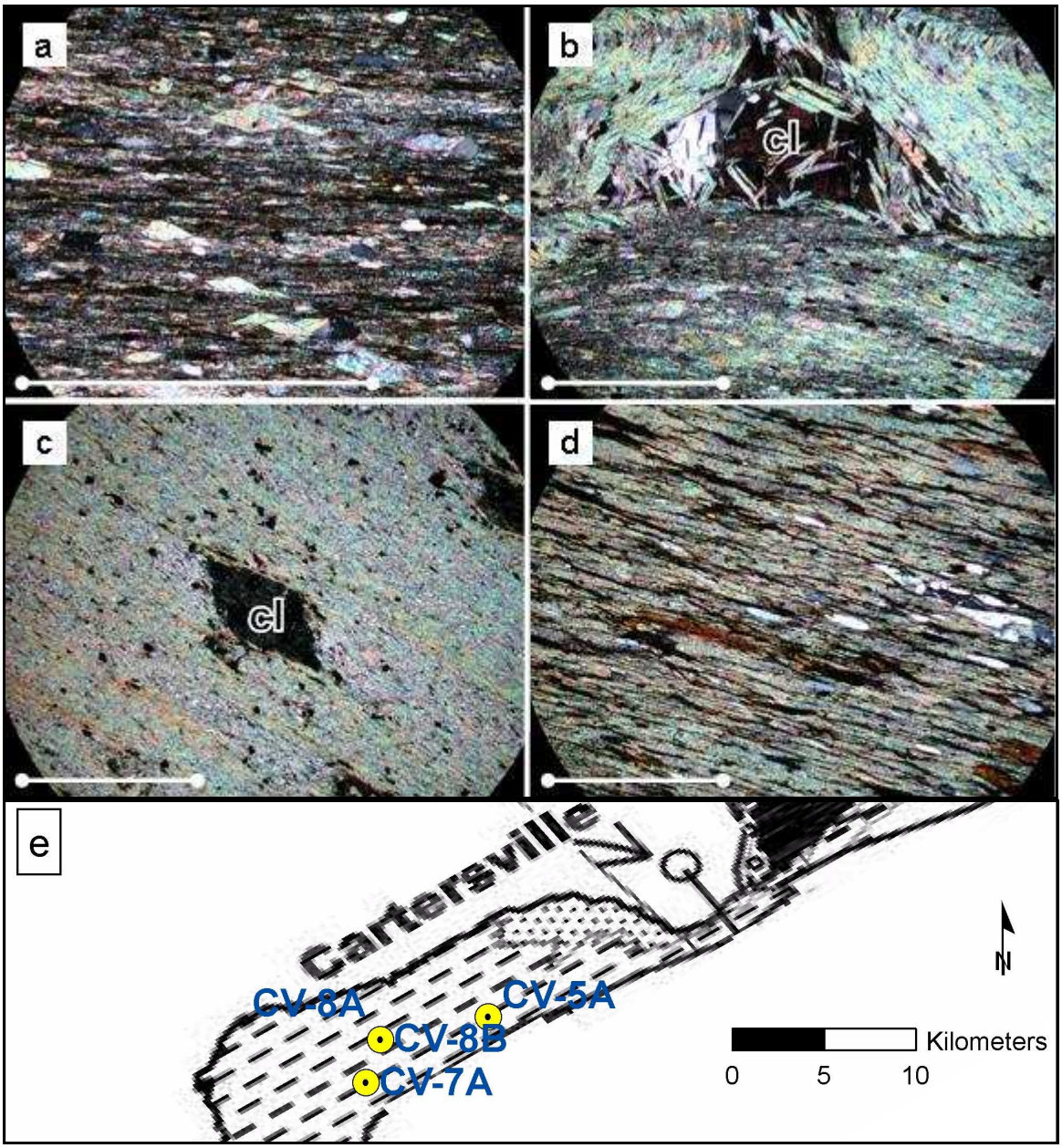

Figure 9: Photomicrographs of metamorphic textures in rocks from the Talladega belt (scale bars are 1.0 mm; cross-polarized light). (a) Sample CV-7a, biotite-muscovite phyllite. Sample characterized by a single-generation foliation. Muscovite porphyroclasts are aligned with foliation. (b) Sample CV-8a, muscovite phyllite. Sample characterized by an early generation, mica-rich fabric cut by a late-generation quartz and retrograde chlorite (cl) rich fabric. (c) Sample CV-8b, muscovite phyllite. Sample characterized by a single-continuous foliation with abundant retrograde chlorite. (d) Sample CV-5a, muscovite phyllite. Sample characterized by a single-continuous foliation defined by fine-grained muscovite and elongated quartz grains. (e) Map of sample localities (adapted from Tull and Holm, 2005).

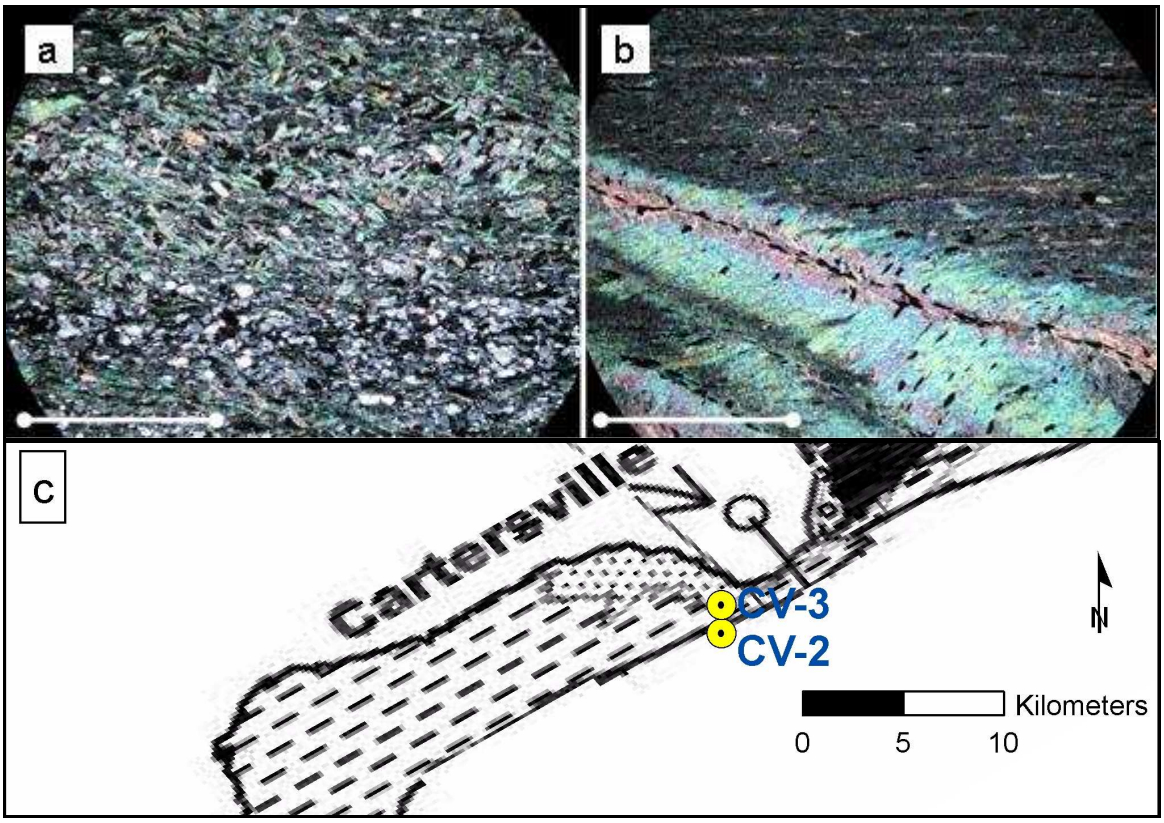

Figure 10: Photomicrographs of metamorphic textures in rocks from the Cartersville transverse zone (scale bars represent 1.0 mm; cross-polarized light). (a) Sample CV-3, muscovite phyllite. Sample characterized by a single generation, spaced foliation. Sample has abundant retrograde chlorite. (b) Sample CV-2, garnet-chlorite-muscovite phyllite. Sample characterized by an early generation, continuous foliation cut by late-stage crenulation. (c) Map of sample localities (adapted from Tull and Holm, 2005).

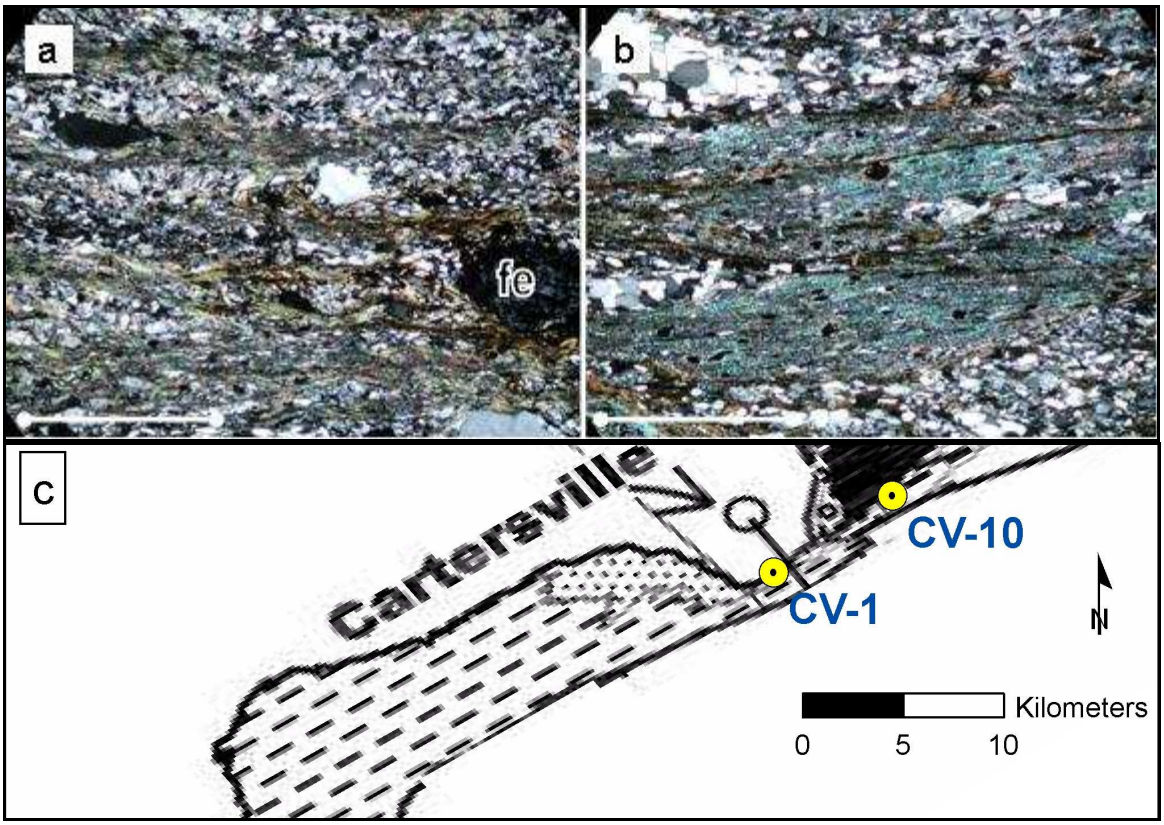

Figure 11: Photomicrographs of metamorphic textures in rocks from the western Blue Ridge-Cartersville transverse zone (scale bars represent 1.0 mm; cross-polarized light). (a) Sample CV-1, muscovite phyllite. Sample characterized by a single generation, spaced foliation and abundant feldspar porphyroclasts. (b) Sample CV-10, muscovite schist. Sample characterized by an early generation, spaced foliation deformed by late-stage fabric development (as evidenced by muscovite porphyroclasts). (c) Map of sample localities (adapted from Tull and Holm, 2005).

Sample CV-7a (Figure 9a) is a biotite-muscovite phyllite of the Lay Dam Formation (alternatively the Mineral Bluff Group of the western Blue Ridge). The sample is characterized by a single-generation fabric, defined by fine-grained muscovite and minor biotite. Muscovite porphyroclasts could be detrital grains or relicts of an earlier generation. Samples CV-8a and CV-8b (Figures 9b and 9c respectively) are muscovite phyllites of the Lay Dam Formation. Sample CV-8a is characterized by a multiple-generation fabric. The early-generation foliation is defined by fine-grained muscovite and chlorite. Late-stage foliation is defined by coarser grained muscovite and abundant retrograde chlorite. The quartz grains are strained as evidenced by undulose extinction. The sample is graphitic and has hematite staining. Sample CV-8b is characterized by a single-generation fabric, defined by very fine-grained muscovite. An abundance of retrograde chlorite is present. Sample CV-5a (Figure 9d) is a muscovite phyllite of the Lay Dam Formation. The sample is characterized by a single-generation fabric, defined by fine-grained muscovite and elongated quartz grains. Undulose extinction, exhibited by the quartz grains, indicates strain.

Sample CV-3 (Figure 10a) is a muscovite phyllite of the Dean Formation, Great Smoky Group. The sample is characterized by two planar fabrics. Early-generation spaced cleavage is defined by fine-grained muscovite. Late-stage deformation has sheared the early foliation. Quartz grains are strained as evidenced by undulose extinction. The sample is predominantly quartz and has abundant retrograde chlorite. Sample CV-2 (Figure 10b) is a garnet-chlorite-muscovite phyllite of the Otto Formation (eastern Blue Ridge). The sample is characterized by a multiple-generation fabric. The early generation, continuous foliation is defined by fine-grained muscovite and chlorite.

Late-stage deformation has crenulated the early foliation. The sample is graphitic and has abundant garnet porphyroblasts. Strain is indicated in the quartz grains by undulose extinction.

Sample CV-1 (Figure 11a) is a muscovite phyllite of the Wilhite Formation, Walden Creek Group. The sample is characterized by a single-generation spaced foliation, defined by fine-grained muscovite. The sample is graphitic and has abundant feldspar porphyroclasts. The quartz and feldspar grains are strained as evidenced by undulose extinction. Sample CV-10 (Figure 11b) is a muscovite schist of the Wilhite Formation. The sample is characterized by a multiple-generation fabric. The early-spaced foliation is defined by fine-grained muscovite. Late-stage deformation crushed the early foliation forming muscovite porphyroclasts. Strain is evident in quartz grains by the exhibition of undulose extinction.

GREAT SMOKY FAULT

The Great Smoky fault is the northwestern most structure of the western Blue Ridge. This region of the western Blue Ridge is characterized by sub-greenschist facies, metasedimentary rocks. Samples WM-9a (Figure 12a) and WM-9c (Figure 12b) were collected near the Carters Lake Dam, approximately 2000 ft. due north of the stop localities indicated in McConnell (1986). Sample WM-10 (Figure 12c) was collected farther north, near Chatsworth along Route 52 (refer to Table 2 for geographic coordinates).

Samples WM-9a and WM-9c are graphitic-muscovite metasiltstones of the Ammons Formation, Great Smoky Group. Both samples have abundant clasts of relict quartz pebbles. These quartz clasts are strongly strained, as evidenced by undulose

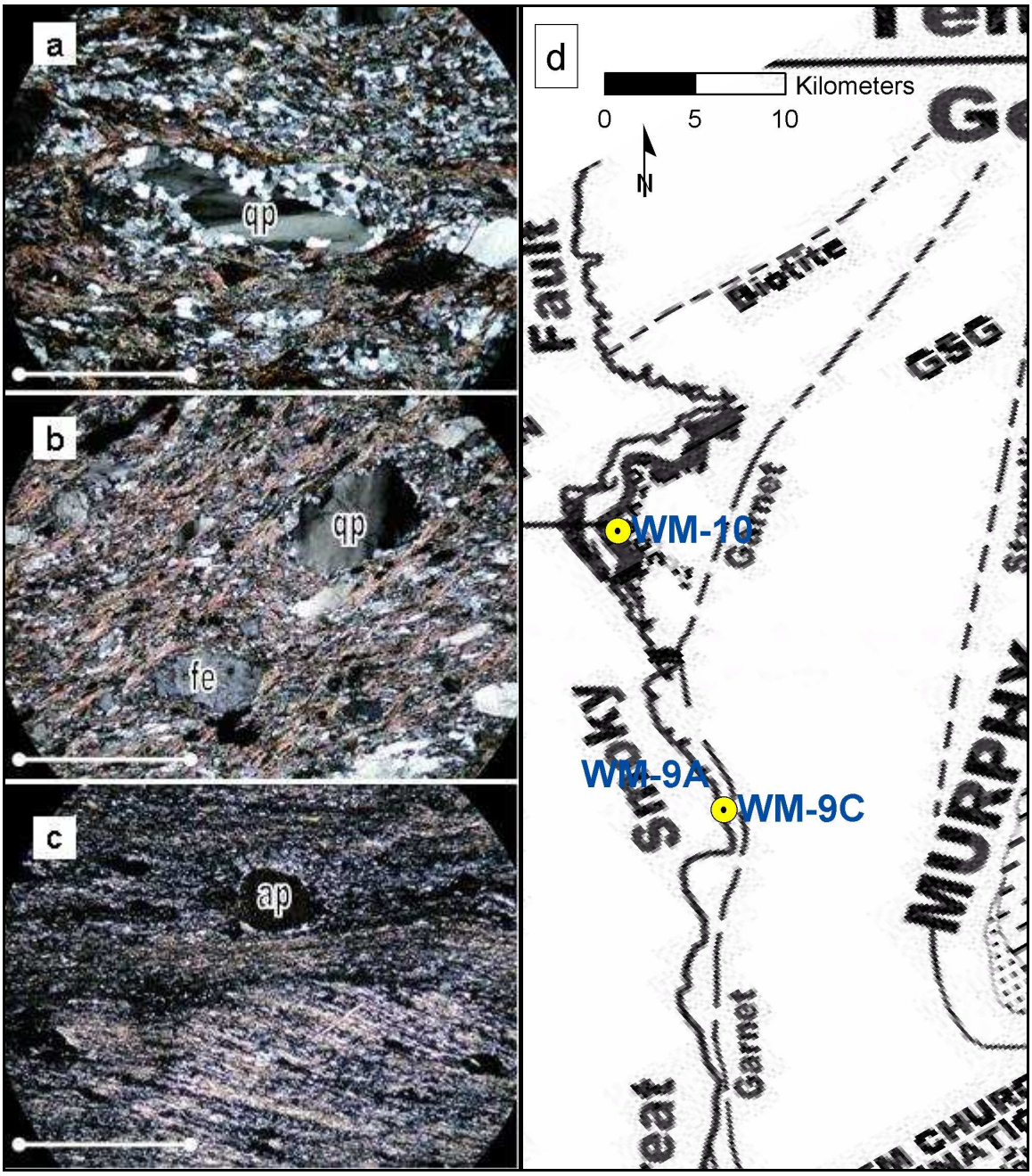

Figure 12: Photomicrographs of metamorphic textures in rocks from the Great Smoky fault (scale bars represent 1.0 mm; cross-polarized light). (a) Sample WM-9a, graphitic-muscovite metasiltstone. Sample characterized by a multiple-generation fabric, plastic deformation of quartz, brittle deformation of micas, and large relict-quartz pebbles or clasts (qp). (b) Sample WM-9c, graphitic-muscovite metasiltstone. Sample has similar fabric with a relatively higher abundance of feldspar clasts (fe) and coarser grained mica. (c) Sample WM-10, muscovite phyllite. Sample characterized by an anastomosing, multiple-generation fabric defined by relatively fine-grained muscovite and relict apatite (ap) clasts. (d) Map of sample localities (adapted from Tull and Holm, 2005).

extinction and subgrains, and are surrounded by recrystallized quartz grains with interlobate boundaries. The mica is characterized by fine-grained muscovite recrystallized from the original sedimentary matrix. These samples have apparently experienced multiple generations of fabric development, with ductile deformation of quartz and brittle deformation of micas. Radiometric data for these samples may be influenced by the presence detrital minerals. Sample WM-10 is a muscovite phyllite of the Pinelog Formation, Snowbird Group. Foliations are defined by very fine-grained muscovite with an anastomosing multiple-generation fabric. The sample is also characterized by an abundance of apatite clasts.

DUCKTOWN ANTICLINORIUM

The Ducktown anticlinorium is a northeast-trending synmetamorphic fold east of the Great Smoky fault. This regional antiform is characterized, as discussed by Hatcher and Goldberg (1991), by a core of staurolite-grade rocks (amphibolite facies) with limbs of garnet and biotite-grade rocks (upper-greenschist facies). Samples BB-1 (Figure 13a) and BB-2 (Figure 13b) were collected from a tailings pile at the Bura Bura Mine in Ducktown. Samples MS-2 (Figure 13c) and MS-3 (Figure 13d) were collected farther east along Route 64 (refer to Table 2 for geographic coordinates).

Samples BB-1 and BB-2 are garnet-biotite-muscovite schists of the Copperhill Formation, Great Smoky Group. The samples are characterized by a multiple-generation fabric, an abundance of garnet porphyroblasts, and crystal-plastically deformed quartz grains as evidenced by undulose extinction and subgrains. An early-generation foliation is defined by coarse muscovite and biotite grains. Late-stage deformation has crenulated the foliation in sample BB-1. Late-stage folding deformed the foliation in sample BB-2.

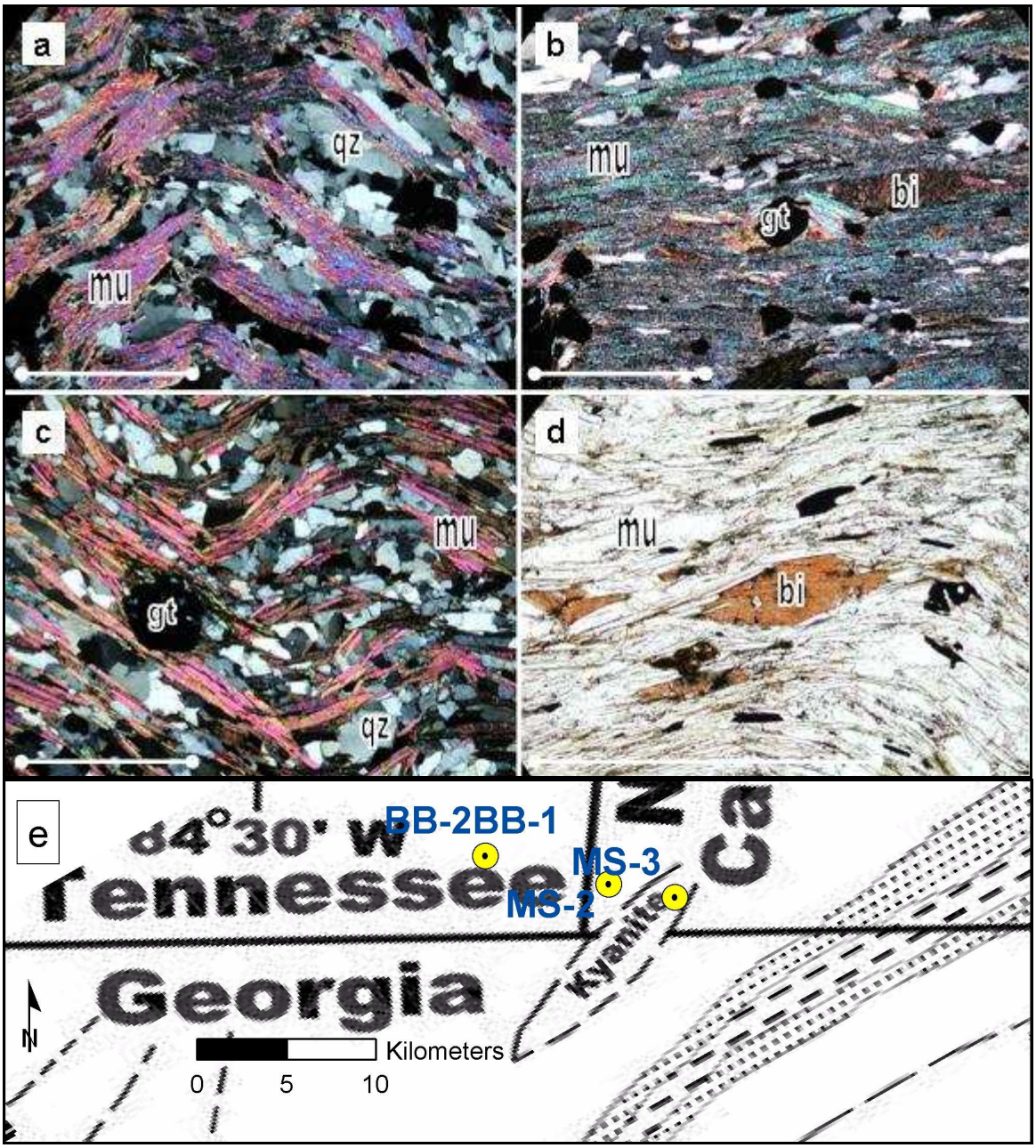

Figure 13: Photomicrographs of metamorphic textures in rocks from the Ducktown anticlinorium (scale bars represent 1.0 mm; cross-polarized light). These garnet-biotite-muscovite schists are characterized by an early-generation foliation, defined by coarse-grained muscovite (mu) and biotite (bi), subsequently deformed by late-stage folds. (a) Sample BB-1. (b) Sample BB-2. (c) Sample MS-2. (d) Sample MS-3. (e) Map of sample localities (adapted from Tull and Holm, 2005).

Sample BB-2 also has minor retrograde chlorite. Sample MS-2 is a garnet-biotite-muscovite schist of the Copperhill Formation. An early-generation foliation is defined by coarse-grained muscovite and biotite. The sample has abundant garnet porphyroblasts. Some quartz grains have recrystallized and some are older-strained grains. Late-stage deformation has crenulated the foliation. Sample MS-3 is a garnet-biotite-muscovite schist of the Upper Anakeesta-Wehutty Formations, Great Smoky Group. An early-generation foliation is defined by coarse muscovite and biotite grains. The biotite grains were subsequently deformed, indicating post-growth shear, as evidenced by lens shaped porphyroclasts and kink bands.

MURPHY SYNCLINORIUM

The Murphy synclinorium is a northeast-trending synmetamorphic fold east of the Ducktown anticlinorium. This regional synform, as discussed by Hatcher and Goldberg (1991), has a core of chlorite-grade rocks (lower-greenschist facies) with limbs of biotite and garnet-grade rocks (upper-greenschist facies). Samples MS-5, 6, 7, and 8 (Figure 14) were collected from the core of the synclinorium along Route 64 (refer to Table 2 for geographic coordinates).

Sample MS-5 (Figure 14a) is a chlorite-muscovite phyllite of the Mineral Bluff Group. The sample is characterized by fine-grained muscovite and chlorite that define an early-generation foliation. Quartz grains consist of recrystallized and strained-host grains. Late-stage deformation has sheared the foliation. Sample MS-6 (Figure 14b) is a chlorite-muscovite phyllite of the Mineral Bluff Group. An early foliation, rich in quartz and chlorite, is deformed and rotated by a later formed foliation, defined by fine-grained muscovite. The quartz grains consist of recrystallized and older-strained grains. Sample

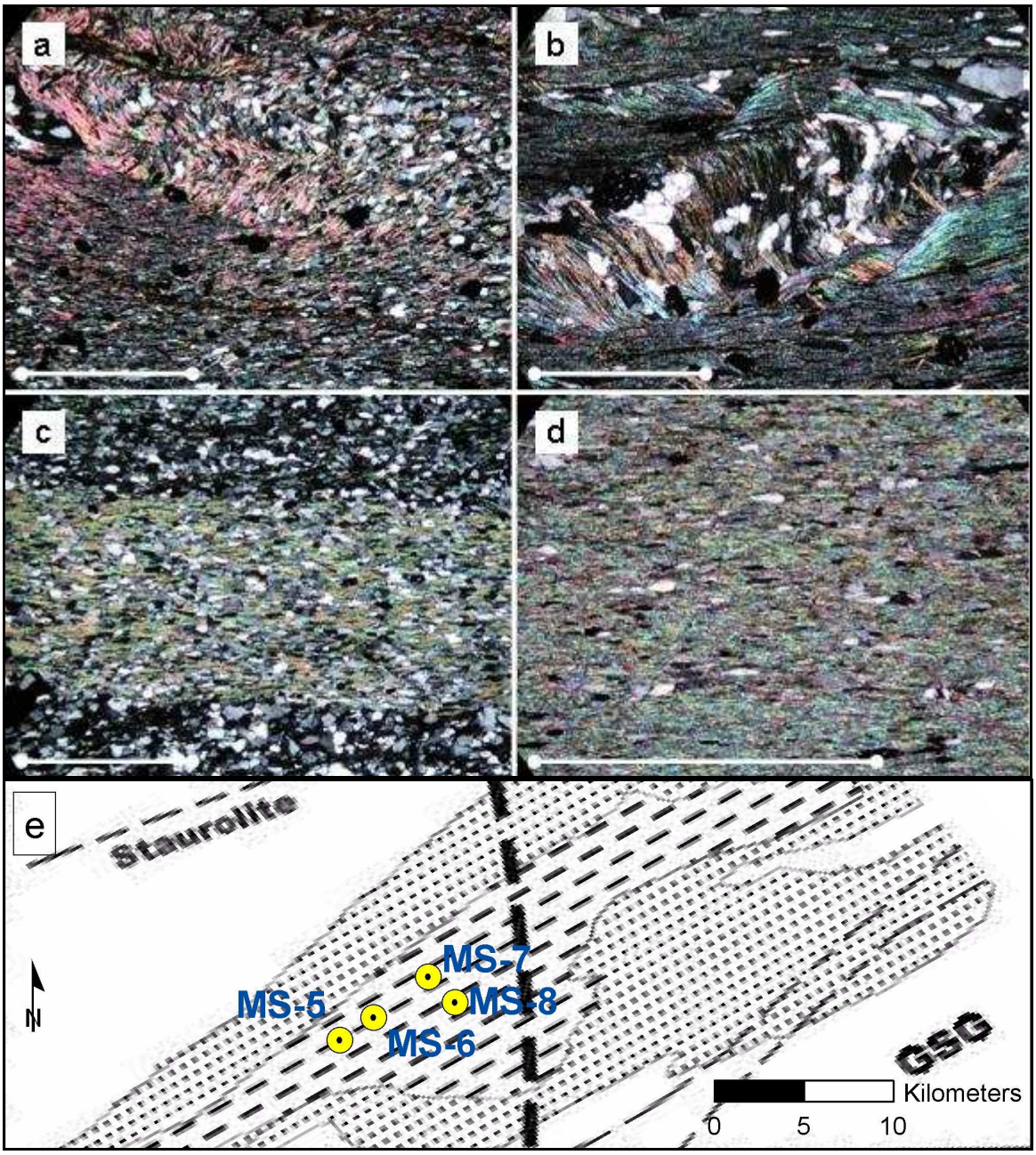

Figure 14: Photomicrographs of metamorphic textures in rocks from the Murphy synclinorium (scale bars = 1.0 mm; cross-polarized light). (a) Sample MS-5, chlorite-muscovite phyllite. Sample characterized by an early-generation planar fabric defined by muscovite sheared by late-stage deformation. (b) Sample MS-6, chlorite-muscovite phyllite. Sample characterized by an early-generation, quartz-rich, fabric rotated by a late-generation, mica-rich, fabric. (c) Sample MS-7, chlorite-muscovite phyllite or slate. Sample characterized by undeformed and fine-grained muscovite laths that define a single cleavage. (d) Sample MS-8, chlorite muscovite slate. Sample characterized by a continuous foliation defined by very finely-grained muscovite and elongated quartz grains. (e) Map of sample localities (adapted from Tull and Holm, 2005).

MS-7 (Figure 14c) is a chlorite-muscovite phyllite of the Mineral Bluff Group. The sample has a single continuous cleavage (phyllitic or slaty) defined by undeformed and fine-grained muscovite laths. The general lack of microstructural evidence for intracrystalline strain in quartz indicates annealing. Sample MS-8 (Figure 14d) is a chlorite-muscovite slate of the Mineral Bluff Group. The sample is characterized by very-fine grained muscovite and elongated quartz grains that define a continuous slaty cleavage. This sample also lacks evidence for intracrystalline strain.

$^{40}Ar/^{39}Ar$ ANALYSIS

BASIS OF THE METHOD

Argon is a noble gas that occurs naturally throughout the atmosphere and potassium is a common element in rock-forming minerals. Several isotopes of these elements pertain to the K/Ar method and $^{40}Ar/^{39}Ar$ technique (Figure 15). ^{40}Ar occurs naturally and is produced by a radioactive-decay branch of ^{40}K, due to electron-capture and positron-emission pathways (Faure, 1986). ^{39}Ar is produced entirely by the decay of ^{39}K and ^{42}Ca, ^{38}Ar occurs naturally and is produced by the radioactive decay of ^{38}Cl, ^{37}Ar is produced entirely by the radioactive decay of ^{40}Ca, and ^{36}Ar occurs naturally and is produced by the radioactive decay of ^{40}Ca (Dickin; 1995). The naturally occurring $^{40}Ar/^{36}Ar$ ratio in the atmosphere is 295.5, enabling the correction for atmospheric ^{40}Ar (Faure, 1986).

The K/Ar method has conventionally been used to date K bearing minerals. Two separate aliquots of ^{40}K and radiogenic ^{40}Ar are measured quantitatively, $^{40}Ar^{*}$ in an inert-gas mass spectrometer and ^{40}K by flame photometry or one of several chemical methods. The fundamental-age equation (as derived in Dalrymple & Lanphere, 1969) is

$$t = (1/\lambda) \ln (^{40}Ar^{*}/ {}^{40}K+1).$$

The decay constant (λ) for $^{40}K \rightarrow {}^{40}Ar$ (as described in McDougall & Harrison, 1999) is $5.543*10^{-10}$/year.

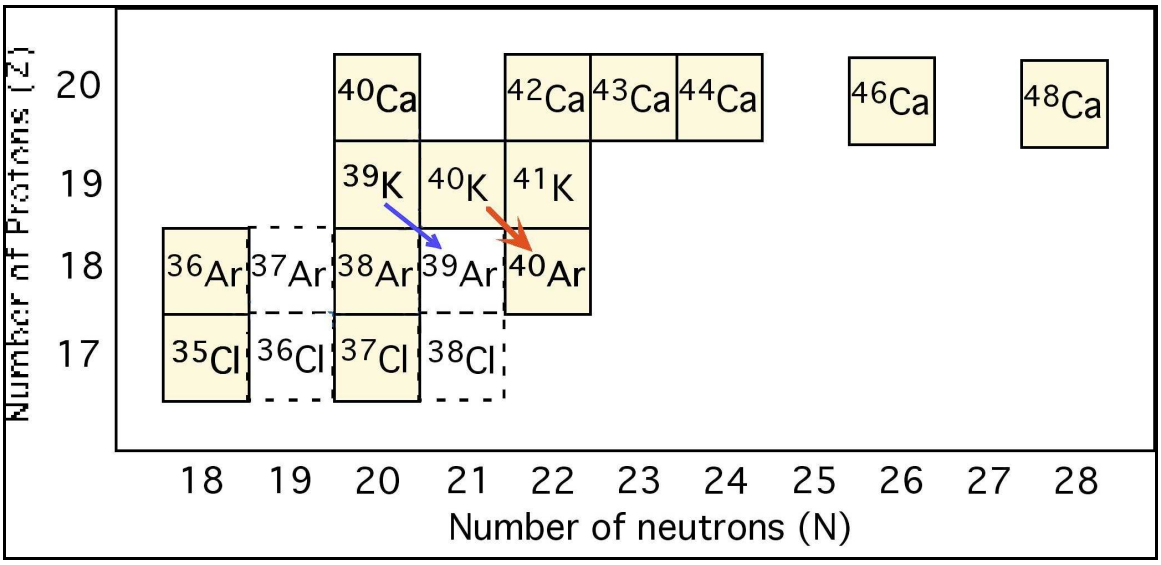

Figure 15: Decay scheme and isotopes relevant to the $^{40}Ar/^{39}Ar$ method. Symbols filled with yellow signify naturally-occurring isotopes. Red arrow signifies the $^{40}K \rightarrow ^{40}Ar^{*}$ decay reaction that occurs in nature. The blue arrow signifies the $^{39}K(n,p)^{39}Ar_K$ reaction that occurs in a nuclear reactor and enables the $^{40}Ar/^{39}Ar$ method.

$^{40}Ar/^{39}Ar$ DATING TECHNIQUES

The $^{40}Ar/^{39}Ar$ technique is a variation of K/Ar. Based on the assumption that the $^{39}K/^{40}K$ ratio is constant in nature and $^{39}Ar_K$ is dependent upon the ^{39}K in the sample, $^{40}Ar^{*}/^{39}Ar_K$ is proportional to $^{40}K/^{40}Ar^{*}$ and $^{39}Ar_K$ can be substituted for ^{40}K (McDougall & Harrison, 1999). The age equation (as discussed in McDougall and Harrison, 1999) is:

$$t = (1/\lambda)\ln(^{40}Ar^{*}/^{39}Ar_K(J)+1).$$

$^{40}Ar^{*}$ is the fraction of ^{40}Ar produced by radioactive decay. $^{39}Ar_K$ is the ^{39}Ar produced through neutron-capture, proton-emission reactions by bombardment with fast, high energy neutrons in a nuclear reactor (Merrihue and Turner, 1966). Determination of the production factor (J; as discussed in Dalrymple et al., 1981) for the $^{39}K \rightarrow ^{39}Ar$ reaction, in the mineral sample and corresponding monitor of known age, during irradiation is

$$J = e^{\lambda t}\text{-}1*1/(^{40}Ar/^{39}Ar).$$

The $^{40}Ar/^{39}Ar$ technique permits precise age determinations on smaller sample sizes (such as single crystals) and allows for simpler data acquisition, as the isotopic ratio data are collected with a single measurement instead of quantitatively analyzing two separate aliquots. This reduces the standard error and lab time for radiometric analysis relative to K/Ar.

The closure temperature (see Petrography section) for any mineral is variable and heavily dependant upon cooling rate and grain size. The cooling of geologic temperature through time (Figure 16a) influences the closure temperature for muscovite. A low cooling rate favors a cooler closure temperature and a high cooling rate favors a higher closure temperature. This influences the ratio of $^{40}Ar/^{40}K$ through geologic time (Figure 16b). Before the closure temperature is reached there is no retention of daughter (^{40}Ar) atoms. Cooling through an interval of partial retention of daughter atoms (the "closure interval"; Dodson, 1973) is shorter for fast cooling rates and longer for slow cooling rates. After muscovite cools through its closure temperature there is complete retention of daughter atoms within the crystal lattice (Giletti; 1972). The grain size of micas also influences the closure temperature (Hames and Bowring, 1994). A smaller muscovite-grain size favors a cooler closure temperature due to the short diffusion dimension and a larger grain size favors a hotter closure temperature due to its longer diffusion dimension. These variables must be considered for reliable interpretation of radiogenic data. In this study the cooling rate of geologic temperature is assumed to be 5˚C/m.y. and the grain size varies between 0.1mm to 0.5 mm (Figure 17). Given the grain size variation, the range of closure temperatures may have varied by as much as 50˚C. Given the 5˚C/m.y. cooling rate, the timing of the retention of argon may have a 10 m.y. variation.

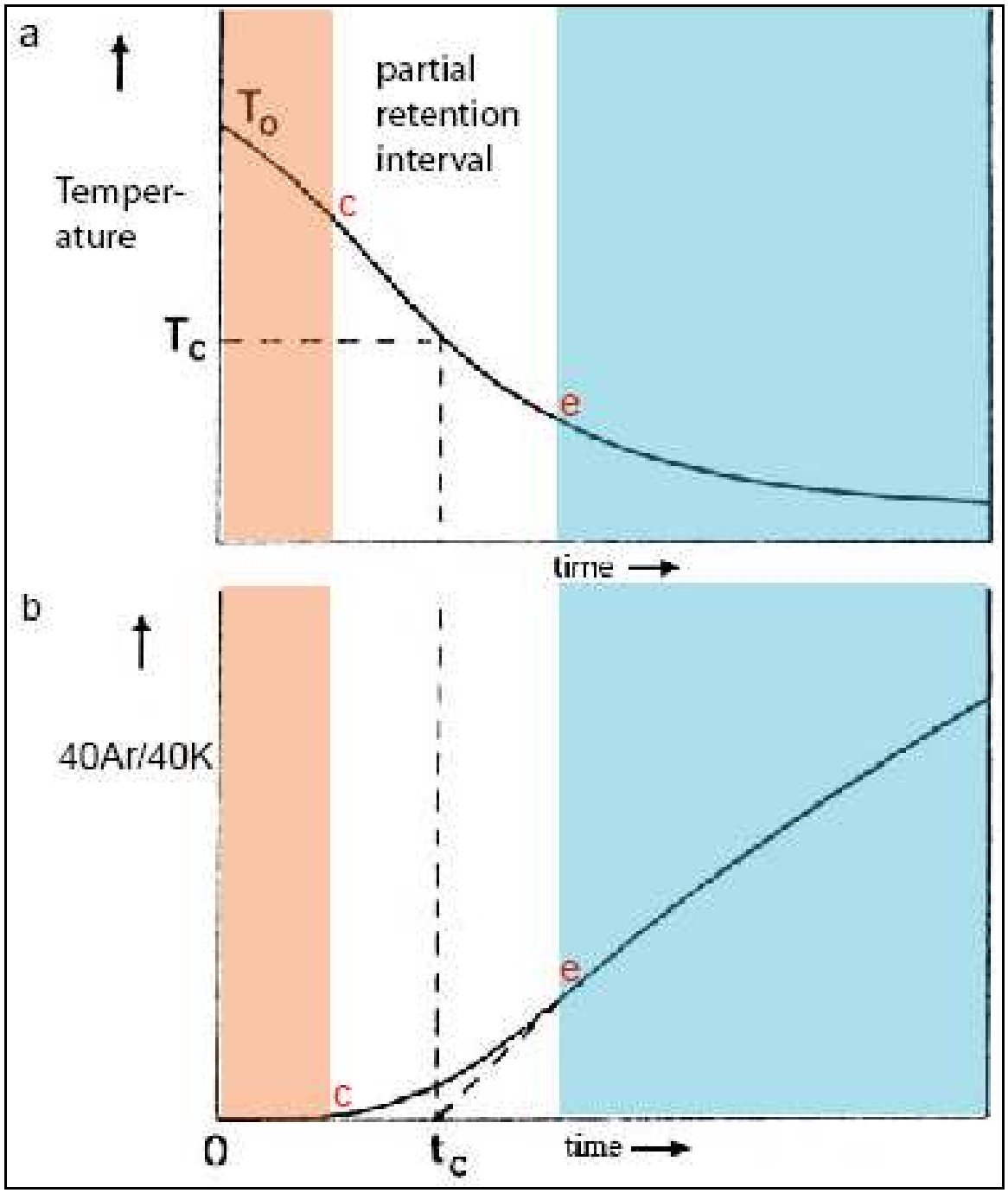

Figure 16: Idealized closure-temperature concept (figure adapted from Dodson, 1973): T_o = initial temperature, T_c = closure temperature, c = argon retention at diffusion-domain centers (crystal cores), e = argon retention throughout diffusion domains; a) Plots geologic temperature against geologic-cooling history (time). b) Plots the daughter/parent ratio ($^{40}Ar/^{40}K$) against geologic time.

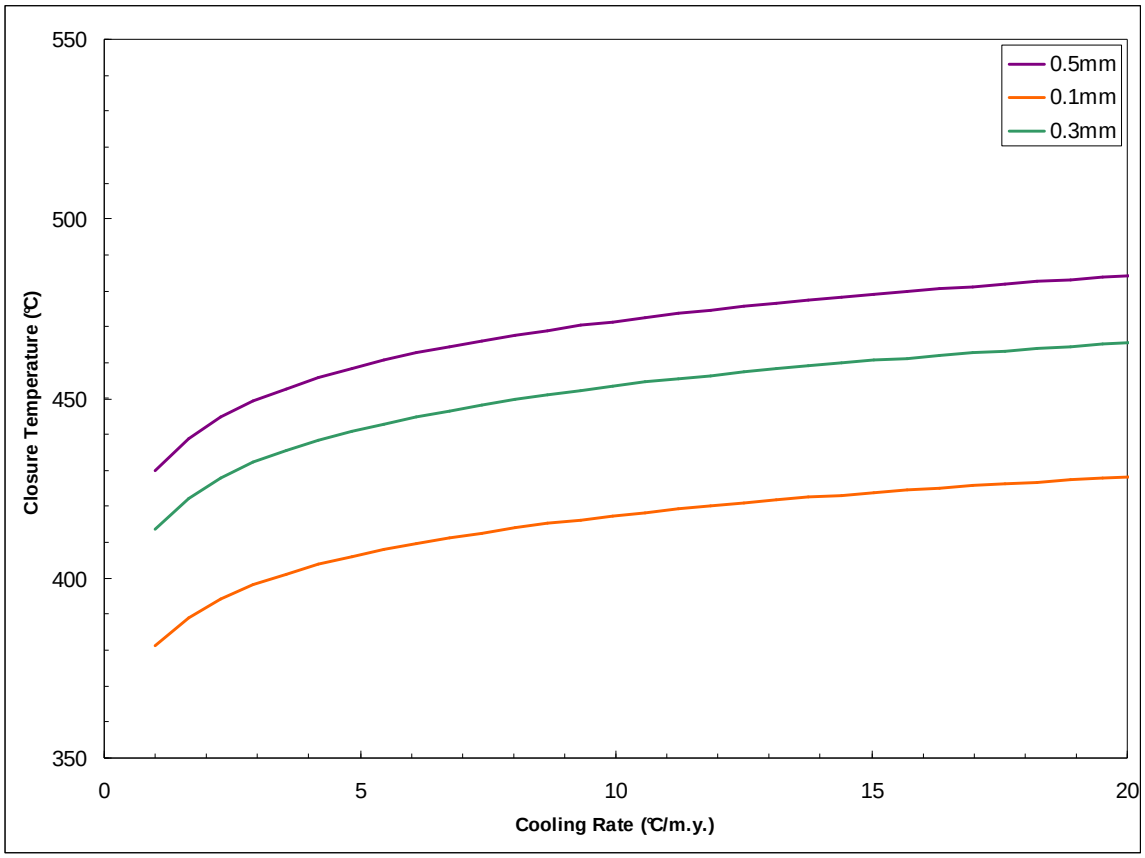

Figure 17: Closure temperature for muscovite grain sizes in this study as a function of geologic-cooling rate (calculated with the model of Dodson, 1973, with muscovite-diffusion parameters from Hames and Bowring, 1994).

ANALYTICAL METHODS

Samples were selected on the basis of structural setting and petrography. Low-grade metamorphic rocks containing muscovite were collected from the Cartersville transverse zone, the Blue Ridge thrust region, and a transect from the Ducktown anticlinorium into the Murphy synclinorium (refer to Table 2). The samples were gently crushed with mortar and pestle, separated into size fractions using standard test sieves, and examined under binocular microscope. Approximately 50 grains of muscovite and biotite (if present) were picked from each sample, immersed in ethanol and stored in centrifuge vials. The mica grains were packaged in aluminum foil along with aliquots of a monitor mineral (Fish Canyon Sanadine; ca. 28.04 Ma; Renne et al, 1998). The sample package was sent to the McMaster University nuclear reactor in Hamilton, Ontario for neutron irradiation.

The mica grains and monitors were analyzed at the Auburn Noble Isotope Mass Analysis Laboratory (ANIMAL; Figures 18 and 19), a facility under the direction of Dr. Hames of the Auburn University Department of Geology and Geography. The lab is set up for single crystal, isotopic analysis utilizing the $^{40}Ar/^{39}Ar$ technique and provides enhanced sensitivity and resolution relative to labs that use bulk sample methods. Single crystals of a single mineral were analyzed individually. This minimizes effects due to extraneous argon and heterogeneous-mineral assemblages inherent to multigrain analysis.

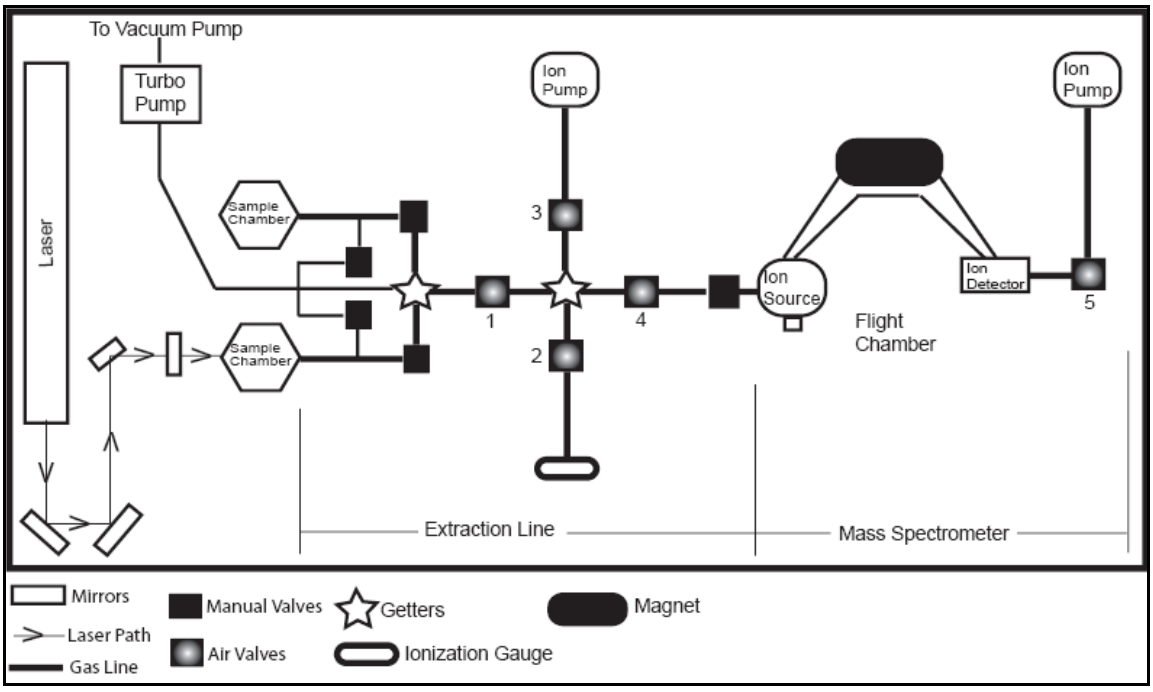

Figure 18: Schematic diagram of the lab apparatus in the Auburn Noble Isotope Mass Analysis Laboratory (ANIMAL facility).

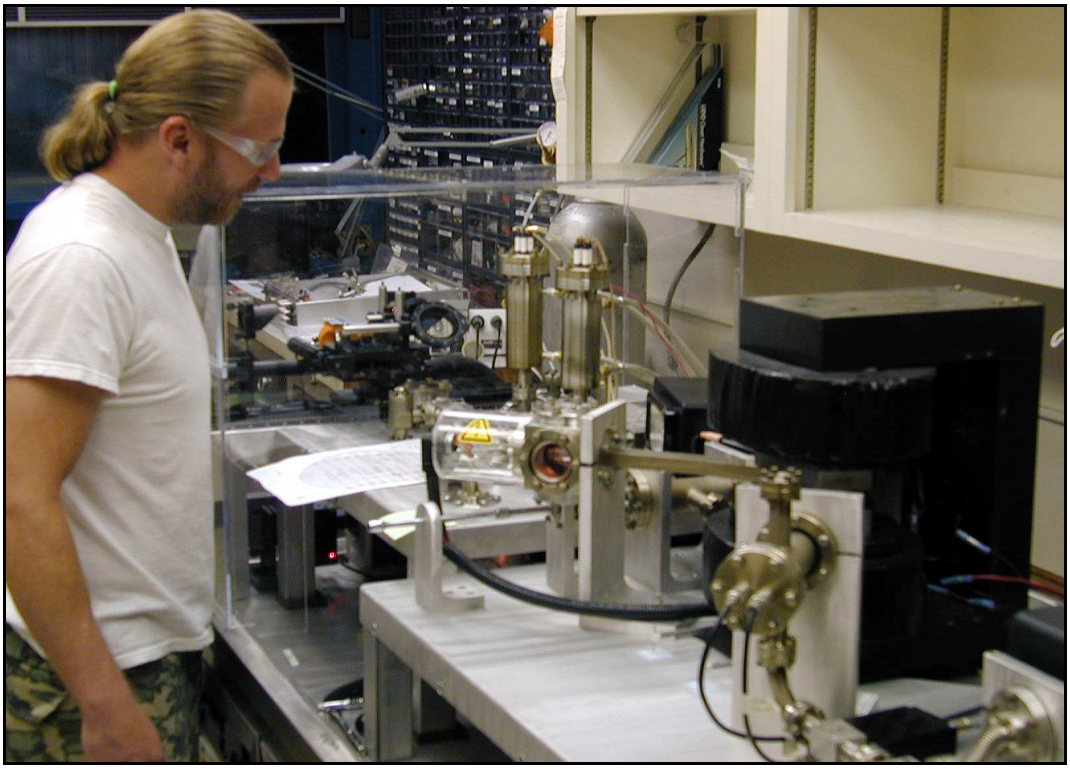

Figure 19: The author analyzing samples in the Auburn Noble Isotope Mass Analysis Laboratory (ANIMAL facility).

The laboratory is equipped with an ultra-high vacuum, 90-degree sector, 10-cm radius spectrometer optimized for single-crystal $^{40}Ar/^{39}Ar$ research. The spectrometer employs second-order focusing (Cross, 1951), and is fitted with a high sensitivity electron-impact source and a single ETP electron multiplier (with signal amplification through a standard pre-amplifier). The total volume of the spectrometer is 400 cc. Resolution in the instrument (with fixed slits for the source and detector) is constrained to ~150. The high sensitivity and low blank of the instrument permits measurement of 10^{-14} mole samples to within 0.3% precision. The extraction line is fitted with a 50W Synrad CO_2 IR laser for heating and fusing silicate minerals and glasses. The sample chamber uses a Cu planchet, KBr cover slips, and low-blank UHV ZnS window (manufactured at Auburn University and based on the design of Cox et al., 2003). The laser system is suitable for fusion analysis of single crystals as employed in this study. The laser beam delivery system utilizes movable optical mounts and a fixed sample chamber to further minimize volume and improve conductance of the extraction line. The extraction line for this system is fully computer automated and utilizes a combination of Varian and Nupro pneumatic valves, and Varian turbomolecular and ion pumps. Residual and sample reactive gases are pumped out of the line through use of SAES AP-10 non-evaporable getters. Pressures in the spectrometer and extraction line are routinely below ~$5x10^{-9}$ torr, as measured with an ionization gauge. An automated pipette delivers standard aliquots for use in measuring sensitivity and mass fractionation. The time required to inlet or equilibrate a 'half-split' of a sample is less than 7 seconds, and the inlet time for a full sample is 20 seconds. Typical blanks for the entire system (4 minute gettering time, while running sanidine monitor minerals) in May of 2006 are as follows (in moles): ^{40}Ar,

$2.1x10^{-16}$; ^{39}Ar, $1.6x10^{-17}$; ^{38}Ar, $3.2x10^{-18}$; ^{37}Ar, $2.6x10^{-18}$; ^{36}Ar, $1.7x10^{-18}$. Computer control of the laser, laser optics, extraction line, mass spectrometer, and data recording is enabled with National Instruments hardware and the Labview programming environment. Initial data reduction is accomplished through an in-house Excel spreadsheet, with final reduction using Isoplot (Ludwig, 2003).

$^{40}Ar/^{39}Ar$ isotopic analyses of the irradiated samples were performed to determine their cooling-crystallization ages. The mica grains were individually arranged in a copper planchet and placed in a vacuum sealed chamber. To determine the background levels of gas in the system, blanks were run before sample analyses and after every fifth sample. Air analyses were run daily to confirm the mass spectrometer yields the $^{40}Ar/^{36}Ar$ ratio of 295.5. Argon was extracted from the mica grains by fusing individual crystals with single laser shots. Hydrocarbon contaminants or other active gases that may have been present were removed by gettering the gas. The gas samples were then passed through the ion source and analyzed in the gas mass spectrometer, measuring the individual voltage for ^{36}Ar, ^{37}Ar, ^{38}Ar, ^{39}Ar, and ^{40}Ar. The argon isotopic ratio data was then reduced; corrections were made for background gases and interfering isotopes and ages were calculated for the $^{40}Ar^*/^{39}Ar_K$ ratios along with corresponding standard error and deviation (as discussed in McDougall and Harrison, 1999).

ANALYTICAL RESULTS

Radiometric age determinations included the systematic laser analysis of single muscovite crystals. The data are reported as the mean and standard error at the 68% confidence level (±1s) of approximately ten analyses for each sample or as a range of single-crystal ages (Table 2). Resulting $^{40}Ar/^{39}Ar$ single-crystal ages vary from 307.1±8.5 Ma to 667.0±3.9 Ma, the younger samples having single mode distributions and the older samples having multiple modes. Younger ages are recorded in muscovite from the Cartersville-thrust region and to the north are represented as younger modes in a more complex record. The oldest ages are recorded for muscovite proximal to the Great Smoky fault, with no single-crystal ages younger than 355 Ma. The overall pattern is a predominance of ages close to 330 Ma for the southern (Cartersville) portion of the Talladega belt-western Blue Ridge, significantly older ages to the north along the Great Smoky fault varying from 355 - 667 Ma (possibly influenced by extraneous argon or a relict/detrital component), and ages varying between 328-465 Ma from along the Ducktown-Murphy transect. The radiometric data will first be discussed for the twelve samples from the Cartersville transverse zone, then for the eleven samples from along the Great Smoky fault, and then west to east for the nine samples across the Ducktown and Murphy structures.

Table 2: $^{40}Ar/^{39}Ar$ data for western Blue Ridge muscovite (SCTF is Single Crystal Total Fusion; n is number of analyses; * Ages (Ma) quoted as a mean at 1σ or as a range).

Study Area	Sample	Quad	Tectonostratigraphic Unit	Longitude	Latitude	Dating Method	n	Age *
Cartersville Transverse Zone	CV-1	Acworth	Wilhite Formation (Walden Creek Group)	-84.746	34.108	SCTF	9	328.6 ± 1.6
	CV-2	Burnt Hickory Ridge	Otto Formation (Muscovite Schist)	-84.769	34.080	SCTF	10	321.7 ± 0.6
	CV-3		Dean Formation (Great Smoky Group)	-84.769	34.092	SCTF	10	322.8 ± 2.0
	CV-4		Lay Dam Formation	-84.847	34.058	SCTF	10	329.0 ± 0.6
	CV-5a			-84.852	34.060	SCTF	9	331.7 ± 1.6
	CV-5b					SCTF	8	330.6 ± 1.4
	CV-6			-84.869	34.075	SCTF	10	322.1 ± 0.8
	CV-7a	Taylorsville		-84.912	34.027	SCTF	10	335.5 ± 0.8
	CV-8a			-84.905	34.048	SCTF	10	331.1 ± 1.1
	CV-8b					SCTF	8	322 - 341
	CV-9	Acworth	Great Smoky Group (undivided)	-84.716	34.115	SCTF	10	321.4 ± 0.3
	CV-10a	Allatoona Dam	Wilhite Formation (Walden Creek Group)	-84.692	34.142	SCTF	9	329.6 ± 0.8
Great Smoky Fault	WM-1a	Waleska	Upper Anakeesta / Wehutty Formations (Great Smoky Group)	-84.561	34.325	SCTF	9	337.6 ± 0.5
	WM 2	White East	Wilhite Formation (Walden Creek Group)	-84.643	34.344	SCTF	10	315.5 ± 0.5
	WM-3	Fairmount	Pinelog Formation (Snowbird Group)	-84.678	34.454	SCTF	10	325 - 345
	WM-4			-84.684	34.454	SCTF	10	334 - 370
	WM-5			-84.681	34.454	SCTF	10	328.6 ± 1.1
	WM-6	Ludville	Upper Anakeesta / Wehutty Formations (Great Smoky Group)	-84.616	34.463	SCTF	10	351.1 ± 1.7
	WM-7a	Talking Rock	Great Smoky Group (undivided)	-84.587	34.546	SCTF	10	338.6 ± 0.7
	WM-9a	Oakman	Ammons Formation (Great Smoky Group)	-84.677	34.615	SCTF	10	355 - 367
	WM-9b					SCTF	10	361 - 480
	WM-9c					SCTF	10	379 - 667
	WM-10	Crandall	Pinelog Formation (Snowbird Group)	-84.730	34.755	SCTF	10	378 - 391
Ducktown-Murphy Transect	BB-1	Ducktown	Copperhill Formation (Great Smoky Group)	-84.380	35.036	SCTF	10	330 - 371
	BB-2					SCTF	10	342 - 381
	MS-2	Isabella		-84.317	35.022	SCTF	9	339.0 ± 0.8
	MS-3		Upper Anakeesta / Wehutty Formations (Great Smoky Group)	-84.284	35.015	SCTF	9	336 - 408
	MS-4b	Persimmon Creek	Ammons Formation (Great Smoky Group)	-84.249	35.021	SCTF	10	336 - 463
	MS-5	Murphy	Mineral Bluff Formation / Nottely Quartzite (Murphy Belt Group)	-84.062	35.063	SCTF	10	334 - 465
	MS-6			-84.045	35.074	SCTF	10	334.7 ± 0.6
	MS-7			-84.018	35.095	SCTF	10	328 - 387
	MS-8			-84.004	35.082	SCTF	9	332.5 ± 0.5

CARTERSVILLE TRANSVERSE ZONE

Laser $^{40}Ar/^{39}Ar$ analysis of twelve samples from the Cartersville-thrust region (Figure 20 and Appendix 2) yield single crystal total fusion ages with means that range between 321.4±4.0 Ma and 335.5±0.8 Ma. Probability distributions and isotope-correlation diagrams (Figures 21 and 22) are presented first for samples collected from the northeast extension of the Talladega Belt. Figures 23 and 24 present the results for samples collected from the zone where the Lay Dam Formation has been correlated along strike into the western Blue Ridge (Tull and Holm, 2005). In general, each sample tends to yield single-crystal ages that are normally distributed, and thus a mean age and standard error of the mean are reported for each. There is no systematic variation among mean ages for samples of the Lay Dam Formation across the Cartersville transverse zone from the Talladega belt into the western Blue Ridge.

A few samples yielded a crystal with an age significantly younger than the mean (CV8a, CV8b, CV6, and CV10). Samples CV6 and CV8a are phyllites of the Lay Dam Formation. CV8b was collected from a boudinaged quartz vein and its age is best expressed as a range (322-341 Ma; Figure 21g). Sample CV10, a schist from the Wilhite Formation, yielded one crystal with an age somewhat younger than the mean (325±1 Ma; Figure 24d). The younger single-crystal ages among these samples could correspond with crystals that had higher defect density or smaller size, and thus lower closure temperature than typical of the group.

Samples CV1 and CV5a, phyllites from the Lay Dam Formation, yielded a few single-crystal ages significantly older than the respective means (Figures 22 and 23). The older single-crystal ages among these samples could be the result of a small proportion of

older muscovite, that could be due to incorporation of detrital minerals or muscovite from an earlier episode of metamorphism.

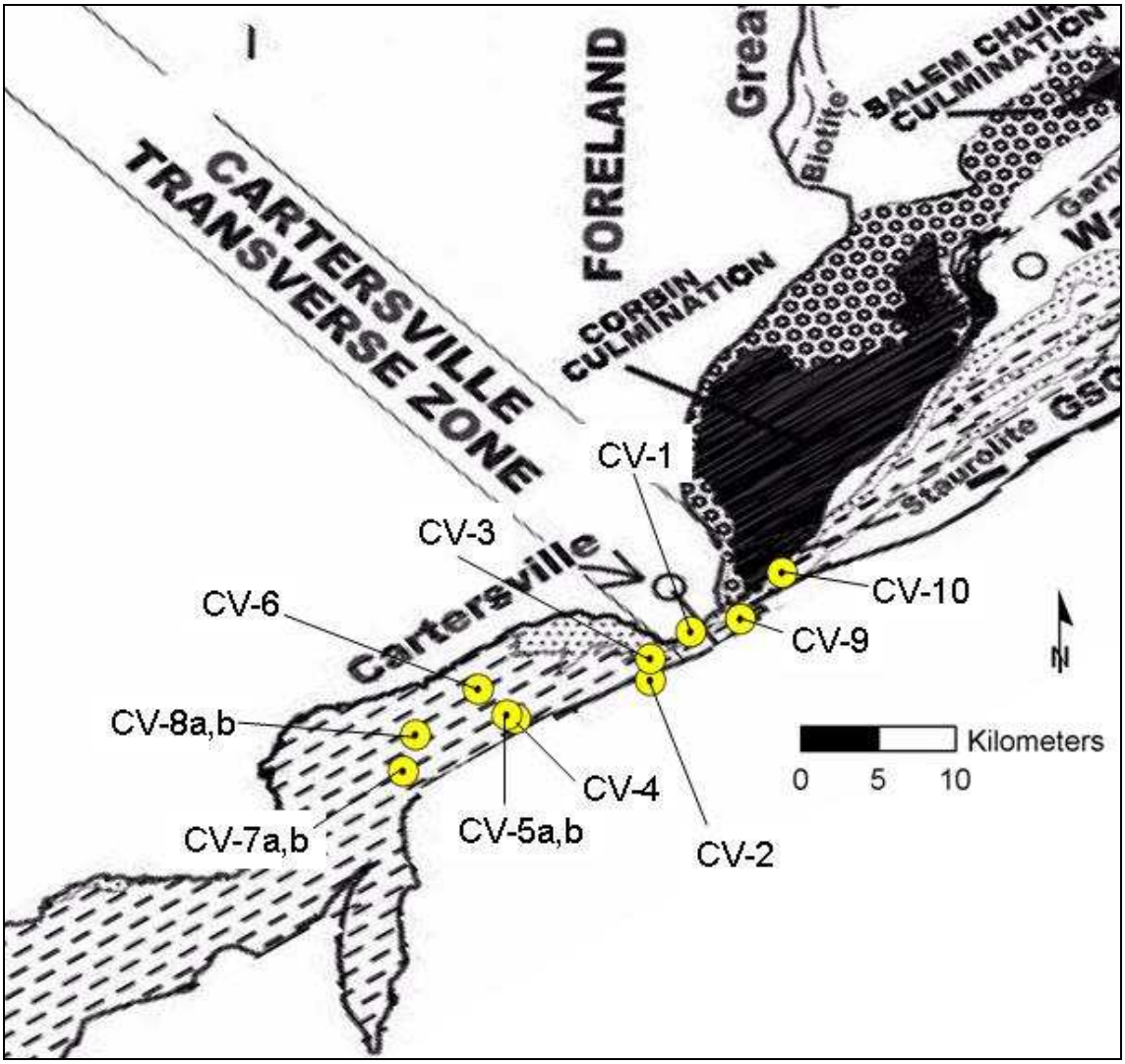

Figure 20: Geologic map of the Cartersville transverse zone and locations for samples represented in Figures 21-24 (adapted from Tull and Holm, 2005).

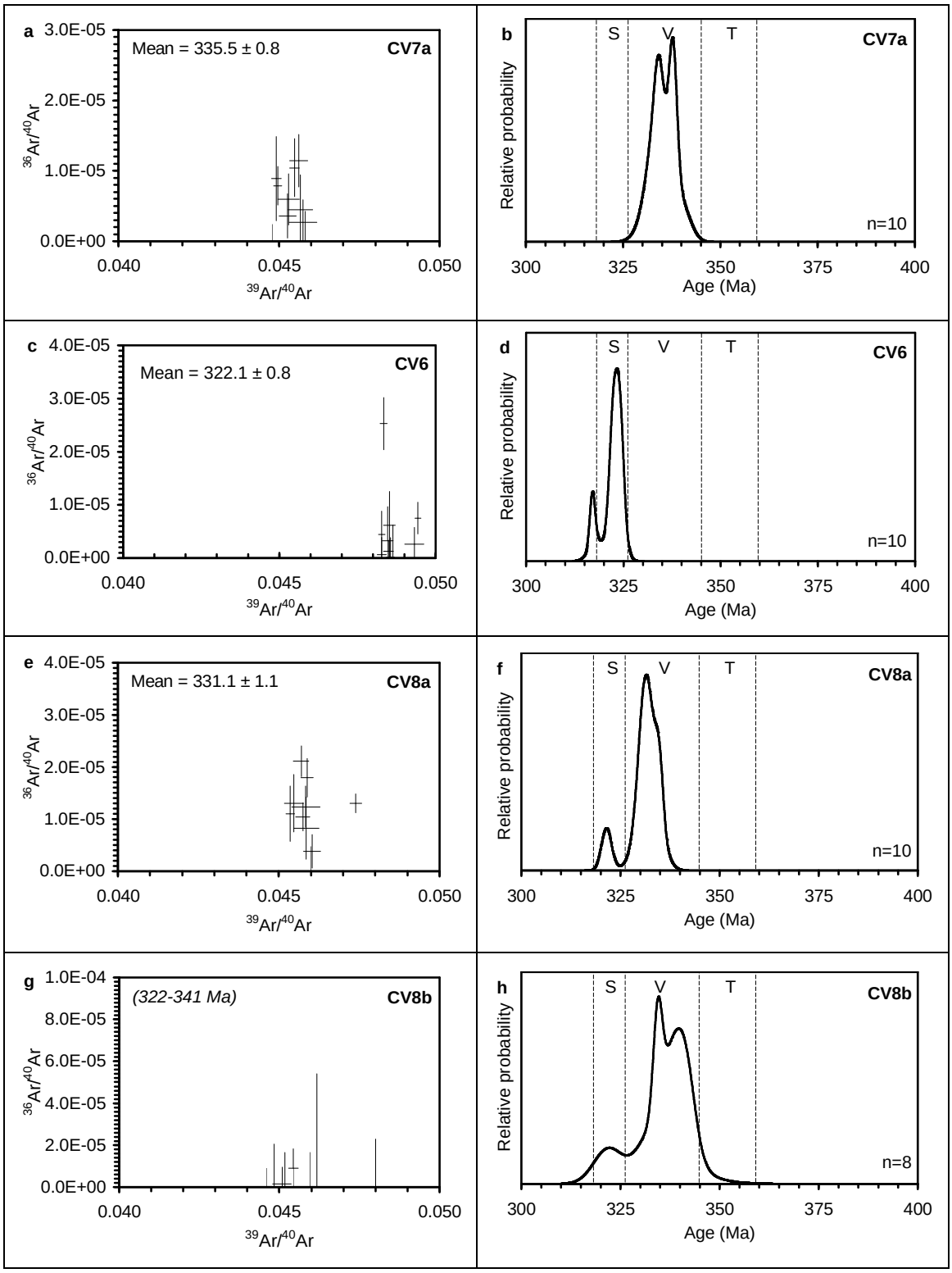

Figure 21: Inverse-isochron and age-probability plots for argon-isotopic data of Cartersville samples CV7a (a-b), CV6 (c-d), CV8a (e-f), and CV8b (g-h) (data-point error crosses are 1σ).

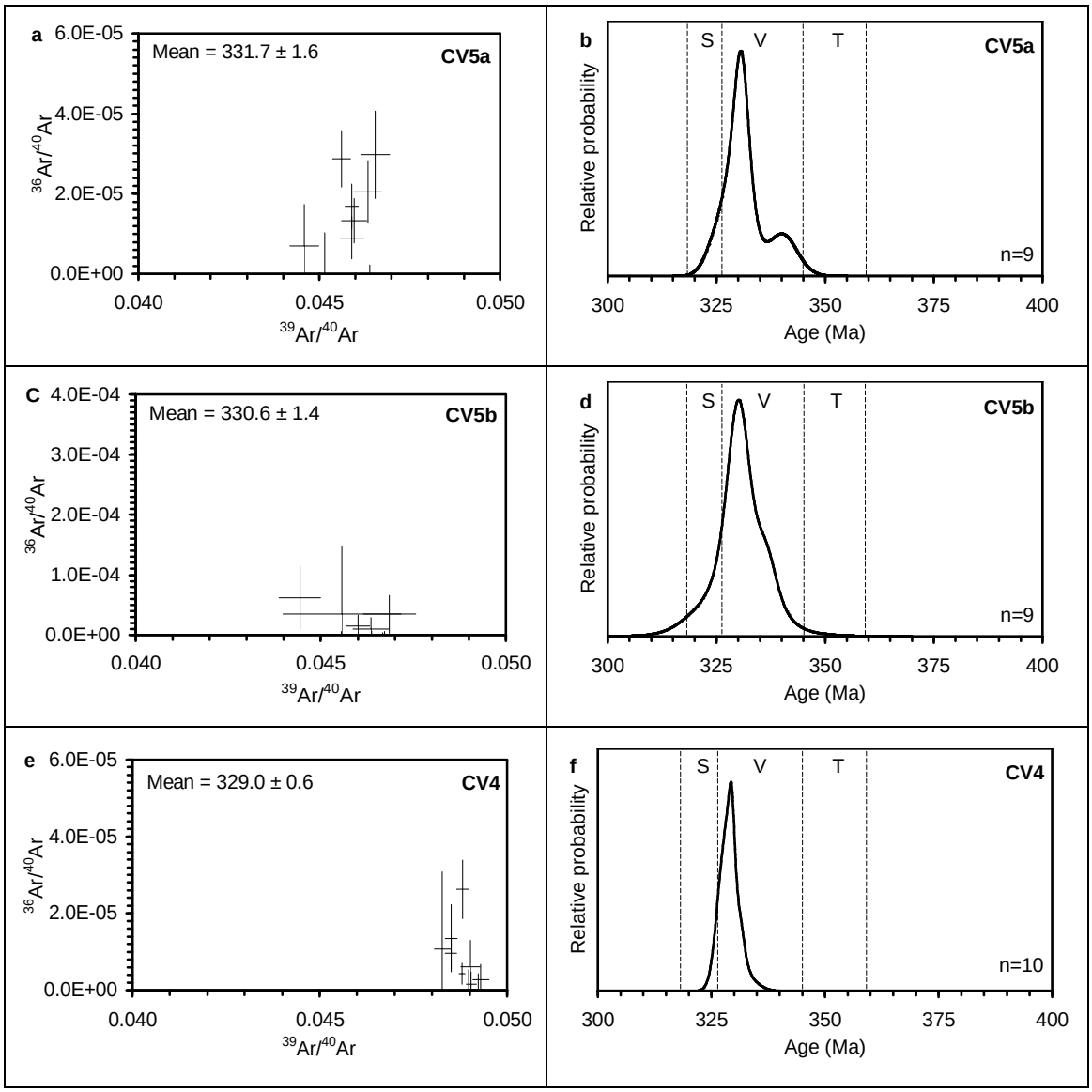

Figure 22: Inverse-isochron and age-probability plots for argon-isotopic data of Cartersville samples CV5a (a-b), CV5b (c-d), and CV4 (e-f) (data-point error crosses are 1σ).

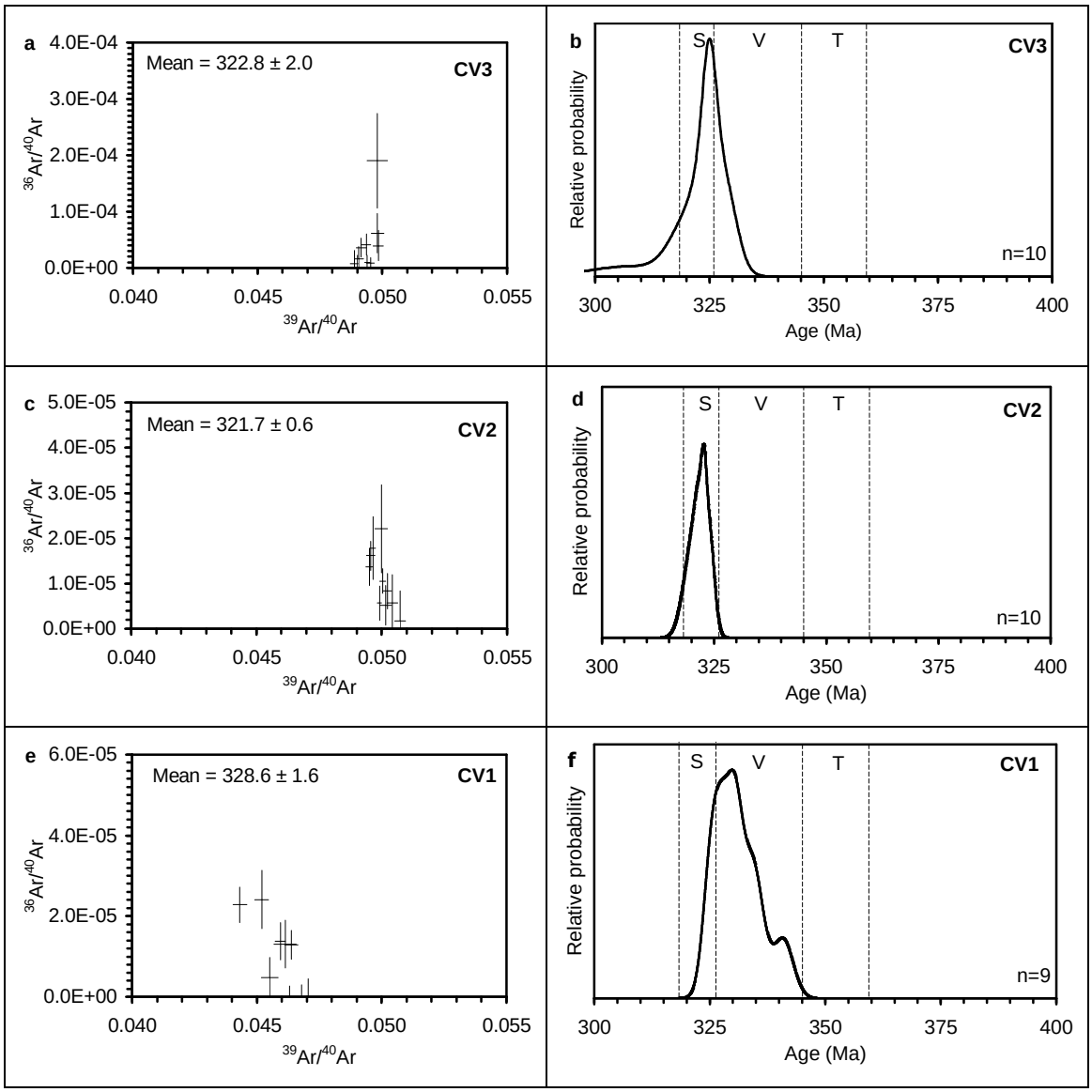

Figure 23: Inverse-isochron and age-probability plots for argon-isotopic data of Cartersville samples CV3 (a-b), CV2 (c-d), and CV1 (e-f) (data-point error crosses are 1σ).

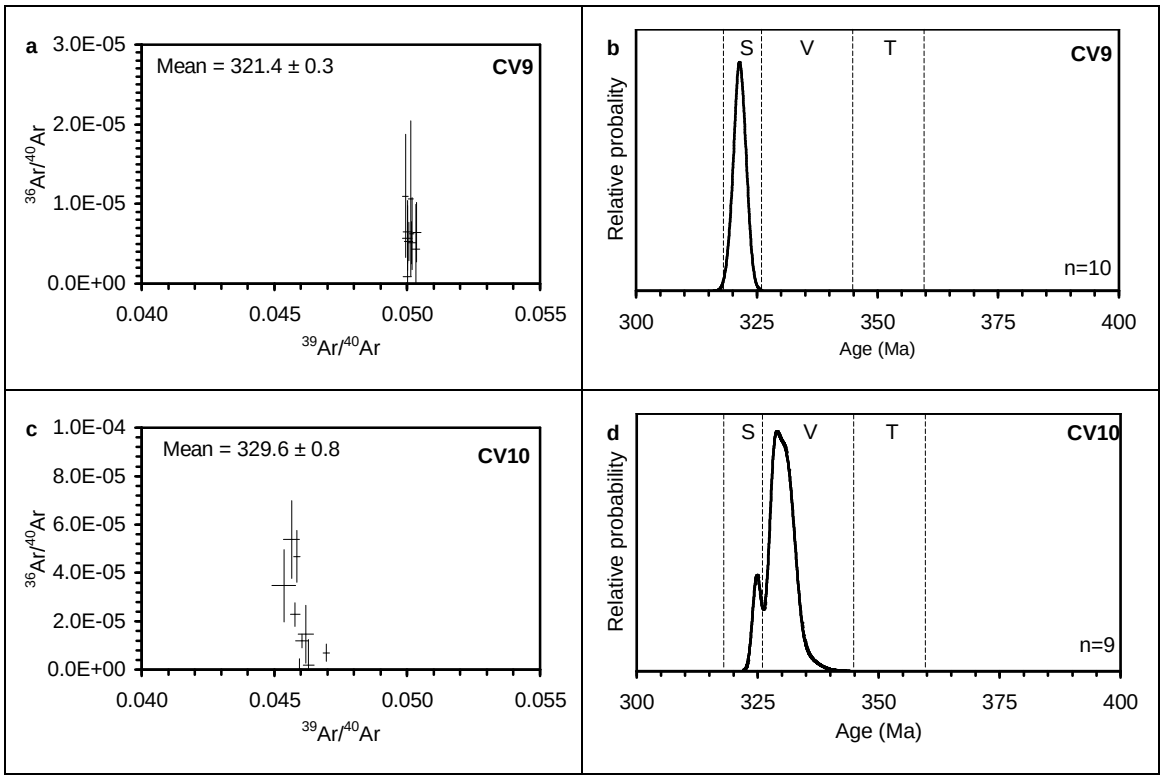

Figure 24: Inverse-isochron and age-probability plots for argon-isotopic data of Cartersville samples CV9 (a-b) and CV10 (c-d) (data-point error crosses are 1σ).

GREAT SMOKY FAULT

Seven samples collected from the vicinity of the Cartersville-Great Smoky fault in the western Blue Ridge (Figure 25 and Appendix 2) yield mean $^{40}Ar/^{39}Ar$ ages that vary between 315.5±0.5 Ma and 351.1±1.7 Ma. Five of these samples tend to yield single-crystal ages that are normally distributed, and thus a mean age and standard error of the mean are reported for each. Figures 26 and 27 present the results for samples collected from various formations of the Ocoee Supergroup, west of the Murphy synclinorium and north of the Cartersville transverse zone. Sample WM2, a phyllite of the Wilhite Formation, yielded the youngest mean age (315.5±0.5 Ma; Figure 26c) of all samples in this study and may be due to a locally-younger zone of deformation. Sample WM6, a phyllite of the Great Smoky Group, yielded a mean age of 351.1±1.7 (Figure 27c) somewhat older than other samples in this region and could be the result of slow cooling from an earlier event. Two samples yielded some crystals with a relatively complex distribution (WM3, WM4). Sample WM3 is a schist of the Pinelog Formation and its single-crystal ages are best expressed as a range from 325-345 Ma (Figure 26e). Also, sample WM4, a phyllite of the Pinelog Formation, yields ages ranging from 334-370 Ma (Figure 26g). The notably wide variation in ages among crystals in samples WM3 and WM4 could be due to polymetamorphism or perhaps the influence of detrital minerals.

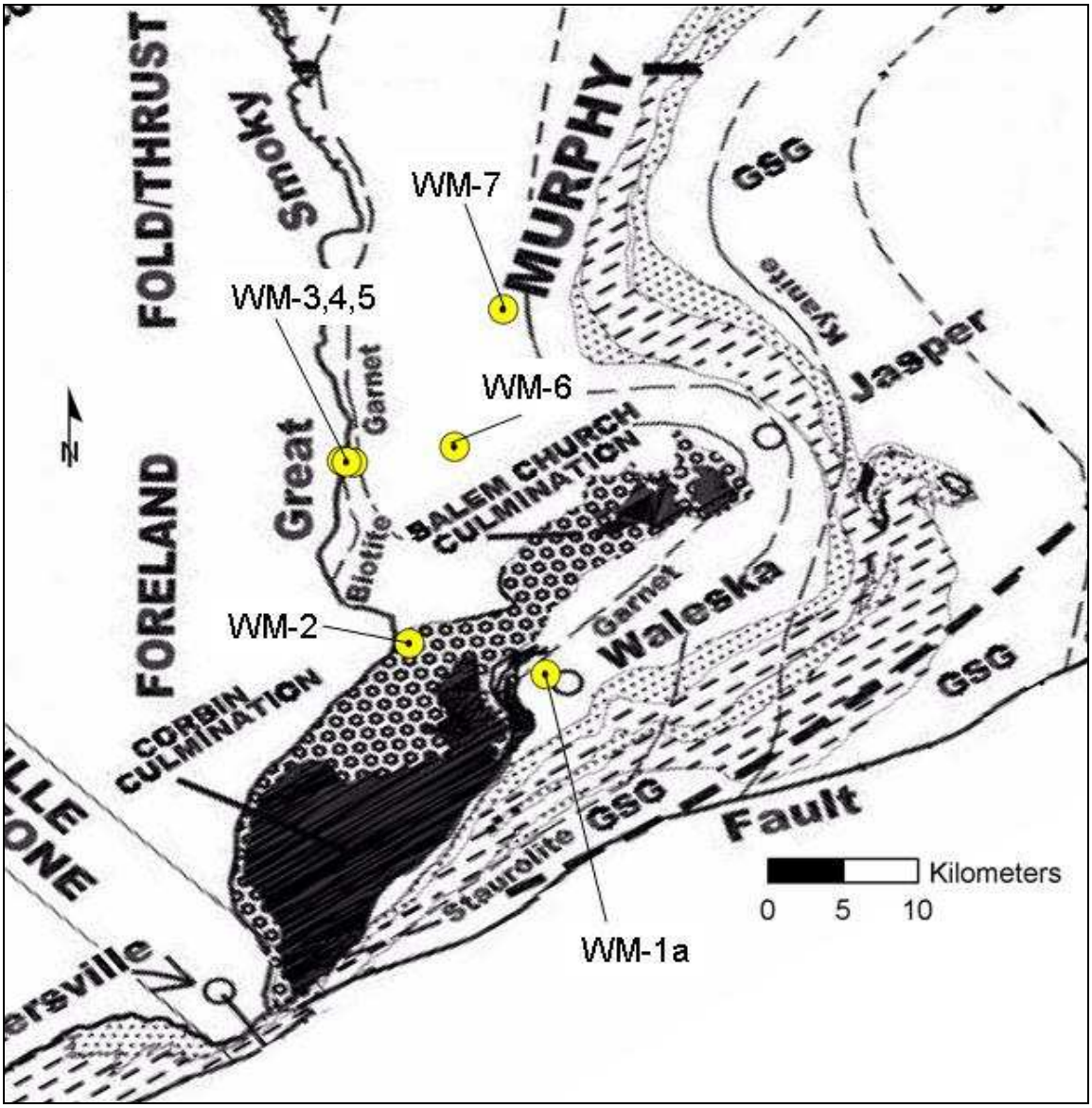

Figure 25: Geologic map of the Cartersville-Great Smoky fault and locations for samples represented in Figures 26-27 (adapted from Tull and Holm, 2005).

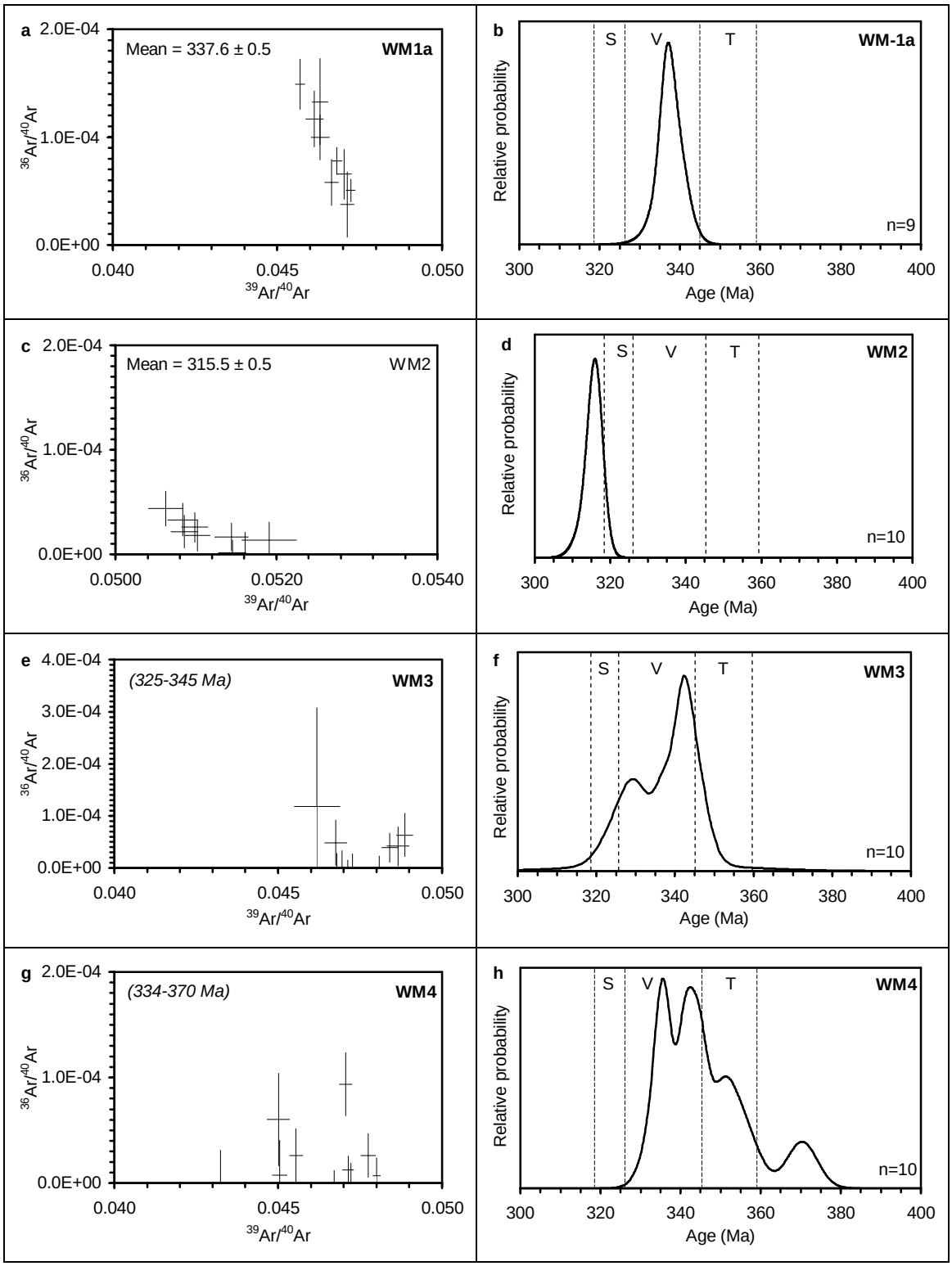

Figure 26: Inverse-isochron and age-probability plots for argon-isotopic data of Cartersville-Great Smoky fault samples WM1a (a-b), WM2 (c-d), WM3 (e-f), and WM4 (g-h) (data-point error crosses are 1σ).

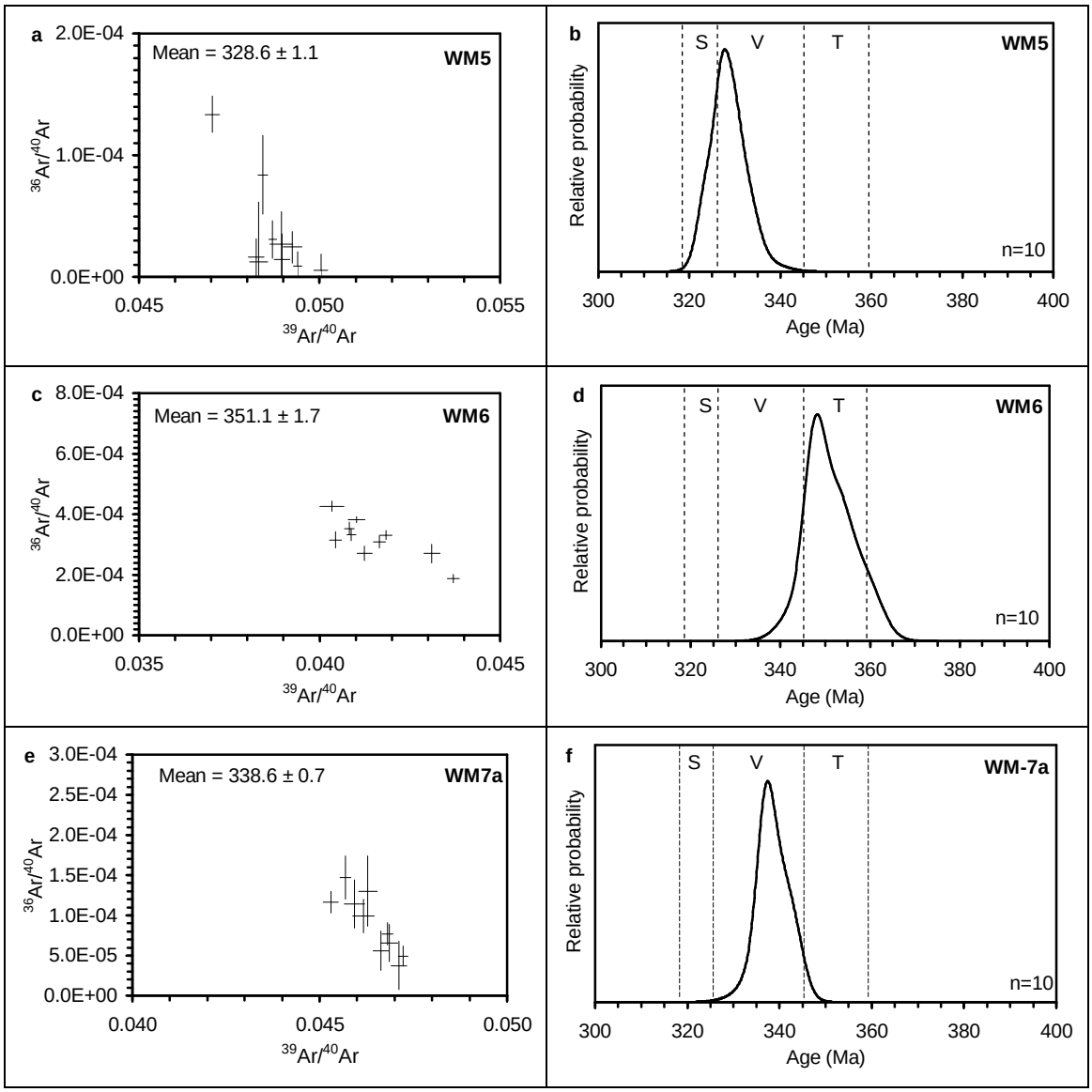

Figure 27: Inverse-isochron and age-probability plots for argon-isotopic data of Cartersville-Great Smoky fault samples WM5 (a-b), WM6 (c-d), and WM7a (e-f) (data-point error crosses are 1σ).

Farther north, four samples from the vicinity of the Cartersville-Great Smoky thrust front in the western Blue Ridge (Figures 28 and 29, and Appendix 2) yield complex distributions of single-crystal ages, and thus an age range is reported for each. The minimum ages are as young as ~355 Ma, however ages older than any plausible timing of Paleozoic metamorphism are also present. Samples WM9a, 9b, and 9c are metasiltstones from the Ammons Formation and were collected proximal to the fault (WM9c directly from the fault zone). Sample WM10 is a phyllite from the Pinelog Formation collected proximal to the Fort Mountain culmination. The age variation among the crystals in these rocks could be due to polymetamorphism, brittle deformation effects that may have introduced extraneous argon, or influence by detrital minerals.

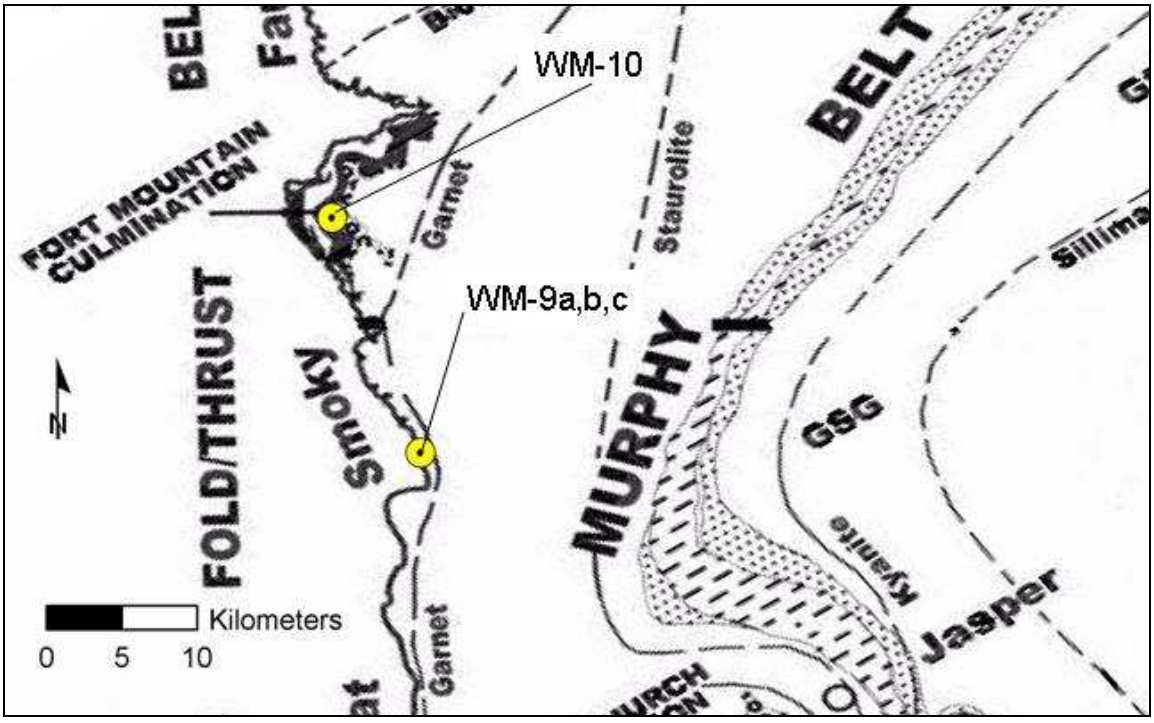

Figure 28: Geologic map of the Great Smoky fault and locations for samples represented in Figure 29 (adapted from Tull and Holm, 2005).

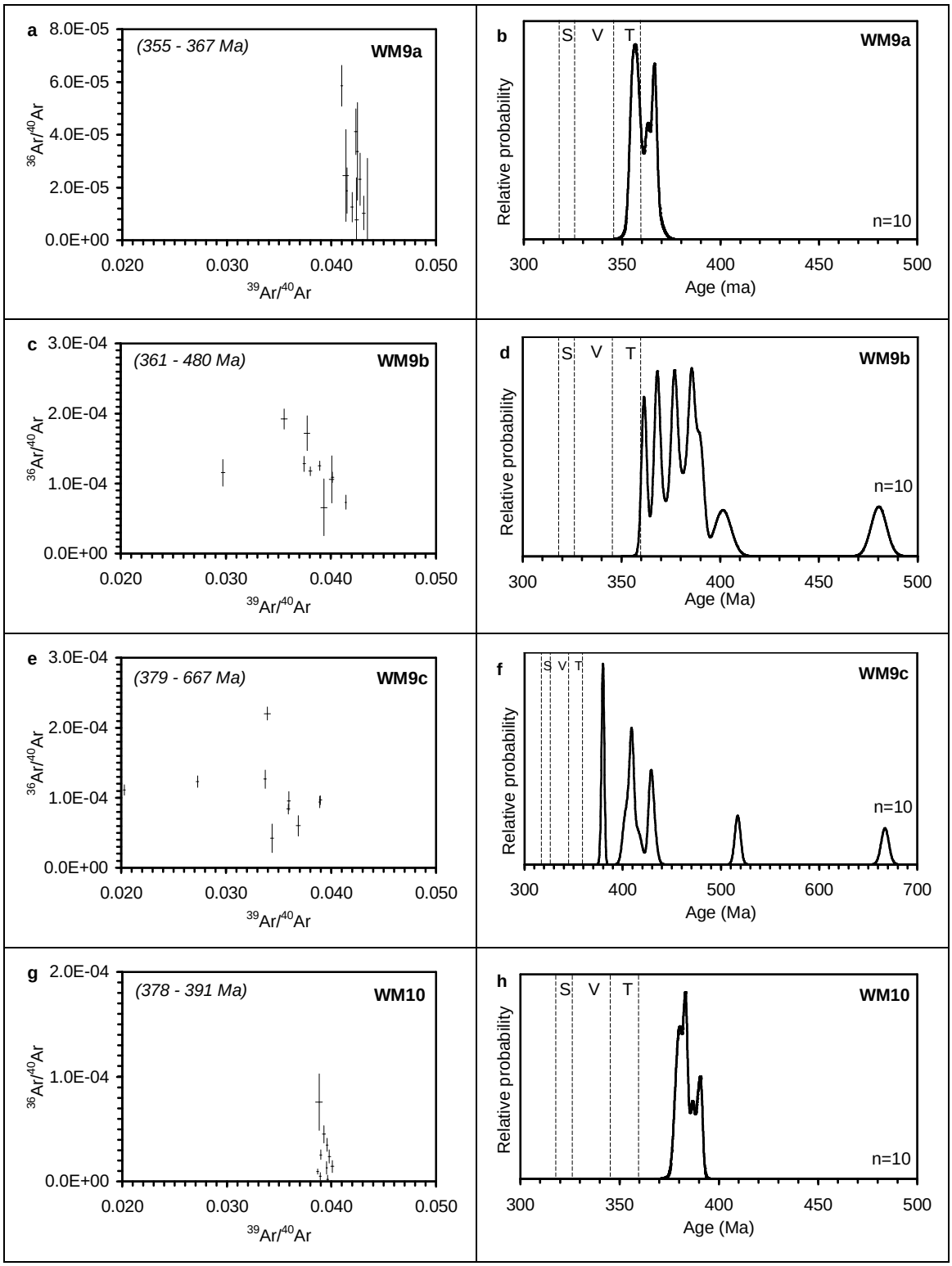

Figure 29: Inverse-isochron and age-probability plots for argon-isotopic data of Carter Lake samples WM9a (a-b), WM9b (c-d), and WM9c (e-f), and Chatsworth sample WM10 (g-h) (data-point error crosses are 1σ).

DUCKTOWN-MURPHY TRANSECT

Nine samples collected along U.S. Hwy. 64 between Ducktown, Tennessee and Murphy, North Carolina in the western Blue Ridge (Figure 30 and Appendix 2) yielded single-crystal $^{40}Ar/^{39}Ar$ ages varying between 327.9±2.6 Ma to 465.5±6.6 Ma. The samples of the Ocoee Supergroup (BB1, BB2, MS2, MS3, and MS4b) tend to yield complex single-crystal age distributions and the samples of the Mineral Bluff Group (MS5, MS6, MS7, and MS8) tend to yield normally distributed single-crystal ages (Figures 31-33). Sample MS2, a metasandstone of the Copperhill Formation in the Ducktown anticlinorium, is an exception as it yielded normally distributed single-crystal ages with one crystal somewhat older than the mean (345±1 Ma; Figure 31e). Samples MS5 and MS7, phyllites of the Mineral Bluff Group in the Murphy synclinorium, both yielded a crystal with an age significantly older than the mean (Figure 32e and 33c).

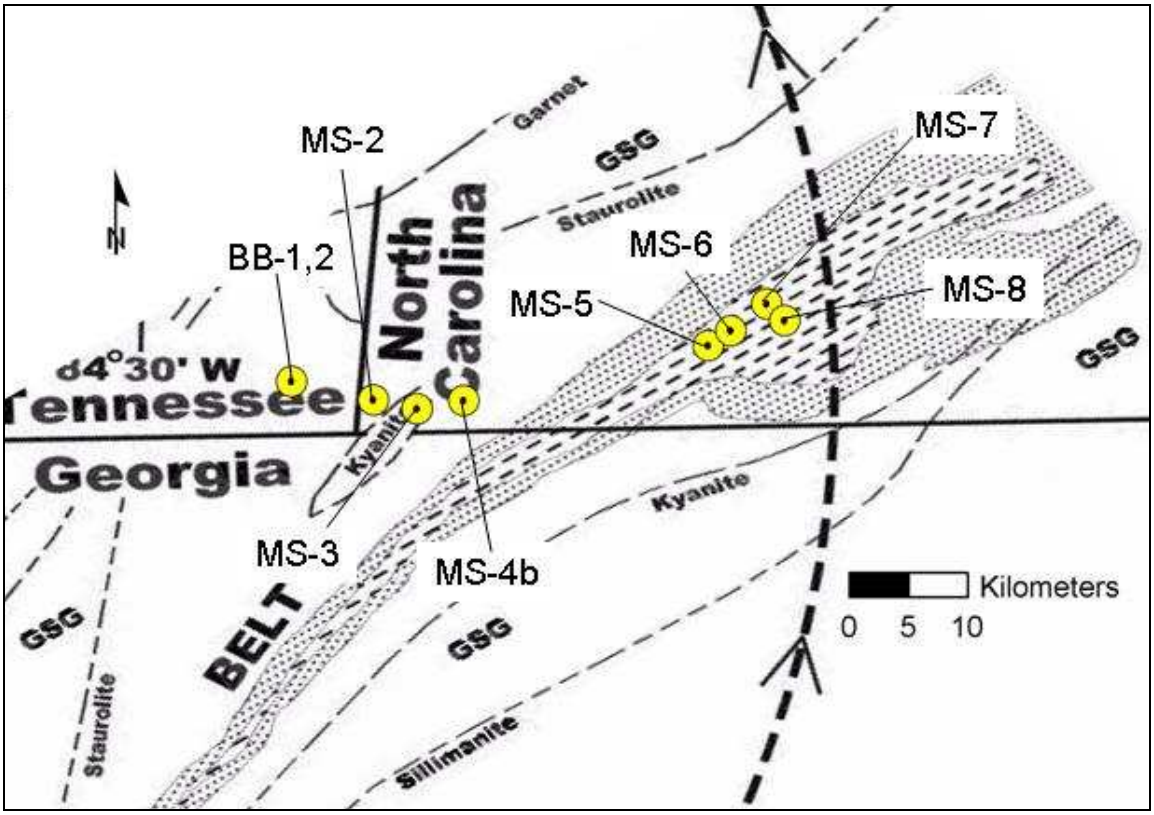

Figure 30: Geologic map of the Ducktown and Murphy structures and locations for samples represented in Figures 31-33 (adapted from Tull and Holm, 2005).

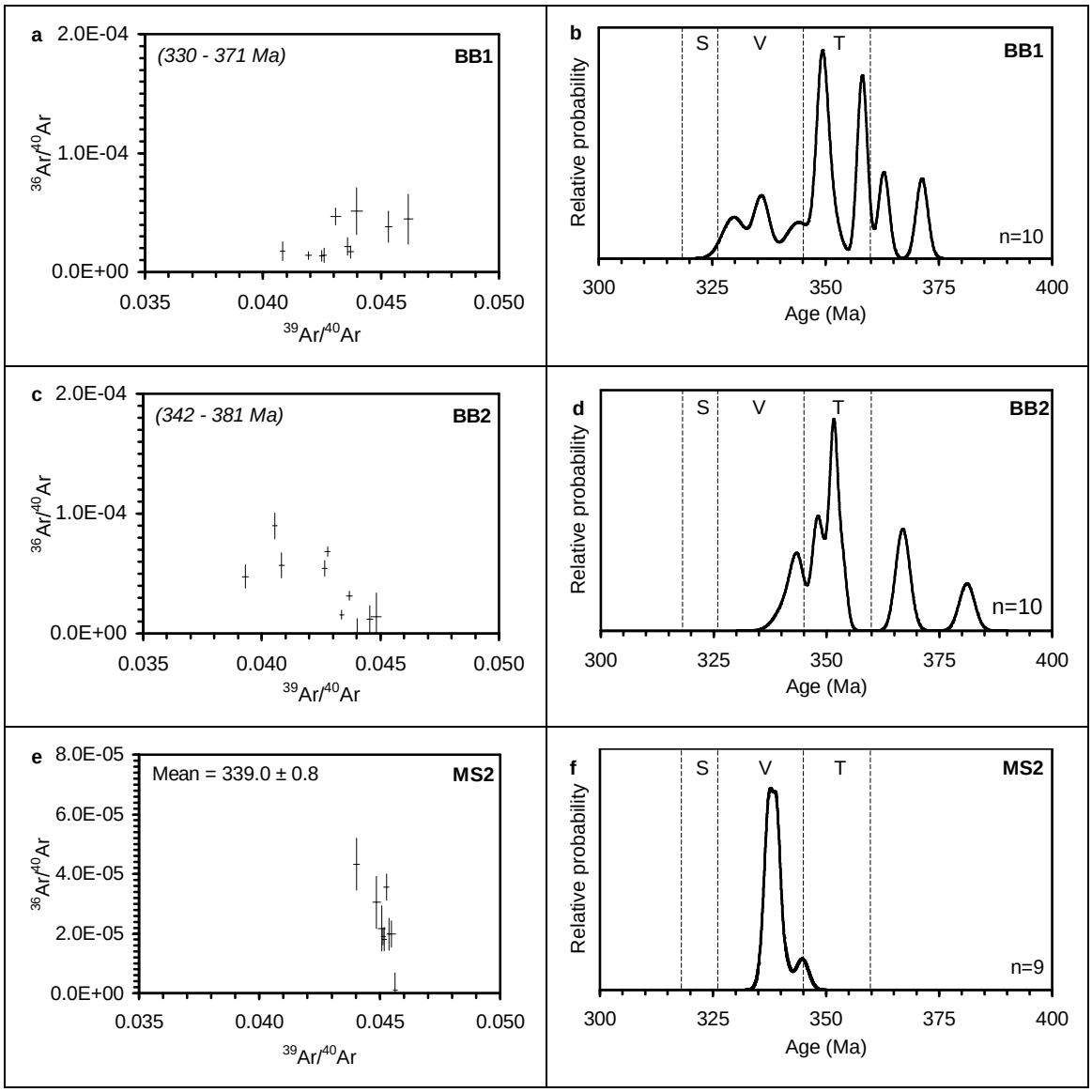

Figure 31: Inverse-isochron and age-probability plots for argon-isotopic data of Ducktown samples BB1 (a-b), BB2 (c-d), and MS2 (e-f) (data-point error crosses are 1σ).

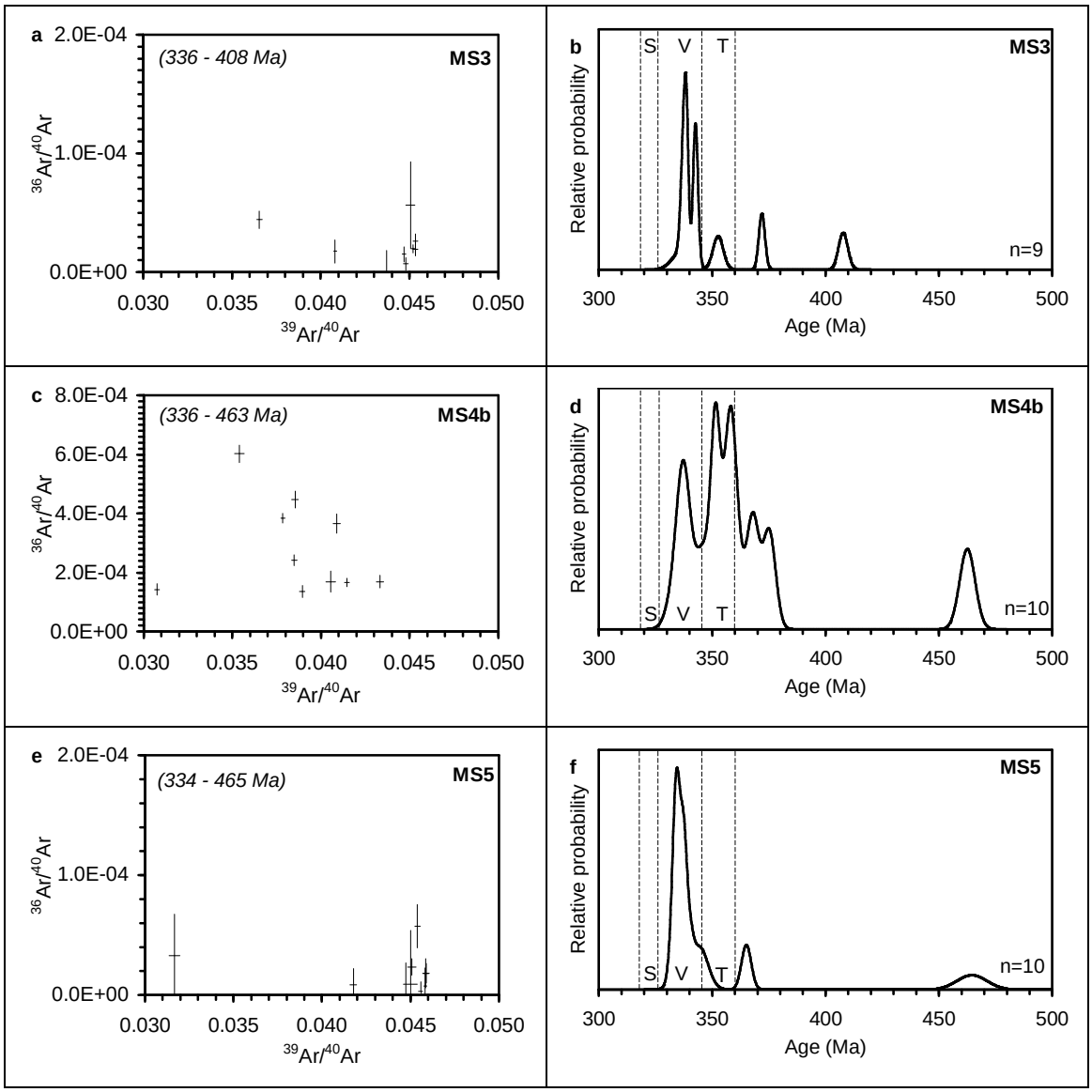

Figure 32: Inverse-isochron and age-probability plots for argon-isotopic data of Ducktown – Murphy samples MS3 (a-b), MS4b (c-d), and MS5 (e-f) (data-point error crosses are 1σ).

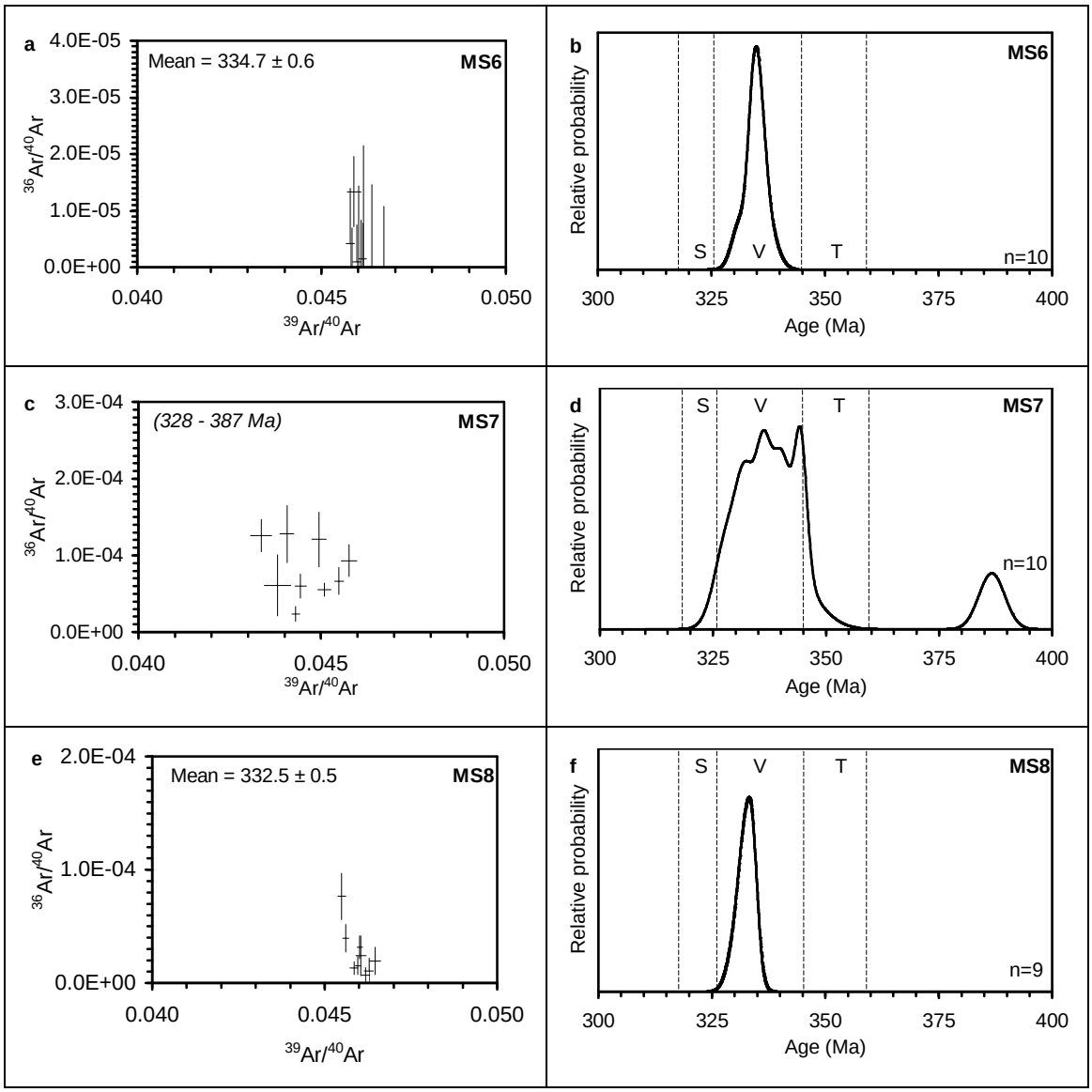

Figure 33: Inverse-isochron and age-probability plots for argon-isotopic data of Murphy samples MS6 (a-b), MS7 (c-d), and MS8 (e-f) (data-point error crosses are 1σ).

INTERPRETATION OF RESULTS

Considering the results for samples obtained near the Cartersville transverse zone (n=12), muscovite appears to record cooling-crystallization over a range of time between 335-320 Ma (see Table 2). These Middle to Late Mississippian ages have a bimodal cumulative distribution and are suggestive of Serpukhovian and Visean components (Figure 34). Individually, all of these samples yielded simple age distribution regardless of metamorphic textural complexity. These results are consistent with work in the Talladega belt (McClellan et al., 2007), and are interpreted to indicate that Middle to Late Mississippian (Alleghanian) tectonic events dominate metamorphic and structural evolution as far north as the Cartersville transverse zone in the western Blue Ridge.

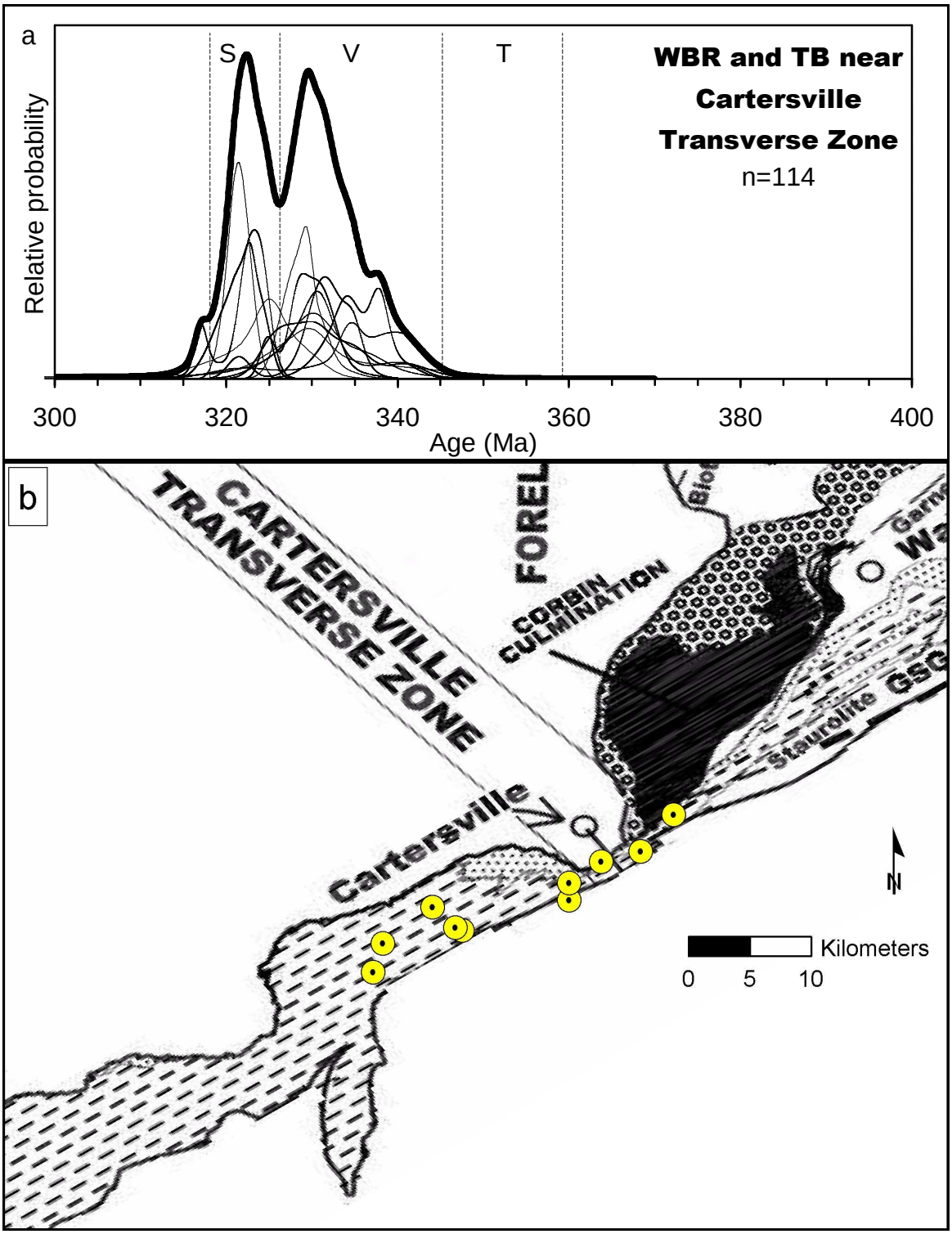

Figure 34: a) Cumulative-distribution plot of age probabilities for muscovite collected from vicinity of the Cartersville transverse zone. b) Map of sample localities (adapted from Tull and Holm, 2005).

Considering the results for samples obtained farther north (Figure 35), along the Cartersville-Great Smoky fault (n=7), muscovite appears to record a complex cooling-crystallization history. In this region, however, the age distribution tends to form a prominent Visean mode (Figure 35a) similar to the Cartersville samples. Results obtained in this region are consistent with a Mississippian (Visean) age of deformation and metamorphism that is superimposed on relict-mineral assemblages of an earlier metamorphic event.

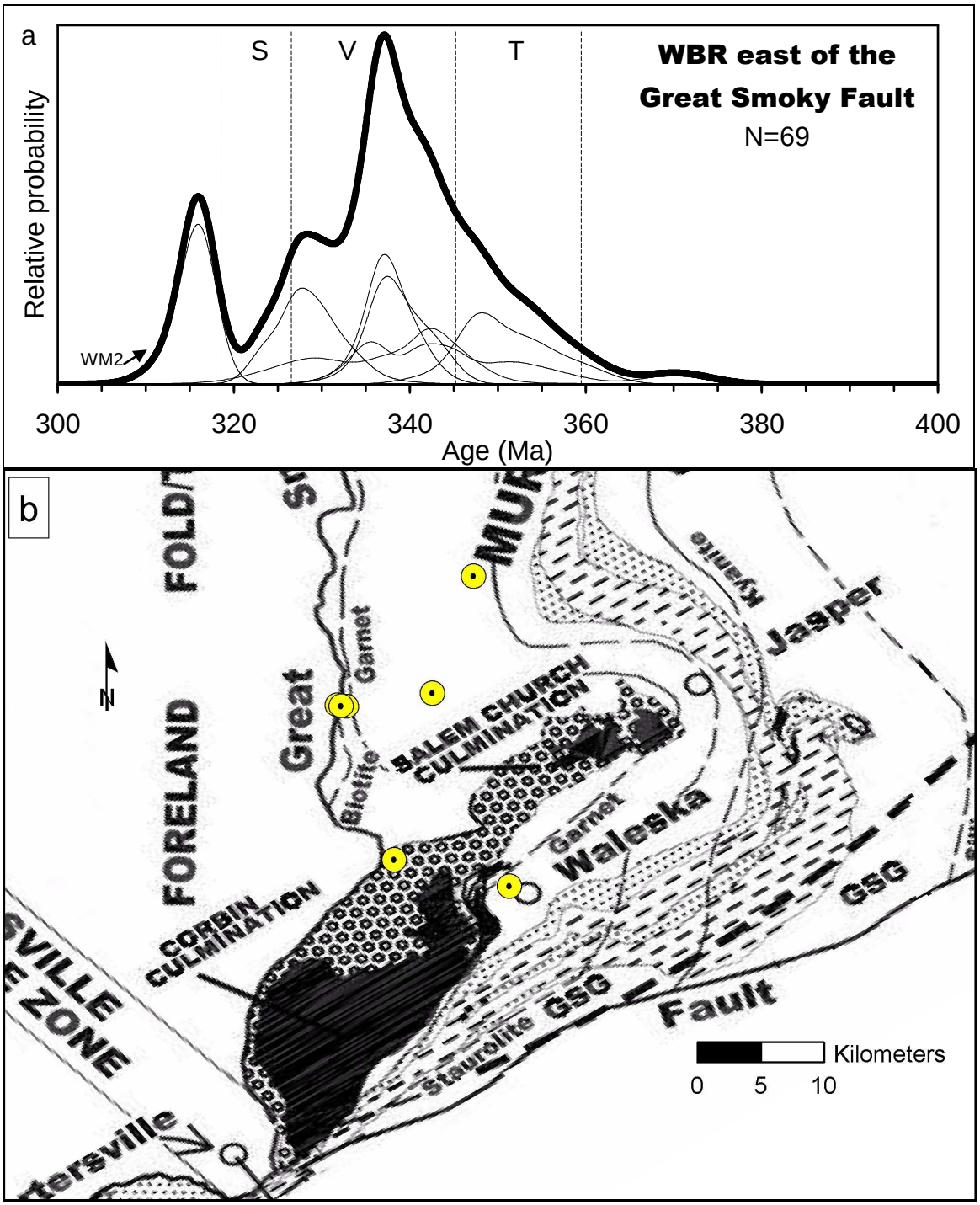

Figure 35: a) Cumulative-distribution plot of age probabilities for muscovite from vicinity of the Cartersville-Great Smoky fault. Sample WM2 (315.5 Ma) yielded the youngest age in this study. b) Map of sample localities (adapted from Tull and Holm, 2005).

Muscovite sampled proximal to the Great Smoky fault, at Carter Lake and Chatsworth, yielded pre-Carboniferous ages with a complex cumulative distribution, showing prominent Middle to Late Devonian modes (Figure 36). Individually, these samples generally yield complex age distributions, have complex metamorphic textures, show evidence of cataclasis, and are considered unreliable due to possible extraneous argon and presence of detrital or relict micas. The Chatsworth sample (WM10) yielded a pre-Carboniferous age with a simple age distribution, showing a prominent Late Devonian peak (Figure 36). A pre-Carboniferous history, possibly relict (Acadian or Taconian), is recorded in western Blue Ridge rocks north of Carter Lake, but that history cannot be discerned from data of this study.

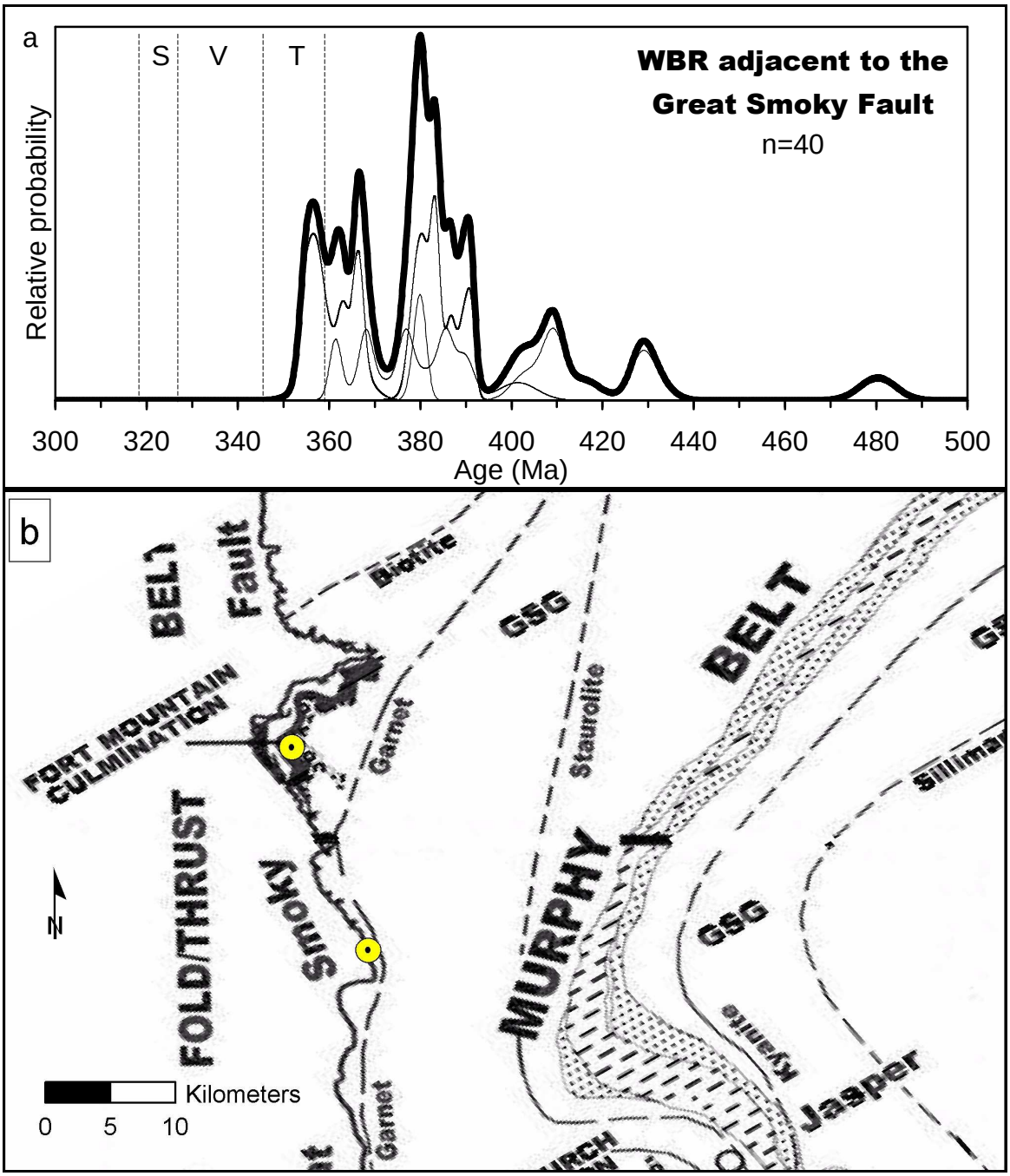

Figure 36: a) Cumulative-distribution plot of age probabilities for muscovite collected farther north (Carter Lake and the Fort Mountain structure) and more directly from fault, yield pre-Carboniferous ages. b) Map of sample localities (adapted from Tull and Holm, 2005).

Considering the results for samples obtained to the northeast, along the Ducktown-Murphy transect (Figure 37), muscovite yielded a complex cooling-crystallization history in Ocoee Supergroup rocks (Ducktown anticlinorium) with prominent Visean and less prominent Tournaisian cumulative-distribution modes. Samples from this transect in rocks of the Mineral Bluff Group (MS-5, MS-6, MS-7, and MS-8; Figures 30, 32, and 33) have a strong tendency to yield normal distributions with prominent Visean modes. A small percentage of the muscovite yielded pre-Carboniferous ages, interpreted to reflect polymetamorphism, relict or detrital grains, the result of accumulating extraneous argon, or combinations of these effects. These results indicate that north of the Cartersville transverse zone, Early-Middle Mississippian (Alleghanian) tectonic events dominate metamorphic and structural evolution in rocks above the Lay Dam unconformity (Mineral Bluff Group). Below the unconformity (Ocoee Supergroup rocks), a record of early-generation muscovite growth is overprinted by Alleghanian tectonothermal effects.

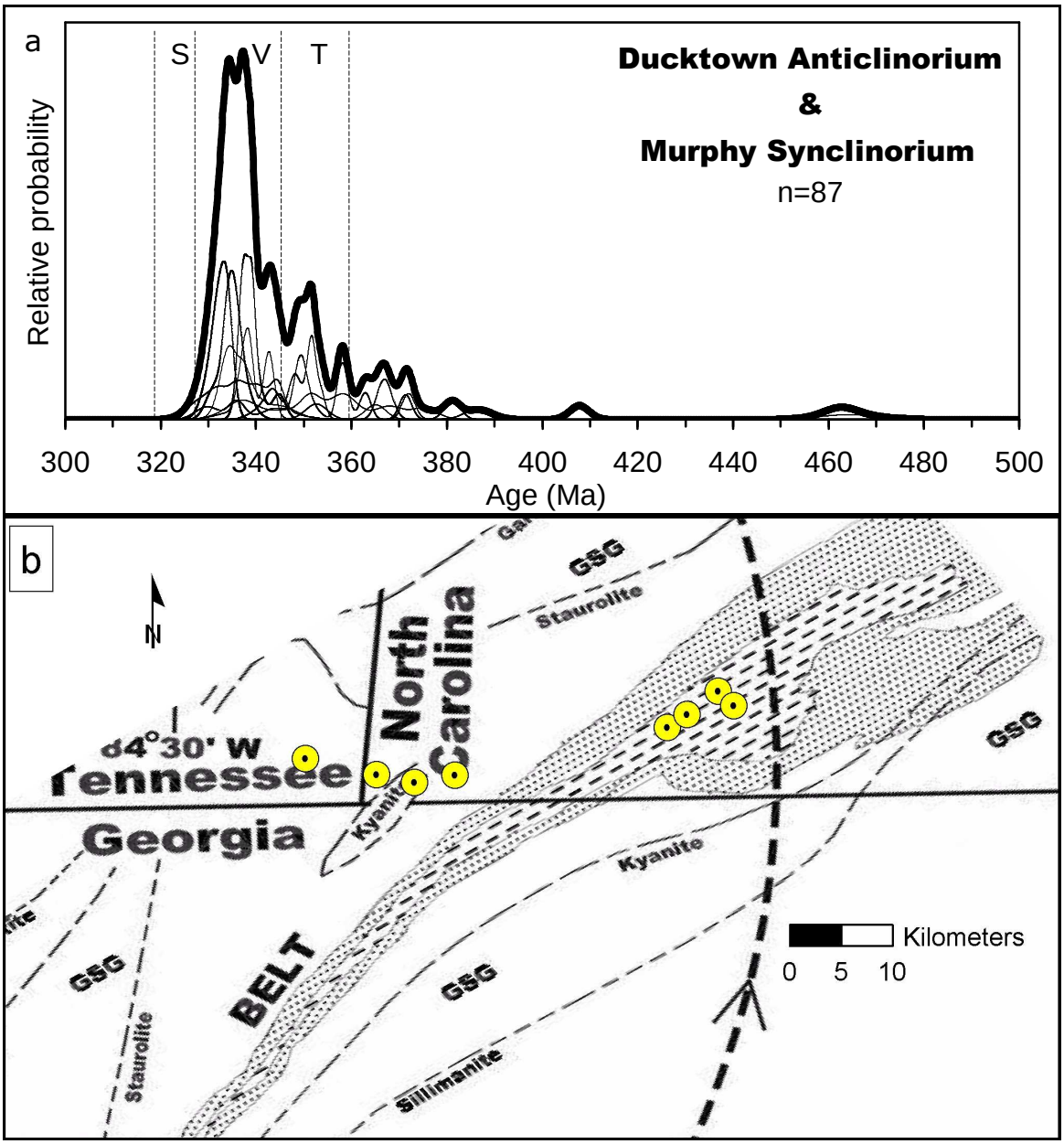

Figure 37: a) Cumulative-distribution plot of age probabilities for muscovite collected from the Ducktown-Murphy structures. b) Map of sample localities (adapted from Tull and Holm, 2005).

DISCUSSION

Middle Mississippian (Visean) ages recorded in muscovite from phyllites and schists of the western Blue Ridge-Talladega belt (see Figure 38) are interpreted to record metamorphism, ductile deformation, and synchronous rapid cooling. These Visean ages are somewhat older than the traditionally accepted Pennsylvanian range for the age of the Alleghanian event (e.g., Hatcher, 1987). The Alleghanian, therefore, comprises orogenic events as old as Early Mississippian. Furthermore, these ages are substantially younger than the Late Devonian to Early Mississippian 'Neoacadian' event (e.g., Hatcher, 2004, 2006). Considering the low metamorphic grade of rocks dated in this study - and thus short time for any post-metamorphic cooling to significantly affect ages - the Visean ages of this study are not likely to result from a Neoacadian event.

The youngest rocks of the southern Appalachian Valley and Ridge (including the lower Pennsylvanian Pottsville Formation) contain syn-orogenic strata that were overridden and deformed by the final emplacement of the western Blue Ridge-Talladega belt (Figure 39). Dominantly Visean ages recorded in muscovite of the western Blue Ridge-Talladega belt are older than the Pottsville Formation. This means the muscovite in low-grade metamorphic rocks of the western Blue Ridge-Talladega belt crystallized and cooled in a distal location, presumably far to the east of their present location, prior to final emplacement and juxtaposition with the Valley and Ridge province.

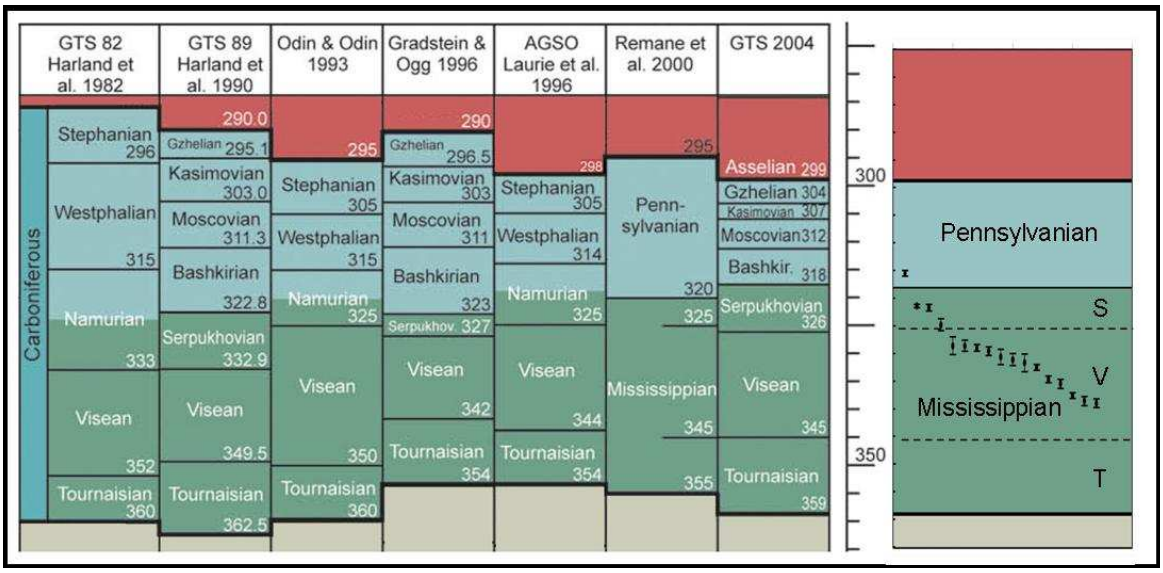

Figure 38: Visean (Mississippian) ages recorded in muscovite of this study (mean ages from Table 2 with error bars representing one standard deviation are shown to the right), in comparison with divisions of the Carboniferous Period. The 'GTS 2004' of the International Commission on Stratigraphy (Gradstein et al., 2004) is the timescale used in this study. See Gradstein et al. (2004) for additional references to earlier timescale versions in this figure. The comparison of timescales above was created with utilities in the International Commission on Stratigraphy web site: http:/www.stratigraphy.org.

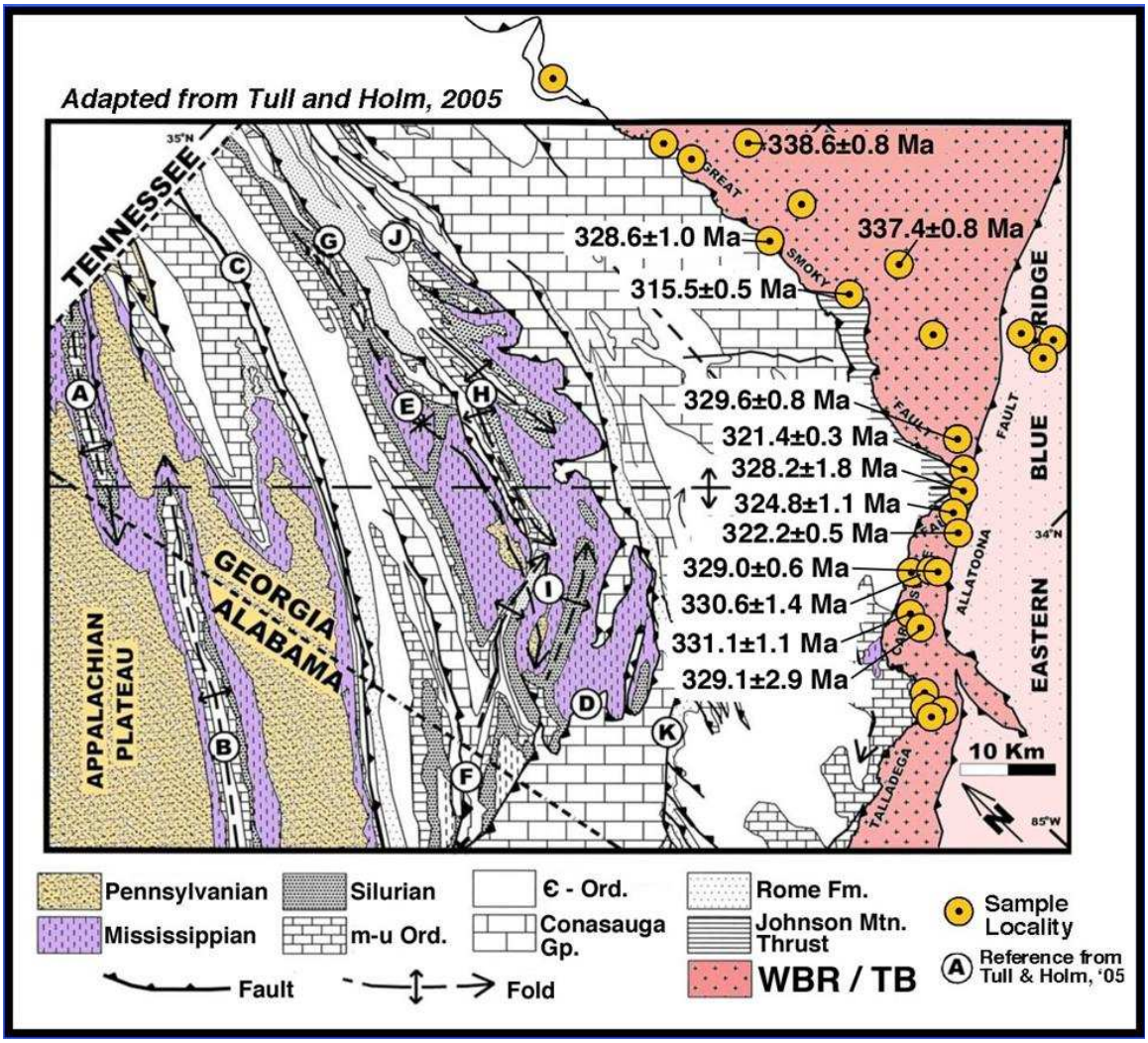

Figure 39: Map of study area showing the distribution of Mississippian ages yielded from rocks of the western Blue Ridge – Talladega Belt and the general stratigraphy of deformed-clastic units in the foreland (adapted from Tull and Holm, 2005). See Table 2 for specific sample coordinates.

Pre-Carboniferous ages recorded in muscovite from schists proximal to the Great Smoky fault and the transect through the Ducktown and Murphy structures are interpreted to reflect Taconian metamorphism and a protracted thermal history. However, it is possible that the effects of extraneous argon, and 'inheritance' of detrital mica, may have strongly influenced these older ages. $^{40}Ar/^{39}Ar$ analyses using incremental-heating methods would clarify the interpretation of these ages because those methods provide a convenient test for the presence of extraneous argon. All ages recorded in muscovite from phyllites near the Cartersville transverse zone of the western Blue Ridge–Talladega belt, and within the Mineral Bluff Group (Murphy synclinorium), tend to define normal distributions and occur within a range from 325-335 Ma. These Visean ages are interpreted to correspond with intense Middle-Late Mississippian deformation and a single, dominant low-grade Alleghanian metamorphic event having affected these units. This finding is consistent with the inference that the Lay Dam Formation (Talladega belt) and Mineral Bluff Group (western Blue Ridge) show evidence of a single low-grade metamorphism (Tull, 1988).

CONCLUSIONS

Middle Mississippian (Visean) ages of ca. 330 Ma record an “early” Alleghanian event, which affected the Laurentian margin, in muscovite from lower-greenschist phyllites and schists of the western Blue Ridge-Talladega belt. These ages are interpreted to record metamorphism and ductile deformation in those terranes, likely synchronous with rapid cooling. No record of pre-Carboniferous thermal disturbance is present, proximal to the Cartersville transverse zone, in muscovite from Lay Dam Formation and Mineral Bluff Group phyllites. Single-crystal ages older than Carboniferous are also relatively rare, farther north, in Mineral Bluff Group phyllites inside the Murphy synclinorium.

The Visean ages do not record final emplacement of the western Blue Ridge-Talladega belt onto non-metamorphosed rocks of the Valley and Ridge province. As final emplacement of the western Blue Ridge-Talladega belt metamorphic terrane occurred along the dominantly brittle Great Smoky-Cartersville thrust and Talladega thrust. Dynamic metamorphism along the thrusts was sufficiently low in metamorphic grade not to result in substantial growth and recrystallization of muscovite.

The present author interprets the Alleghanian orogeny in the southern Appalachians to comprise multiple Early Mississippian to Permian events. First, during the Mississippian, terrane accretion and continent-continent collision resulted in regional metamorphism and the associated ductile deformation and muscovite growth. Later,

during the Pennsylvanian to Permian, further thrusting of this metamorphosed coastal margin terrane resulting in brittle deformation and final emplacement onto the Valley and Ridge province.

A Taconian metamorphic event and subsequent protracted thermal history is interpreted to be reflected in the complex single-crystal age distributions typical of muscovite found in phyllites and schists of the western Blue Ridge below the Lay Dam unconformity and away from the Cartersville transverse zone. As there are complex distributions of single-crystal ages in these polymetamorphic rocks, techniques that tend to homogenize muscovite (specifically, K/Ar sample processing and *in vacuo* $^{40}Ar/^{39}Ar$ incremental-heating analyses) seem likely to yield average, or hybrid, results that may not accurately record geologic history.

REFERENCES

Aylor, J.G., Jr., 1994, Paleozoic history of the Nantahala and Brasstown Formations of the basal Murphy belt, southwesternmost North Carolina and northwestern-most Georgia [Ph.D. thesis]: Tallahassee, Florida State University, 421 p.

Carrarat, P., Frestat, G., and Rampini, A., 2003, BANCO: An SVG-based approach to create Web sites for the management of remote sensing, spatial and non-spatial data: International Journal of Remote Sensing, v. 24, p. 3903-3916.

Carrington, T.J., 1973, Metamorphosed Paleozoic sedimentary rocks in Chilton, Shelby, and Talladega Counties, Alabama, *in* Carrington, T.J., ed., Talladega metamorphic front: Alabama Geological Society, 11th Annual Field Trip, Guidebook, p. 22-38.

Cecconi, A. and Galanda, M., 2002, Adaptive zooming in web cartography: Computer Graphics Forum, v. 21, p. 787-799.

Connelly, J.B., and Dallmeyer, R.D., 1993, Polymetamorphic evolution of the western Blue Ridge: Evidence from $^{40}Ar/^{39}Ar$ whole-rock slate/phyllite and muscovite ages: American Journal of Science, v. 293, p. 322-359.

Corrie, S.L. and Kohn, M.J., 2007, Resolving the timing of orogenesis in the western Blue Ridge, southern Appalachians, via in situ ID-TIMS monazite geochronology: Geology, v. 35, p. 627-630.

Cox, S.G., Griffin, P. F., Adams, C. S., DeMille, D., and Riis, E., 2003, Reusable ultrahigh vacuum viewport bakeable to 240˚C: Review of Scientific Instruments, v. 74, p. 3185-3187.

Cross, W.G., 1951, Two-directional focusing of charged particles with a sector-shaped, uniform magnetic field: Reviews of Scientific Instruments, v. 22, p. 717-722.

Dallmeyer, R.D., 1989, Late Paleozoic thermal evolution of crystalline terranes within portions of the U.S. Appalachian orogen, *in* Hatcher, R.D., Jr., Thomas, W.A., and Veile, G.W., eds., The Appalachian-Ouchita orogen in the United States: Geological Society of America, The Geology of North America, v. F-2, p. 417-444.

Dalrymple, G.B., and Lanphere, M.A., 1969, Potassium-Argon Dating, Principles, Techniques and Applications to Geochronology: San Francisco, W.H. Freeman, 258 p.

Dalrymple, G.B., Alexander, E.C., Jr., Lanphere, M.A., and Kraker, G.P., 1981, Irradiation of samples for $^{40}Ar/^{39}Ar$ dating using the Geological Survey TRIGA reactor: U.S. Geological Survey Professional Paper, n. 1176, 55p.

Dickin, A.P., 1995, Radiogenic Isotope Geology: New York, Cambridge Press, 452 p.

Dodson, M.H., 1973, Closure temperature in cooling geochronological and petrological systems: Contributions to Mineralogy and Petrology, v. 40, p. 259-274.

Drake, A.A., Jr., Sinha, A.K., Laird, J., and Guy, R.E., 1989, The Taconic orogen, *in* Hatcher, R.D., Jr., Thomas, W.A., and Veile, G.W., eds., The Appalachian-Ouchita orogen in the United States: Geological Society of America, The Geology of North America, v. F-2, p. 101-177.

Duce, D., Herman, I., and Hopgood, B., 2002, Web 2D graphics file formats: Computer Graphics Forum, v. 21, p. 43-64.

Dunlap, W.J., Teyssier, C., McDougall, I., and Baldwin, S., 1991, Ages of deformation from K/Ar and $^{40}Ar/^{39}Ar$ dating of white micas: Geology, v. 19, p. 1213-1216.

Faure, G., 1986, Principles of Isotope Geology, second edition: New York, John Wiley and Sons, 589 p.

Gastaldo, R.A., Guthrie, G.M., and Steltenpohl, M.G., 1993, Mississippian fossils from southern Appalachian metamorphic rocks and their implications for late Paleozoic tectonic evolution: Science, v. 262, p. 732-734.

Gradstein, F.M., Ogg, F.G., Smith, A.G., Agterberg, F.P., Bleeker, W., Cooper, R.A., Davydov, V., Gibbard, P., Hinnov, L.A., House, M.R., Lourens, L., Luterbacher, H.P., McArthur, J., Melchin, M.J., Robb, L.J., Shergold, J., Villeneuve, M., Wardlaw, B.R., Ali, J., Brinkhuis, H., Hilgen, F.J., Hooker, J., Howarth, R.J., Knoll, A.H., Laskar, J., Monechi, S., Plumb, K.A., Powell, J., Raffi, I., Röhl, U., Sadler, P., Sanfilippo, A., Schmitz, B., Shackleton, N.J., Shields, G.A., Strauss, H., Van Dam, J., van Kolfschoten, T., Veizer, J., and Wilson, D., 2004, A Geologic Time Scale 2004: Cambridge University Press, 589 p.

Giletti, B.J., 1972, Diffusion of alkalis and radiogenic argon-40 in phlogopite: American Geophysical Union, v. 53, p. 557.

Hadley, J.B., 1970, The Ocoee Series and its possible correlatives, *in* Fisher, G.W. et al., eds., Studies of Appalachian geology – central and southern: New York, Interscience Publishers, p. 247-259.

Hames, W.E., and Bowring, S.A., 1994, An empirical evaluation of the argon diffusion geometry: Earth and Planetary Science Letters, v. 124, p. 161-169.

Hatcher, R.D., Jr., 1987, Tectonics of the southern and central Appalachian internides: Annual Reviews of Earth and Planetary Sciences, v. 15, p. 337-362.

Hatcher, R.D., Jr., 1989, Tectonic synthesis of the U.S. Appalachians, *in* Hatcher, R.D., Jr., Thomas, W.A., and Veile, G.W., eds., The Appalachian-Ouchita orogen in the United States: Geological Society of America, The Geology of North America, v. F-2, p. 511-535.

Hatcher, R.D., Jr., 2002, Alleghanian (Appalachian) orogeny, a product of zipper tectonics: Rotational transpressive continent-continent collision and closing of ancient oceans along irregular margins, *in* Martinez Catalan, J.R., Hatcher, R.D., Jr., Arenas, R., and Diaz Garcia, F., eds., Variscan-Appalachian dynamics: The building of the late Paleozoic basement: Geological Society of America Special Paper 364, p. 199-208.

Hatcher, R.D., Jr., and Goldberg, S.A., 1991, The Blue Ridge Province, *in* Horton, J. W., Jr., and Zullo, V.A., eds., The Geology of the Carolinas - Carolina Geological Society 50th Anniversary Volume: Knoxville, University of Tennessee Press, p. 11-35.

Hatcher, R.D., Jr., and Odom, A.L., 1980, Timing of thrusting in the southern Appalachians, USA: model for orogeny?: Journal of the Geological Society, v. 137, p. 321-327.

Hatcher, R.D., Jr., Osberg, P.H., Drake, A.A., Jr., Robinson, P., and Thomas, W.A., 1990, TECTONIC MAP OF THE U.S. APPALACHIANS: The Appalachian-Ouachita orogen in the United States, The Geology of North America, v. F-2.

Hatcher, R.D., Jr., Thomas, W.A., Greiser, P.A., Snoke, A.W., Mosher, S., and Wiltschko, D.V., 1989, Alleghanian orogen, *in* Hatcher, R.D., Jr., Thomas, W.A., and Veile, G.W., eds., The Appalachian-Ouchita orogen in the United States: Geological Society of America, The Geology of North America, v. F-2, p. 233-318.

Herman, I., and Dardailler, D., 2002, SVG Linearization and Accessibility: Computer Graphics Forum, v. 21, p. 777-786.

Hopson, J.L., Hatcher, R.D., Jr., and Stieve, A.L., 1989, Geology of the eastern Blue Ridge, northeastern Georgia and the adjacent Carolinas: Georgia Geological Society Guidebooks, v. 9, n. 3, p. 1-40.

Horton, J.W., Jr., Drake, A.A., and Rankin, D.W., 1989, Tectonostratigraphic terranes and their boundaries in the central and southern Appalachians: Geological Society of America Special Paper 230, p. 213-245.

Hurst, V.J., 1955, Stratigraphy, structure, and mineral resources of the Mineral Bluff Quadrangle, Georgia: Georgia Geological Survey Bulletin, n. 63, 137 p.

Hurst, V.J., 1973, Geology Of The Southern Blue Ridge Belt: American Journal of Science, v. 273, p. 643-670.

Keith, A., 1907, Description of the Nantahala Quadrangle, North Carolina and Tennessee: U.S. Geological Survey Geological Atlas Folio, v. 143, p. 11.

King, P.B., 1964, Geology of the central Great Smoky Mountains, Tennessee: U.S. Geological Survey Professional Paper 349-C, 148 p.

King, P.B., Hadley, J.B., Neuman, R.B., Hamilton, W. B., 1958, Stratigraphy of the Ocoee Series, Great Smoky Mountains, Tennessee and North Carolina: Geological Society of America Bulletin, v. 69, p. 947-966.

Kish, S.A., 1983, A geochronological study of deformation and metamorphism in the Blue Ridge and Piedmont of the Carolinas [Ph. D. thesis]: Chapel Hill, University of North Carolina, 220 p.

Kish, S.A., 1990, Timing of Middle Paleozoic (Acadian) metamorphism in the southern Appalachians: K-Ar Studies in the Talladega belt, Alabama: Geology, v. 18, p. 650-653.

Kish, S.A., 1991, Potassium-argon dating in the Western Blue Ridge of North Carolina and Tennessee, *in* Kish, S.A., ed., Studies of Precambrian and Paleozoic stratigraphy in the western Blue Ridge: Carolina Geological Society, p. 69-77.

Kunk, M.J., Southworth, S.C., Aleinikoff, J.N., Naeser, C.W., Merschat, C.E., Cattanach, B. L., 2006, Preliminary U-Pb, $^{40}Ar/^{39}Ar$ and fission-track ages support a long and complex tectonic history in the western Blue Ridge in North Carolina and Tennessee: Geological Society of America Abstracts with Programs, v. 38, n. 3, p. 66.

Lavallee, S.B., 2003, Timing of the accretion of the Carolina zone to Laurentia: Petrologic and geochronologic analysis [MS thesis]: Auburn, Auburn University, 74 p.

Li, Li, and Tull, J.F., 1998, Cover stratigraphy and structure of the southernmost external basement massifs in the southern Appalachian Blue Ridge: Evidence for two-stage Late Proterozoic rifting: American Journal of Science, v. 298, p. 829-867.

Ludwig, K.R., 2003, User's manual for ISOPLOT, version 3, A geochronological toolkit for Microsoft Excel: Berkeley Geochronological Center, Special Publication, n. 4, 70 p.

McClellan, E.A., Steltenpohl, M.G., Thomas, C., and Miller, C.F., 2005, Isotopic age constraints and metamorphic history of the Talladega belt: New evidence for timing of arc metamorphism and terrane emplacement along the southern Laurentian margin, *in* Steltenpohl, M.G., ed., Southernmost Appalachian Terranes, Alabama and Georgia: Tuscaloosa, Alabama, Southeast Section of the Geological Society of America, p. 19-50.

McClellan, E.A., Steltenpohl, M.G., Thomas, C., and Miller, C.F., 2007, Isotopic age constraints and metamorphic history of the Talladega belt: New evidence for timing of arc metamorphism and terrane emplacement along the southern Laurentian margin: Journal of Geology, v. 115, p. 541-561.

McConnell, K.I., 1986, The Cartersville fault at Carters Dam, *in* Neathery, T. L., ed., Geological Society of America Centennial Field Guide Southeastern Section: v. 6, p. 271-274.

McDougall, I., and Harrison, M.T., 1999, Geochronology and thermochronology by the $^{40}Ar/^{39}Ar$ method: New York, Oxford University Press, 269 p.

Merrihue, C., and Turner, G., 1966, Potassium-argon dating by activation with fast neutrons: Journal of Geophysical Research, v. 71, p. 2852-2856.

Mueller, P., Heatherington, A., Wooden, J.L., Steltenpohl, M.G., and Hanley, T.B., 2005, Age and Provenance of Precambrian Crust in the Southernmost Appalachians, *in* Steltenpohl, M.G., ed., Southernmost Appalachian Terranes, Alabama and Georgia: Tuscaloosa, Alabama, Southeast Section of the Geological Society of America, p. 98-114.

Osberg, P.H., Tull, J.F., Robinson, P., Hon, R., and Butler, J.R., 1989, The Acadian orogen, *in* Hatcher, R.D., Jr., Thomas, W.A., and Veile, G.W., eds., The Appalachian-Ouchita orogen in the United States: Geological Society of America, The Geology of North America, v. F-2, p. 179-232.

Plewe, B., 1997, GIS online: information retrieval, mapping, and the internet: Santa Fe, OnWord Press, 336 p.

Purdy, J.W. and Jager, E., 1976, K-Ar ages on rock-forming minerals from the central Alps: Institute of Geology and Mineralogy Memoir, Padova University, v. 30, p. 1-31.

Rankin, D.W., 1975, The continental margin of the eastern North America in the Southern Appalachians: The opening and closing of the proto-Atlantic Ocean: American Journal of Science, v. 275-A, p. 298-336.

Renne, P.R., Swisher, C.C., Deino, A.L. Karner, D.B., Owens, T.L., DePaolo, D.J., 1998, Intercalibration of standards, absolute ages and uncertainties in $^{40}Ar/^{39}Ar$ dating: Chemical Geology, v. 145, p.117-152.

Rinner, C., 1998, Online maps in GeoMed-Internet Mapping, online GIS and their application in Collaborative Spatial Decision-Making: *in* proceedings of GIS PlaNET '98 International Conference on Geographic Information: Lisbon, 9 p.

Rodgers, J., 1970, The tectonics of the Appalachians: New York, John Wiley and Sons, 271 p.

Rodgers, J., 1972, Latest Precambrain (post-Grenville) rocks of the Appalachian region: American Journal of Science, v. 272, p. 507-520.

Ruffle, S. and Richens, P., 2004, Stylist and scaleable-vector graphics for all on the Web: International Journal of Architectural Computing, v. 2, p. 333-350.

Secor, D.S., Jr., Snoke, A.W., and Dallmeyer, R.D., 1986, Character of the Alleghanian orogeny in the southern Appalachians: Part 3. Regional tectonic relations: Geological Society of America Bulletin, v. 97, p. 1345-1353.

Shaig, A., 2001, An overview of web based Geographic Information Systems: *in* Whigham, P.A., ed., The 13th Annual Colloquium of the Spatial Information Research Centre: Dunedin, University of Otago, 10 p.

Steltenpohl, M.G., and Kunk, M. J., 1993, $^{40}Ar/^{39}Ar$ thermochronology and Alleghanian development of the southernmost Appalachian Piedmont, Alabama and southwest Georgia: Geological Society of America Bulletin, v. 105, p. 819-833.

Steltenpohl, M.G., Heatherington, A., Mueller, P., and Miller, B.V., 2005, New isotopic dates on crystalline rocks from Alabama and Georgia, *in* Steltenpohl, M.G., ed., Southernmost Appalachian terranes, Alabama and Georgia: Tuscaloosa, Southeast Section of the Geological Society of America, p. 51-69.

Stevens, G.C. and Wright, T.O., 1981, Stratigraphy of the Martinsburg Formation, West of Harrisburg in the Great Valley of Pennsylvania: American Journal of Science, v. 281, p. 1009-1020.

Thigpen, J.R. and Hatcher, R.D., 2006, Geologic map of the western Blue Ridge and portions of the eastern Blue Ridge and Valley and Ridge Provinces in southeast Tennessee, southwest North Carolina, and northern Georgia, *in* Hibbard, J. P., van Staal, C.R., Rankin, D.W., and Williams, H., eds., Lithotectonic map of the Appalachian Orogen, Canada-United States of America: Geological Survey of Canada, Map 2096A, scale 1:1500000.

Thomas, W.A., 1977, Evolution of Appalachian-Ouachita salients and recesses from reentrants and promontories in the continental margin: American Journal of Science, v. 277, p. 1233-1278.

Thomas, W.A., 1983, Continental margins, orogenic belts, and intracratonic structures: Geology, v. 11, p. 270-272.

Thomas, W.A., 1991, The Appalachian-Ouchita rifted margin of southeastern North America: Geological Society of America Bulletin, v. 103, p. 415-431.

Tull, J.F., 1982, Stratigraphic framework of the Talladega slate belt, Alabama Appalachians, *in* Bearce, D.N., Black, W.W., Kish, S.A., and Tull, J.F., eds., Tectonic studies in the Talladega and Carolina slate belts, southern Appalachian orogen: Geological Society of America Special Paper, n. 191, p. 13-18.

Tull, J. F., 1998, Analysis of a regional middle Paleozoic unconformity along the distal southeastern Laurentian margin, southernmost Appalachians: implications for tectonic evolution: Geological Society of America Bulletin, v. 110, p. 1149-1162.

Tull, J.F., 2002, Southeastern margin of the middle Paleozoic shelf, southwesternmost Appalachians: Regional stability bracketed by Acadian and Alleghanian tectonism: Geological Society of America Bulletin, v. 114, p. 643-655.

Tull, J.F. and Holm, C.S., 2005, Structural evolution of a major Appalachian salient-recess junction: Consequences of oblique collisional convergence across a continental margin transform fault: Geological Society of America Bulletin, v. 117, p. 482-499.

Tull, J.F., Ausich, W.I., Groszos, M.S., and Thompson, T.W., 1993, Appalachian Blue Ridge cover sequence ranges at least into the Ordovician: Geology, v. 21, p. 215-218.

Tull, J.F., Harris, A.G., Repetski, J.E., McKinney, F.K., Garret, C.B., and Bearce, D.N., 1988, New paleontologic evidence constraining the age and paleotectonic setting of The Talladega slate belt, southern Appalachians: Geological Society of America Bulletin, v. 100, p. 1291-1299.

Tull, J.F., Thompson, T.W., Grozos, M.S., Aylor, J.G., and Kish, S.A., 1991, Murphy belt lithostratigraphic nomenclature, *in* Kish, S.A., ed., Studies of Precambrian and Paleozoic stratigraphy in the western Blue Ridge: Durham, North Carolina, Carolina Geological Society Field Trip Guidebook, p. 79-86.

Weaver, K.N., 1970, The Valley and Ridge and Appalachian Plateau-structure and tectonics: Introduction, *in* Fisher, G.W., Pettijohn, F.J., Reed, J.C., Jr., and Weaver, K.W., eds., Studies of Appalachian geology - central and southern: New York, John Wiley and Sons, p. 125-126.

Williams, H. and Hatcher, R.D., Jr., 1982, Suspect terranes and accretionary history of the Appalachian orogen: Geology, v. 10, p. 530-536.

Wilson, J.T., 1966, Did the Atlantic close and then reopen?: Nature, v. 211, p. 676-681.

APPENDICES

APPENDIX A: MONITOR DATA

monitor	J	n	^{40}Ar(*+atm)		^{39}Ar(K)		^{38}Ar(Cl+atm)		^{37}Ar(Ca)		^{36}Ar(Atm)		%Rad	R	J-Value	
au3.2L.san	± 3.146 E-05	0.00938	1.211E-13	±	7.225E-14	±	8.5E-16	±	1.435E-15	±	1.5E-18	±	100%	1.670	0.00938	± 2.408E-05
		2	1.151E-13	±	6.886E-14	±	8.1E-16	±	1.536E-15	±	1.4E-18	±	100%	1.666	0.00940	± 2.015E-05
		3	8.662E-14	±	5.211E-14	±	6.1E-16	±	1.034E-15	±	1.2E-19	±	100%	1.662	0.00943	± 1.930E-05
		4	8.414E-14	±	4.930E-14	±	5.8E-16	±	9.058E-16	±	5.7E-18	±	98%	1.673	0.00936	± 1.906E-05
		5	5.142E-14	±	3.065E-14	±	3.6E-16	±	6.408E-16	±	2.1E-19	±	100%	1.676	0.00935	± 2.193E-05
au3.3j.san	± 9.312 E-05	1	6.385E-14	±	3.680E-14	±	4.3E-16	±	2.252E-17	±	4.6E-19	±	100%	1.731	0.00905	± 1.418E-05
		2	4.026E-14	±	2.354E-14	±	2.8E-16	±	1.584E-17	±	5.0E-19	±	100%	1.704	0.00919	± 2.210E-05
		3	4.242E-14	±	2.501E-14	±	3.0E-16	±	1.914E-17	±	7.4E-19	±	99%	1.688	0.00928	± 1.494E-05
		4	4.620E-14	±	2.697E-14	±	3.2E-16	±	1.893E-17	±	1.6E-18	±	99%	1.696	0.00924	± 1.703E-05
(a)au3.3j.san	± 2.473 E-04	1	4.682E-14	±	2.757E-14	±	3.2E-16	±	1.749E-17	±	5.9E-19	±	100%	1.692	0.00926	± 2.041E-05
		2	3.187E-15	±	1.912E-15	±	4.7E-18	±	-1.662E-20	±	-1.0E-19	±	101%	1.681	0.00931	± 4.714E-05
		3	7.191E-15	±	4.411E-15	±	1.1E-17	±	4.787E-20	±	1.9E-19	±	99%	1.617	0.00968	± 2.704E-05
		4	2.162E-14	±	1.244E-14	±	3.1E-17	±	-6.377E-21	±	1.5E-18	±	98%	1.702	0.00919	± 1.240E-05
(b)au3.3j.san	0.00952	5	2.053E-14	±	1.273E-14	±	3.2E-17	±	1.837E-19	±	2.0E-19	±	100%	1.607	0.00974	± 1.034E-05
		1	2.718E-14	±	1.657E-14	±	4.2E-17	±	5.513E-20	±	1.1E-18	±	99%	1.619	0.00967	± 1.058E-05
		2	6.686E-14	±	3.961E-14	±	4.7E-16	±	9.3E-20	±	7.5E-20	±	99%	1.677	0.00934	± 9.577E-06
		3	4.4E-17	±	3.120E-14	±	3.7E-16	±	2.295E-17	±	1.5E-18	±	99%	1.683	0.00930	± 1.466E-05
(a)au3.4k.san	± 3.361 E-05	4	5.288E-14	±	3.120E-14	±	3.5E-17	±	2.922E-17	±	1.2E-18	±	99%	1.680	0.00933	± 9.176E-06
		5	8.409E-14	±	4.981E-14	±	5.9E-16	±	2.658E-17	±	1.5E-18	±	99%	1.681	0.00932	± 1.900E-05
		1	7.414E-14	±	4.384E-14	±	5.2E-16	±	3.032E-17	±	1.4E-18	±	98%	1.693	0.00925	± 1.074E-05
(b)au3.4k.san	± 4.029 E-05	2	6.650E-14	±	3.864E-14	±	4.8E-16	±	3.086E-17	±	3.7E-18	±	100%	1.595	0.00982	± 1.553E-05
		3	1.664E-14	±	1.040E-14	±	4.5E-17	±	1.045E-19	±	1.8E-19	±	99%	1.608	0.00974	± 1.520E-05
		4	1.723E-14	±	1.059E-14	±	3.0E-17	±	-9.790E-20	±	6.6E-19	±	99%	1.593	0.00982	± 1.271E-05
		5	2.666E-14	±	1.666E-14	±	4.2E-17	±	8.734E-20	±	3.3E-19	±	100%	1.593	0.00982	± 2.082E-05
au4.3k.san	0.00984	1	1.171E-14	±	7.321E-15	±	1.8E-17	±	-3.686E-20	±	1.2E-19	±	100%	1.593	0.00977	± 1.321E-05
		2	2.917E-14	±	1.804E-14	±	4.7E-17	±	4.285E-20	±	8.4E-19	±	99%	1.603	0.00991	± 1.025E-05
		3	7.296E-14	±	4.562E-14	±	1.2E-16	±	3.598E-19	±	2.9E-18	±	99%	1.580	0.00983	± 1.953E-05
		4	4.727E-14	±	2.855E-14	±	7.5E-17	±	2.390E-19	±	6.0E-18	±	96%	1.593	0.00986	± 8.642E-06
au4.4k.san	± 4.774 E-05	5	6.136E-14	±	3.833E-14	±	9.1E-17	±	1.533E-19	±	1.6E-18	±	99%	1.587	0.00978	± 3.640E-05
		1	1.618E-14	±	1.011E-14	±	2.5E-17	±	3.657E-19	±	-1.5E-20	±	100%	1.601	0.00983	± 1.340E-05
		2	7.686E-14	±	4.784E-14	±	1.2E-16	±	-2.683E-19	±	2.0E-18	±	99%	1.593	0.00944	± 6.538E-06
		3	1.033E-13	±	6.241E-14	±	7.4E-16	±	4.694E-16	±	-8.9E-19	±	100%	1.660	0.00936	± 7.975E-06
au4.4k.san	0.00938	4	8.662E-14	±	5.165E-14	±	6.2E-16	±	3.565E-16	±	6.9E-19	±	100%	1.673	0.00942	± 1.417E-05
		5	9.728E-14	±	5.829E-14	±	6.9E-16	±	5.856E-16	±	1.2E-18	±	100%	1.663	0.00935	± 1.339E-05
		1	1.048E-13	±	6.229E-14	±	7.3E-16	±	4.780E-16	±	1.5E-18	±	100%	1.676	0.00933	± 2.666E-05
au4.5j.san	± 3.496 E-05	2	8.465E-14	±	5.055E-14	±	6.0E-16	±	4.040E-16	±	-8.5E-19	±	100%	1.680	0.00936	± 5.409E-06
		3	1.019E-13	±	6.033E-14	±	7.2E-16	±	5.473E-16	±	3.1E-18	±	99%	1.673	0.00946	± 1.322E-05
		4	7.216E-14	±	4.315E-14	±	5.3E-16	±	3.542E-16	±	2.4E-18	±	99%	1.656	0.00940	± 9.066E-06
		5	6.024E-14	±	3.578E-14	±	4.2E-16	±	4.111E-16	±	2.1E-18	±	99%	1.666	0.00940	± 1.502E-05
		1	6.995E-14	±	4.174E-14	±	4.9E-16	±	3.191E-16	±	1.4E-18	±	99%	1.666	0.00940	± 9.706E-06
		2	1.159E-13	±	6.949E-14	±	8.3E-16	±	5.903E-16	±	3.5E-19	±	100%	1.666	0.00940	

Laser single-crystal measurements of FC-2 (prepared by New Mexico Tech; 20-28 mesh size), and J-values calculated assuming an age of 28.02 Ma (Renne et al., 1998). Data are in moles, corrected for mass discrimination, blank, and interfering nuclear reactions. Errors are quoted as the standard deviation, and a weighted mean J-value is presented for each

APPENDIX B: $^{40}Ar/^{39}Ar$ DATA FOR AGE DETERMINATIONS

CV-1(AU3.3F.mus)	328.6 Ma ± 1.6			J = 0.00920																				
n	^{40}Ar(*+atm)			^{39}Ar(K)			^{38}Ar(Cl+atm)			^{37}Ar(Ca)			^{36}Ar(Atm)			%Rad	R	Age (Ma)		
1	5.486E-14	±	7.4E-17	2.479E-15	±	1.4E-17	2.6E-17	±	3.8E-19	5.3E-19	±	3.5E-18	1.3E-18	±	3.9E-19	99%	21.972	332.3	±	2.0
2	1.132E-13	±	1.4E-16	5.295E-15	±	3.4E-17	6.2E-17	±	7.6E-19	-1.1E-18	±	-3.5E-18	-4.5E-19	±	-3.4E-19	100%	21.396	324.3	±	2.1
3	7.400E-14	±	1.1E-16	3.368E-15	±	2.4E-17	4.0E-17	±	1.4E-18	1.7E-18	±	3.5E-18	3.5E-19	±	3.8E-19	100%	21.941	331.9	±	2.4
4	5.638E-14	±	1.1E-16	2.499E-15	±	1.5E-17	3.3E-17	±	1.3E-18	-1.5E-18	±	-3.3E-18	1.3E-18	±	2.5E-19	99%	22.413	338.3	±	2.1
5	9.950E-14	±	1.1E-16	4.607E-15	±	3.8E-17	5.1E-17	±	1.8E-18	-4.4E-19	±	-3.3E-18	-2.1E-19	±	-2.6E-19	100%	21.613	327.3	±	2.7
6	8.515E-14	±	9.9E-17	3.912E-15	±	1.7E-17	4.7E-17	±	1.6E-18	8.9E-20	±	3.3E-18	1.2E-18	±	3.9E-19	100%	21.679	328.2	±	1.5
7	5.028E-14	±	9.5E-17	2.319E-15	±	2.2E-17	2.5E-17	±	1.5E-18	1.2E-18	±	3.2E-18	6.6E-19	±	3.0E-19	100%	21.593	327.0	±	3.2
8	8.043E-14	±	3.5E-17	3.784E-15	±	1.9E-17	4.3E-17	±	1.2E-18	4.4E-19	±	3.9E-18	-2.4E-19	±	-3.6E-19	100%	21.275	322.6	±	1.6
9	9.221E-14	±	1.3E-16	4.276E-15	±	2.5E-17	4.6E-17	±	4.1E-19	-2.3E-19	±	-3.3E-18	1.2E-18	±	3.3E-19	100%	21.480	325.5	±	1.9
CV-2(AU3.4C.mus)	**321.7 Ma ± 0.6**			**J = 0.00979**																				
n	^{40}Ar(*+atm)			^{39}Ar(K)			^{38}Ar(Cl+atm)			^{37}Ar(Ca)			^{36}Ar(Atm)			%Rad	R	Age (Ma)		
1	1.857E-14	±	5.4E-17	9.324E-16	±	1.9E-18	3.2E-18	±	2.8E-20	2.0E-19	±	8.5E-20	1.5E-19	±	7.2E-20	100%	19.863	320.7	±	1.2
2	9.710E-15	±	2.8E-17	4.896E-16	±	1.5E-18	1.9E-18	±	3.5E-20	3.4E-19	±	8.3E-20	5.5E-20	±	6.0E-20	100%	19.796	319.7	±	1.5
3	8.362E-15	±	2.4E-17	4.242E-16	±	1.5E-18	1.8E-18	±	2.5E-20	3.0E-19	±	8.6E-20	1.5E-20	±	5.5E-20	100%	19.699	318.3	±	1.5
4	1.998E-14	±	2.3E-17	9.973E-16	±	9.5E-19	2.6E-18	±	3.1E-20	1.2E-19	±	8.7E-20	1.1E-19	±	7.6E-20	100%	20.002	322.7	±	0.6
5	1.456E-14	±	6.0E-17	7.300E-16	±	1.6E-18	2.0E-18	±	2.7E-20	9.2E-20	±	6.3E-20	7.5E-20	±	6.4E-20	100%	19.908	321.3	±	1.6
6	9.717E-15	±	8.5E-18	4.825E-16	±	9.7E-19	1.1E-18	±	1.8E-20	-5.5E-20	±	7.7E-20	1.7E-19	±	6.7E-20	99%	20.032	323.2	±	1.0
7	1.680E-14	±	3.7E-17	8.315E-16	±	1.2E-18	1.8E-18	±	2.2E-20	-1.5E-19	±	6.7E-20	2.3E-19	±	6.9E-20	100%	20.119	324.5	±	1.0
8	1.803E-14	±	3.0E-17	9.023E-16	±	1.5E-18	2.2E-18	±	2.7E-20	-7.4E-20	±	8.3E-20	1.9E-19	±	4.9E-20	100%	19.923	321.6	±	0.8
9	1.387E-14	±	2.6E-17	6.875E-16	±	1.9E-18	1.7E-18	±	2.5E-20	-7.7E-20	±	8.7E-20	2.2E-19	±	4.5E-20	100%	20.075	323.8	±	1.1
10	5.531E-15	±	1.7E-17	2.765E-16	±	1.1E-18	7.1E-19	±	2.2E-20	-1.1E-19	±	1.1E-19	1.2E-19	±	5.4E-20	99%	19.874	320.8	±	1.9
CV-3(AU3.4B.mus)	**322.8 Ma ± 2.0**			**J = 0.00979**																				
n	^{40}Ar(*+atm)			^{39}Ar(K)			^{38}Ar(Cl+atm)			^{37}Ar(Ca)			^{36}Ar(Atm)			%Rad	R	Age (Ma)		
1	3.528E-15	±	1.1E-17	1.742E-16	±	3.7E-19	5.8E-19	±	1.9E-20	-2.3E-19	±	7.9E-20	1.5E-19	±	6.8E-20	99%	20.013	322.9	±	2.2
2	7.695E-15	±	1.1E-17	3.801E-16	±	7.0E-19	1.1E-18	±	2.3E-20	-1.3E-19	±	7.3E-20	7.0E-20	±	1.0E-19	100%	20.188	325.5	±	1.5
3	2.115E-15	±	2.9E-18	1.054E-16	±	4.3E-19	4.9E-19	±	3.0E-20	1.3E-20	±	8.9E-20	8.4E-20	±	5.8E-20	99%	19.829	320.2	±	3.0
4	2.344E-15	±	2.8E-18	1.149E-16	±	5.4E-19	2.3E-19	±	1.5E-20	8.0E-20	±	9.5E-20	1.2E-22	±	5.2E-20	100%	20.403	328.6	±	2.7
5	3.102E-15	±	1.8E-18	1.516E-16	±	4.5E-19	3.4E-19	±	1.9E-20	1.1E-20	±	8.2E-20	2.4E-20	±	7.1E-20	100%	20.413	328.8	±	2.4
6	2.417E-15	±	2.6E-18	1.186E-16	±	4.0E-19	2.7E-19	±	1.9E-20	-8.6E-20	±	9.0E-20	3.9E-20	±	5.5E-20	100%	20.285	326.9	±	2.5
7	3.477E-15	±	4.7E-18	1.709E-16	±	6.5E-19	5.7E-19	±	2.3E-20	5.9E-20	±	9.4E-20	1.3E-19	±	6.0E-20	99%	20.123	324.5	±	2.1
8	5.923E-15	±	5.8E-18	2.934E-16	±	8.7E-19	9.5E-19	±	2.2E-20	9.1E-20	±	9.5E-20	5.2E-20	±	5.8E-20	100%	20.136	324.7	±	1.4
9	1.406E-15	±	9.2E-19	7.003E-17	±	3.4E-19	2.6E-19	±	2.2E-20	3.3E-20	±	8.4E-20	8.7E-20	±	5.0E-20	98%	19.710	318.4	±	3.7
10	6.362E-16	±	1.3E-18	3.168E-17	±	2.5E-19	3.5E-19	±	4.1E-20	1.1E-19	±	8.4E-20	1.2E-19	±	5.3E-20	94%	18.949	307.1	±	8.5
CV-4(AU3.4a.mus)	329.0 Ma ± 0.6			J = 0.00979																				
n	^{40}Ar(*+atm)			^{39}Ar(K)			^{38}Ar(Cl+atm)			^{37}Ar(Ca)			^{36}Ar(Atm)			%Rad	R	Age (Ma)		
1	5.648E-15	±	8.4E-18	2.740E-16	±	8.0E-19	7.8E-19	±	2.4E-20	6.6E-20	±	9.9E-20	7.6E-20	±	5.0E-20	100%	20.530	330.5	±	1.4
2	1.090E-14	±	2.5E-17	5.287E-16	±	1.1E-18	1.7E-18	±	3.1E-20	1.2E-19	±	9.1E-20	1.0E-19	±	4.5E-20	100%	20.557	330.9	±	1.1
3	7.291E-15	±	6.1E-18	3.559E-16	±	1.1E-18	1.1E-18	±	2.2E-20	1.7E-19	±	9.3E-20	1.9E-19	±	5.6E-20	99%	20.325	327.5	±	1.3
4	7.968E-15	±	4.4E-18	3.902E-16	±	7.0E-19	1.0E-18	±	1.8E-20	2.1E-20	±	1.2E-19	-1.7E-20	±	-4.3E-20	100%	20.429	329.0	±	0.8
5	1.355E-14	±	1.0E-17	6.614E-16	±	9.3E-19	1.7E-18	±	2.1E-20	-3.4E-20	±	1.0E-19	5.9E-20	±	3.7E-20	100%	20.464	329.5	±	0.6
6	1.163E-14	±	1.2E-17	5.724E-16	±	2.0E-18	1.4E-18	±	2.7E-20	-5.3E-20	±	7.7E-20	2.1E-21	±	4.9E-20	100%	20.311	327.3	±	1.2
7	1.039E-14	±	1.9E-17	5.121E-16	±	2.0E-18	9.9E-19	±	2.1E-20	-1.0E-19	±	8.9E-20	2.8E-20	±	4.1E-20	100%	20.267	326.6	±	1.5
8	6.506E-15	±	1.0E-17	3.189E-16	±	1.6E-18	7.5E-19	±	1.9E-20	-1.5E-19	±	9.0E-20	4.0E-20	±	4.5E-20	100%	20.363	328.1	±	1.8
9	1.451E-14	±	1.2E-17	7.117E-16	±	1.9E-18	1.9E-18	±	2.5E-20	2.4E-20	±	7.1E-20	2.4E-20	±	4.7E-20	100%	20.378	328.3	±	1.0
10	2.630E-15	±	4.8E-18	1.269E-16	±	5.2E-19	3.2E-19	±	1.6E-20	-4.7E-20	±	6.2E-20	2.8E-20	±	5.3E-20	100%	20.649	332.3	±	2.5
Laser muscovite data for this study, with corrections and presentation as in Appendix A.																								

CV-5a(AU3.4D.mus)	331.7 Ma ± 1.6			J = 0.00931																				
n	^{40}Ar(*+atm)			^{39}Ar(K)			^{38}Ar(Cl+atm)			^{37}Ar(Ca)			^{36}Ar(Atm)			%Rad	R	Age (Ma)		
1	6.709E-14	±	1.4E-16	3.109E-15	±	2.5E-17	3.3E-17	±	1.6E-18	1.2E-18	±	3.7E-18	1.4E-18	±	5.2E-19	99%	21.449	327.5	±	2.7
2	3.283E-14	±	6.3E-17	1.463E-15	±	1.3E-17	1.7E-17	±	3.5E-19	-1.7E-18	±	-4.9E-18	2.3E-19	±	3.4E-19	100%	22.384	340.5	±	3.1
3	2.073E-14	±	5.6E-17	9.359E-16	±	1.2E-17	9.3E-18	±	6.9E-19	-3.8E-18	±	-5.0E-18	-2.0E-19	±	-2.1E-19	100%	22.213	338.1	±	4.6
4	1.215E-13	±	1.0E-16	5.635E-15	±	3.3E-17	6.3E-17	±	9.5E-19	1.1E-18	±	5.2E-18	-6.5E-19	±	-2.8E-19	100%	21.588	329.4	±	2.0
5	9.888E-14	±	8.6E-17	4.538E-15	±	1.8E-17	5.5E-17	±	1.1E-18	7.7E-18	±	3.8E-18	1.7E-18	±	5.5E-19	99%	21.679	330.7	±	1.3
6	6.747E-14	±	4.8E-17	3.097E-15	±	2.3E-17	3.5E-17	±	1.5E-18	2.4E-19	±	3.3E-18	6.1E-19	±	3.6E-19	100%	21.726	331.4	±	2.4
7	4.421E-14	±	5.9E-17	2.057E-15	±	1.7E-17	2.4E-17	±	1.0E-18	3.3E-18	±	3.5E-18	1.3E-18	±	4.8E-19	99%	21.298	325.4	±	2.8
8	4.843E-14	±	5.7E-17	2.209E-15	±	1.2E-17	2.5E-17	±	7.6E-19	-1.3E-18	±	-3.9E-18	1.4E-18	±	3.4E-19	99%	21.735	331.5	±	1.8
9	6.249E-14	±	1.2E-16	2.872E-15	±	2.1E-17	3.7E-17	±	7.2E-19	3.7E-18	±	3.6E-18	8.3E-19	±	3.5E-19	100%	21.670	330.6	±	2.5
CV-5b(AU3.2F.mus)	**330.6 Ma ± 1.4**			**J = 0.00938**																				
n	^{40}Ar(*+atm)			^{39}Ar(K)			^{38}Ar(Cl+atm)			^{37}Ar(Ca)			^{36}Ar(Atm)			%Rad	R	Age (Ma)		
1a	5.235E-14	±	1.8E-16	2.427E-15	±	2.4E-17	2.8E-17	±	1.8E-18	1.6E-18	±	3.3E-18	5.4E-19	±	9.9E-19	100%	21.505	328.3	±	3.4
1b	9.177E-15	±	7.2E-17	4.182E-16	±	1.4E-17	5.4E-18	±	1.1E-18	-9.4E-19	±	-2.6E-18	3.2E-19	±	1.0E-18	99%	21.716	331.2	±	11.6
2	5.842E-14	±	1.4E-16	2.687E-15	±	1.8E-17	3.3E-17	±	2.6E-18	-1.3E-18	±	-3.1E-18	8.9E-19	±	1.0E-18	100%	21.641	330.2	±	2.3
3	1.919E-14	±	6.5E-17	8.529E-16	±	1.0E-17	9.0E-18	±	8.8E-19	2.4E-18	±	3.1E-18	1.2E-18	±	1.0E-18	98%	22.090	336.4	±	4.2
4	3.904E-14	±	2.5E-16	1.829E-15	±	2.5E-17	2.2E-17	±	9.6E-19	-6.4E-20	±	-2.6E-18	1.3E-18	±	1.2E-18	99%	21.123	322.9	±	4.8
5	8.050E-14	±	2.3E-16	3.668E-15	±	2.3E-17	4.3E-17	±	1.8E-18	-2.3E-18	±	-3.5E-18	-1.5E-18	±	-4.8E-19	101%	22.073	336.2	±	2.3
6	1.068E-13	±	2.2E-16	4.991E-15	±	4.5E-17	5.6E-17	±	1.5E-18	1.8E-18	±	2.8E-18	-2.8E-18	±	-6.7E-19	101%	21.571	329.2	±	3.0
7	1.022E-13	±	2.3E-16	4.772E-15	±	2.8E-17	5.7E-17	±	1.7E-18	-5.5E-18	±	-2.6E-18	-3.5E-18	±	-3.9E-19	101%	21.642	330.2	±	2.1
8	7.940E-14	±	1.4E-16	3.682E-15	±	2.9E-17	4.2E-17	±	6.6E-19	-1.0E-18	±	-3.1E-18	-1.6E-18	±	-5.2E-19	101%	21.691	330.9	±	2.6
CV-6(AU3.3i.mus)	**322.1 Ma ± 0.8**			**0.00952**																				
n	^{40}Ar(*+atm)			^{39}Ar(K)			^{38}Ar(Cl+atm)			^{37}Ar(Ca)			^{36}Ar(Atm)			%Rad	R	Age (Ma)		
1	1.324E-14	±	1.2E-17	6.399E-16	±	1.4E-18	1.8E-18	±	2.0E-20	-8.2E-20	±	1.3E-19	3.3E-19	±	6.5E-20	99%	20.531	322.0	±	0.9
2	1.330E-14	±	1.2E-17	6.422E-16	±	1.3E-18	1.7E-18	±	2.2E-20	-5.2E-20	±	1.4E-19	5.9E-20	±	5.9E-20	100%	20.685	324.2	±	0.8
3	9.475E-15	±	7.3E-18	4.592E-16	±	1.6E-18	1.1E-18	±	2.6E-20	-1.4E-19	±	1.3E-19	3.1E-20	±	6.0E-20	100%	20.612	323.2	±	1.3
4	9.104E-15	±	2.6E-17	4.417E-16	±	1.1E-18	1.2E-18	±	2.6E-20	-1.3E-19	±	7.3E-20	5.6E-20	±	5.7E-20	100%	20.570	322.6	±	1.4
5	1.814E-14	±	2.6E-17	8.968E-16	±	1.2E-18	2.3E-18	±	3.4E-20	-5.1E-20	±	8.5E-20	1.4E-19	±	5.4E-20	100%	20.184	317.0	±	0.7
6	1.851E-14	±	1.0E-16	9.131E-16	±	2.3E-18	2.3E-18	±	4.0E-20	6.7E-20	±	9.3E-20	4.8E-20	±	5.9E-20	100%	20.259	318.1	±	2.0
7	2.423E-14	±	3.5E-17	1.177E-15	±	2.7E-18	2.7E-18	±	3.0E-20	4.2E-20	±	1.0E-19	3.9E-21	±	9.0E-20	100%	20.593	322.9	±	1.0
8	2.280E-14	±	3.8E-17	1.101E-15	±	2.8E-18	2.7E-18	±	2.2E-20	-3.4E-20	±	1.1E-19	1.4E-20	±	7.4E-20	100%	20.709	324.6	±	1.0
9	3.318E-14	±	6.4E-17	1.609E-15	±	4.3E-18	4.1E-18	±	2.8E-20	8.7E-20	±	1.1E-19	4.2E-20	±	7.0E-20	100%	20.612	323.2	±	1.1
10	1.227E-14	±	4.0E-17	5.965E-16	±	2.8E-18	1.6E-18	±	3.0E-20	-4.0E-20	±	1.1E-19	-7.2E-20	±	-7.7E-20	100%	20.598	323.0	±	1.9
CV-7a(AU3.4E.mus)	**335.5 Ma ± 0.8**			**J = 0.00931**																				
n	^{40}Ar(*+atm)			^{39}Ar(K)			^{38}Ar(Cl+atm)			^{37}Ar(Ca)			^{36}Ar(Atm)			%Rad	R	Age (Ma)		
1	9.410E-14	±	1.4E-16	4.305E-15	±	4.0E-17	4.7E-17	±	1.6E-18	6.2E-18	±	3.9E-18	2.5E-19	±	3.0E-19	100%	21.840	332.9	±	3.1
2	7.438E-14	±	9.2E-17	3.393E-15	±	2.1E-17	3.7E-17	±	4.9E-19	3.5E-19	±	3.9E-18	8.5E-19	±	2.8E-19	100%	21.849	333.1	±	2.1
3	7.924E-14	±	1.0E-16	3.559E-15	±	1.0E-17	3.8E-17	±	5.7E-19	2.1E-18	±	4.0E-18	7.0E-19	±	4.7E-19	100%	22.204	338.0	±	1.1
4	7.464E-14	±	1.0E-16	3.379E-15	±	1.9E-17	4.1E-17	±	1.8E-18	4.3E-19	±	3.7E-18	2.7E-19	±	2.4E-19	100%	22.070	336.1	±	1.9
5	6.813E-14	±	3.2E-16	3.121E-15	±	2.4E-17	3.6E-17	±	9.0E-19	-1.9E-18	±	-3.8E-18	-7.1E-19	±	-2.9E-19	100%	21.897	333.7	±	3.0
6	1.042E-13	±	1.5E-16	4.687E-15	±	1.1E-17	5.2E-17	±	6.7E-19	3.0E-18	±	2.0E-18	8.2E-19	±	2.8E-19	100%	22.189	337.8	±	0.9
7	8.266E-14	±	1.0E-16	3.759E-15	±	1.2E-17	4.3E-17	±	7.4E-19	7.0E-18	±	2.3E-18	8.6E-19	±	3.4E-19	100%	21.919	334.0	±	1.1
8	9.011E-14	±	1.1E-16	4.083E-15	±	3.0E-17	4.6E-17	±	9.1E-19	6.0E-18	±	2.5E-18	5.4E-19	±	3.3E-19	100%	22.033	335.6	±	2.5
9	9.616E-14	±	1.8E-16	4.392E-15	±	3.6E-17	5.1E-17	±	1.7E-18	1.4E-17	±	2.9E-18	4.3E-19	±	4.8E-19	100%	21.867	333.3	±	2.8
10	1.213E-13	±	1.4E-16	5.432E-15	±	3.3E-17	6.5E-17	±	8.1E-19	7.1E-18	±	2.1E-18	-8.3E-19	±	-2.8E-19	100%	22.375	340.4	±	2.1

Laser muscovite data for this study, with corrections and presentation as in Appendix A.

CV-8a(AU3.4F.mus)	331.1 Ma ± 1.1			J = 0.00931																				
n	^{40}Ar(*+atm)			^{39}Ar(K)			^{38}Ar(Cl+atm)			^{37}Ar(Ca)			^{36}Ar(Atm)			%Rad	R	Age (Ma)		
1	2.457E-13	±	8.2E-16	1.165E-14	±	2.5E-17	1.3E-16	±	2.0E-18	5.7E-18	±	3.9E-18	3.2E-18	±	4.5E-19	100%	21.017	321.4	±	1.3
2	1.096E-13	±	2.6E-16	5.011E-15	±	2.4E-17	5.6E-17	±	1.6E-18	-4.4E-18	±	-3.0E-18	2.3E-18	±	3.3E-19	99%	21.745	331.6	±	1.8
3	1.088E-13	±	1.8E-16	5.009E-15	±	2.8E-17	5.1E-17	±	2.0E-18	-6.7E-18	±	-2.6E-18	4.1E-19	±	3.5E-19	100%	21.696	330.9	±	1.9
4	1.293E-13	±	1.8E-16	5.934E-15	±	2.3E-17	6.3E-17	±	1.2E-18	-6.4E-18	±	-2.6E-18	2.3E-18	±	4.8E-19	99%	21.679	330.7	±	1.3
5	1.044E-13	±	2.3E-16	4.777E-15	±	2.1E-17	5.3E-17	±	1.2E-18	-2.7E-18	±	-3.0E-18	1.1E-18	±	2.8E-19	100%	21.791	332.3	±	1.6
6	7.817E-14	±	1.7E-16	3.595E-15	±	2.3E-17	4.1E-17	±	8.4E-19	-7.8E-18	±	-3.8E-18	-4.1E-20	±	-3.7E-19	100%	21.747	331.6	±	2.2
7	7.853E-14	±	1.4E-16	3.562E-15	±	8.1E-18	4.1E-17	±	9.6E-19	-2.2E-18	±	-3.9E-18	8.6E-19	±	4.2E-19	100%	21.977	334.8	±	1.0
8	8.792E-14	±	1.5E-16	4.030E-15	±	3.8E-17	4.4E-17	±	8.3E-19	-3.0E-18	±	-4.0E-18	1.1E-18	±	3.5E-19	100%	21.734	331.5	±	3.2
9	7.164E-14	±	1.3E-16	3.258E-15	±	2.0E-17	3.6E-17	±	5.0E-19	-6.1E-18	±	-3.8E-18	9.3E-19	±	3.9E-19	100%	21.906	333.9	±	2.2
10	6.867E-14	±	8.8E-17	3.149E-15	±	2.6E-17	3.6E-17	±	3.9E-19	-1.9E-18	±	-4.0E-18	5.7E-19	±	4.1E-19	100%	21.754	331.7	±	2.8
CV-8b(AU3.2E.mus)	**335.5 Ma ± 2.1**			**J = 0.00938**																				
n	^{40}Ar(*+atm)			^{39}Ar(K)			^{38}Ar(Cl+atm)			^{37}Ar(Ca)			^{36}Ar(Atm)			%Rad	R	Age (Ma)		
1	1.144E-13	±	2.2E-16	5.197E-15	±	1.5E-17	6.0E-17	±	1.2E-18	5.7E-18	±	4.1E-18	1.0E-18	±	1.0E-18	100%	21.947	334.4	±	1.1
2	5.942E-14	±	1.5E-16	2.730E-15	±	3.1E-17	3.2E-17	±	9.3E-19	-1.7E-18	±	-3.6E-18	-7.2E-19	±	-9.8E-19	100%	21.840	332.9	±	3.8
3	1.391E-13	±	3.1E-16	6.272E-15	±	3.7E-17	7.8E-17	±	9.7E-19	6.4E-18	±	4.1E-18	2.1E-19	±	1.1E-18	100%	22.170	337.5	±	2.1
4	4.786E-14	±	1.2E-16	2.146E-15	±	1.5E-17	2.9E-17	±	1.7E-18	1.1E-18	±	3.5E-18	-9.5E-19	±	-9.8E-19	101%	22.431	341.1	±	2.5
5	1.025E-13	±	2.5E-16	4.572E-15	±	3.0E-17	5.5E-17	±	2.0E-18	4.4E-18	±	3.4E-18	-2.2E-19	±	-9.1E-19	100%	22.437	341.2	±	2.4
6	3.866E-14	±	9.3E-17	1.855E-15	±	2.0E-17	2.0E-17	±	1.3E-18	2.5E-18	±	3.4E-18	-1.3E-18	±	-8.9E-19	101%	21.037	321.7	±	3.6
7a	1.716E-14	±	8.9E-17	7.922E-16	±	1.9E-17	1.1E-17	±	1.1E-18	-2.3E-18	±	-3.3E-18	-1.4E-18	±	-9.3E-19	102%	22.164	337.4	±	8.3
7b	5.778E-14	±	9.7E-17	2.611E-15	±	3.7E-17	3.2E-17	±	1.4E-18	5.0E-18	±	3.6E-18	-4.4E-19	±	-9.5E-19	100%	22.183	337.7	±	4.9
CV-9(AU3.3H.mus)	**321.4 Ma ± 0.3**			**J = 0.00952**																				
n	^{40}Ar(*+atm)			^{39}Ar(K)			^{38}Ar(Cl+atm)			^{37}Ar(Ca)			^{36}Ar(Atm)			%Rad	R	Age (Ma)		
1	1.616E-14	±	9.7E-18	8.133E-16	±	2.4E-18	2.1E-18	±	3.0E-20	6.9E-20	±	8.9E-20	7.0E-20	±	9.2E-20	100%	19.842	320.4	±	1.1
2	9.758E-15	±	8.3E-18	4.892E-16	±	9.1E-19	1.1E-18	±	2.2E-20	8.2E-20	±	8.3E-20	1.0E-19	±	9.5E-20	100%	19.884	321.0	±	1.1
3	1.174E-14	±	1.5E-17	5.862E-16	±	1.0E-18	1.5E-18	±	2.2E-20	9.5E-20	±	8.9E-20	1.3E-19	±	9.1E-20	100%	19.961	322.1	±	1.0
4	2.369E-14	±	3.0E-17	1.193E-15	±	3.5E-18	3.2E-18	±	3.4E-20	-4.8E-20	±	1.1E-19	1.5E-19	±	8.8E-20	100%	19.818	320.0	±	1.1
5	2.180E-14	±	3.0E-17	1.090E-15	±	3.6E-18	2.6E-18	±	2.6E-20	1.4E-19	±	1.1E-19	1.2E-19	±	8.8E-20	100%	19.961	322.1	±	1.2
6	2.468E-14	±	2.1E-17	1.238E-15	±	1.8E-18	3.2E-18	±	2.9E-20	4.6E-20	±	7.0E-20	1.6E-19	±	1.1E-19	100%	19.893	321.1	±	0.7
7	2.145E-14	±	2.7E-17	1.074E-15	±	3.2E-18	2.6E-18	±	3.0E-20	8.7E-20	±	7.1E-20	1.1E-19	±	5.2E-20	100%	19.946	321.9	±	1.1
8	2.396E-14	±	3.5E-17	1.202E-15	±	3.3E-18	3.2E-18	±	3.0E-20	1.4E-19	±	6.1E-20	1.2E-19	±	6.4E-20	100%	19.904	321.3	±	1.0
9	1.526E-14	±	1.6E-17	7.630E-16	±	2.3E-18	1.8E-18	±	2.0E-20	1.2E-19	±	5.7E-20	9.9E-20	±	6.0E-20	100%	19.954	322.0	±	1.1
10	9.798E-15	±	1.2E-17	4.900E-16	±	1.3E-18	1.3E-18	±	2.1E-20	1.0E-19	±	5.9E-20	8.8E-21	±	5.5E-20	100%	19.991	322.6	±	1.1
CV-10a(AU3.4G.mus)	**329.6 Ma ± 0.8**			**J = 0.00931**																				
n	^{40}Ar(*+atm)			^{39}Ar(K)			^{38}Ar(Cl+atm)			^{37}Ar(Ca)			^{36}Ar(Atm)			%Rad	R	Age (Ma)		
1	7.557E-14	±	2.5E-16	3.498E-15	±	1.0E-17	4.1E-17	±	1.7E-18	6.6E-18	±	4.5E-18	1.3E-19	±	8.0E-19	100%	21.589	329.4	±	1.5
2	1.009E-13	±	2.2E-16	4.628E-15	±	6.9E-18	5.2E-17	±	2.0E-18	2.3E-17	±	4.0E-18	4.7E-18	±	1.1E-18	99%	21.508	328.3	±	0.9
3	1.400E-13	±	1.9E-16	6.431E-15	±	2.3E-17	8.0E-17	±	2.9E-18	3.7E-17	±	3.8E-18	-5.3E-19	±	-6.3E-19	100%	21.794	332.3	±	1.3
4	1.038E-13	±	2.1E-16	4.736E-15	±	3.0E-17	6.0E-17	±	1.6E-18	9.7E-18	±	5.1E-18	5.6E-18	±	1.7E-18	98%	21.558	329.0	±	2.2
5	1.102E-13	±	1.6E-16	4.999E-15	±	4.9E-17	6.1E-17	±	1.9E-18	1.7E-16	±	9.6E-18	3.8E-18	±	1.7E-18	99%	21.818	332.6	±	3.3
6	1.380E-13	±	2.1E-16	6.375E-15	±	3.7E-17	7.6E-17	±	2.6E-18	2.1E-17	±	5.8E-18	2.0E-18	±	1.7E-18	100%	21.556	329.0	±	2.0
7	1.218E-13	±	8.8E-17	5.610E-15	±	2.8E-17	6.5E-17	±	1.6E-18	5.0E-18	±	3.5E-18	1.4E-18	±	3.5E-19	100%	21.644	330.2	±	1.7
8	9.445E-14	±	1.1E-16	4.324E-15	±	1.6E-17	5.1E-17	±	1.8E-18	7.0E-18	±	4.1E-18	2.2E-18	±	4.5E-19	99%	21.696	330.9	±	1.3
9	1.194E-13	±	2.1E-16	5.607E-15	±	1.1E-17	6.3E-17	±	2.3E-18	1.2E-17	±	3.5E-18	8.3E-19	±	4.4E-19	100%	21.254	324.8	±	0.8

Laser muscovite data for this study, with corrections and presentation as in Appendix A.

WM-1a(AU4.3B.mus)	337.6 Ma ± 0.5						J = 0.00984																	
n	^{40}Ar(*+atm)			^{39}Ar(K)			^{38}Ar(Cl+atm)			^{37}Ar(Ca)			^{36}Ar(Atm)			%Rad	R	Age (Ma)		
1	3.567E-15	±	4.7E-18	1.677E-16	±	7.3E-19	4.4E-19	±	2.9E-20	-3.9E-20	±	2.0E-19	2.3E-19	±	8.2E-20	98%	20.848	336.6	±	2.8
2	4.957E-15	±	1.0E-17	2.336E-16	±	9.3E-19	6.2E-19	±	4.0E-20	6.6E-20	±	1.9E-19	1.9E-19	±	1.5E-19	99%	20.986	338.7	±	3.4
3	3.916E-15	±	3.9E-18	1.813E-16	±	1.1E-18	4.1E-19	±	3.2E-20	3.4E-20	±	2.0E-19	3.9E-19	±	8.2E-20	97%	20.960	338.3	±	3.0
4	7.523E-15	±	1.1E-17	3.553E-16	±	8.4E-19	1.3E-18	±	5.0E-20	2.4E-19	±	2.2E-19	3.8E-19	±	7.8E-20	99%	20.855	336.8	±	1.4
5	9.168E-15	±	9.6E-18	4.292E-16	±	1.3E-18	1.5E-18	±	5.0E-20	-7.6E-20	±	2.2E-19	7.1E-19	±	1.2E-19	98%	20.870	337.0	±	1.7
6	3.989E-15	±	5.7E-18	1.823E-16	±	4.9E-19	7.6E-19	±	5.0E-20	1.4E-19	±	2.3E-19	5.9E-19	±	9.3E-20	96%	20.920	337.7	±	2.7
7	3.415E-15	±	4.1E-18	1.575E-16	±	8.9E-19	6.6E-19	±	4.9E-20	1.3E-20	±	2.0E-19	4.0E-19	±	8.9E-20	97%	20.930	337.9	±	3.4
8	2.923E-15	±	3.5E-18	1.353E-16	±	6.8E-19	5.1E-19	±	3.2E-20	1.7E-19	±	2.1E-19	3.9E-19	±	1.2E-19	96%	20.754	335.3	±	4.5
9	3.938E-15	±	6.0E-18	1.837E-16	±	7.6E-19	3.6E-19	±	3.3E-20	-7.0E-20	±	2.2E-19	2.3E-19	±	8.4E-20	98%	21.071	339.9	±	2.7
WM-2(AU4.3C.mus)	**315.5 Ma ± 0.5**						**J = 0.00984**																	
n	^{40}Ar(*+atm)			^{39}Ar(K)			^{38}Ar(Cl+atm)			^{37}Ar(Ca)			^{36}Ar(Atm)			%Rad	R	Age (Ma)		
1	6.376E-15	±	1.1E-17	3.228E-16	±	1.3E-18	6.6E-19	±	2.4E-20	-1.2E-19	±	2.1E-19	2.8E-19	±	1.1E-19	99%	19.496	316.6	±	2.1
2	6.662E-15	±	4.8E-18	3.427E-16	±	1.4E-18	4.7E-19	±	2.3E-20	3.5E-20	±	1.8E-19	1.1E-19	±	8.7E-20	100%	19.342	314.3	±	1.8
3	1.052E-14	±	6.3E-18	5.367E-16	±	1.6E-18	1.4E-18	±	3.0E-20	-8.9E-20	±	1.7E-19	1.9E-19	±	1.6E-19	99%	19.494	316.6	±	1.7
4	7.254E-15	±	1.8E-17	3.699E-16	±	7.3E-19	7.4E-19	±	2.9E-20	-2.7E-20	±	1.6E-19	1.9E-19	±	1.0E-19	99%	19.460	316.1	±	1.7
5	7.650E-15	±	1.4E-17	3.936E-16	±	1.1E-18	1.1E-18	±	4.0E-20	6.5E-20	±	1.2E-19	1.2E-20	±	9.2E-20	100%	19.425	315.6	±	1.5
6	5.682E-15	±	3.1E-18	2.933E-16	±	1.0E-18	6.3E-19	±	2.7E-20	2.2E-19	±	1.0E-19	-2.9E-20	±	-1.2E-19	100%	19.404	315.3	±	2.2
7	5.772E-15	±	1.8E-17	2.996E-16	±	1.7E-18	9.1E-19	±	4.2E-20	-1.6E-20	±	1.9E-19	7.8E-20	±	1.0E-19	100%	19.186	312.0	±	2.6
8	6.717E-15	±	6.0E-18	3.416E-16	±	1.1E-18	1.1E-18	±	4.7E-20	3.5E-20	±	1.3E-19	1.5E-19	±	1.0E-19	99%	19.535	317.2	±	1.8
9	5.297E-15	±	4.0E-18	2.693E-16	±	9.6E-19	5.6E-19	±	2.9E-20	1.6E-20	±	1.6E-19	1.8E-19	±	8.4E-20	99%	19.477	316.3	±	1.9
10	5.317E-15	±	6.1E-18	2.645E-16	±	1.1E-18	6.7E-19	±	4.0E-20	2.1E-22	±	1.5E-19	6.2E-19	±	1.2E-19	97%	19.413	315.4	±	2.6
WM-3(AU4.3d.mus)	**337.3 Ma ± 2.3**						**J = 0.00984**																	
n	^{40}Ar(*+atm)			^{39}Ar(K)			^{38}Ar(Cl+atm)			^{37}Ar(Ca)			^{36}Ar(Atm)			%Rad	R	Age (Ma)		
1	4.811E-15	±	8.4E-18	2.314E-16	±	6.7E-19	5.0E-19	±	4.1E-20	-1.6E-19	±	1.6E-19	-7.5E-20	±	-1.1E-19	100%	20.889	337.3	±	2.5
2	8.862E-15	±	1.0E-17	4.177E-16	±	1.1E-18	1.3E-18	±	4.1E-20	-2.8E-19	±	2.1E-19	-2.7E-21	±	-1.3E-19	100%	21.219	342.1	±	1.8
3	2.891E-15	±	4.8E-18	1.366E-16	±	9.2E-19	3.2E-19	±	3.4E-20	1.0E-20	±	1.6E-19	-7.9E-20	±	-7.7E-20	101%	21.325	343.7	±	3.6
4	2.643E-15	±	5.5E-18	1.236E-16	±	8.4E-19	1.7E-19	±	1.8E-20	1.3E-19	±	2.0E-19	1.3E-19	±	1.1E-19	99%	21.080	340.1	±	5.0
5	2.730E-15	±	5.3E-18	1.334E-16	±	6.3E-19	2.9E-19	±	2.2E-20	2.4E-19	±	2.2E-19	1.7E-19	±	1.1E-19	98%	20.081	325.3	±	4.4
6	3.244E-15	±	6.7E-18	1.579E-16	±	1.0E-18	2.9E-19	±	2.2E-20	3.1E-19	±	2.1E-19	1.4E-19	±	1.2E-19	99%	20.296	328.5	±	4.3
7	2.615E-15	±	3.6E-18	1.228E-16	±	6.4E-19	1.8E-19	±	1.5E-20	-5.5E-21	±	1.3E-19	-3.0E-20	±	-8.6E-20	100%	21.369	344.3	±	3.8
8	3.755E-15	±	3.9E-18	1.757E-16	±	6.1E-19	2.9E-19	±	2.1E-20	2.1E-19	±	1.4E-19	-3.7E-21	±	-1.0E-19	100%	21.380	344.5	±	3.1
9	6.250E-16	±	3.8E-18	2.887E-17	±	4.0E-19	-1.2E-19	±	-9.2E-20	2.1E-19	±	1.6E-19	7.4E-20	±	1.2E-19	97%	20.896	337.3	±	20.3
10	4.820E-15	±	1.2E-17	2.333E-16	±	1.0E-18	7.4E-19	±	3.8E-20	2.5E-19	±	1.5E-19	1.9E-19	±	1.4E-19	99%	20.418	330.3	±	3.3
WM-4(AU4.3E.mus)	**346.1 Ma ± 3.5**						**J = 0.00984**																	
n	^{40}Ar(*+atm)			^{39}Ar(K)			^{38}Ar(Cl+atm)			^{37}Ar(Ca)			^{36}Ar(Atm)			%Rad	R	Age (Ma)		
1	5.538E-15	±	4.3E-18	2.606E-16	±	1.1E-18	7.8E-19	±	5.1E-20	2.8E-19	±	1.8E-19	5.2E-19	±	1.7E-19	97.2%	20.659	333.9	±	3.4
2	7.470E-15	±	9.1E-18	3.566E-16	±	1.6E-18	7.2E-19	±	3.0E-20	9.6E-20	±	2.1E-19	1.9E-19	±	1.5E-19	99.2%	20.783	335.7	±	2.6
3	8.184E-15	±	7.8E-18	3.858E-16	±	1.3E-18	6.7E-19	±	3.2E-20	-6.9E-20	±	2.9E-19	1.0E-19	±	1.1E-19	99.6%	21.135	340.9	±	1.8
4	5.241E-15	±	5.9E-18	2.387E-16	±	1.0E-18	4.9E-19	±	2.8E-20	-7.0E-20	±	2.8E-19	1.4E-19	±	1.3E-19	99.2%	21.784	350.4	±	3.1
5	5.036E-15	±	3.7E-18	2.378E-16	±	7.0E-19	3.7E-19	±	3.7E-20	5.2E-20	±	2.5E-19	-7.5E-20	±	-9.4E-20	100.4%	21.269	342.8	±	2.2
6	8.502E-15	±	7.2E-18	3.972E-16	±	1.8E-18	1.6E-18	±	5.8E-20	-4.0E-20	±	1.7E-19	-1.4E-20	±	-1.0E-19	100.0%	21.417	345.0	±	2.0
7	3.553E-15	±	4.5E-18	1.601E-16	±	7.5E-19	7.3E-19	±	7.9E-20	9.9E-20	±	2.0E-19	2.6E-20	±	1.2E-19	99.8%	22.149	355.7	±	3.9
8	6.852E-15	±	5.2E-18	3.289E-16	±	7.5E-19	1.3E-18	±	5.8E-20	-3.7E-19	±	2.4E-19	4.7E-20	±	1.2E-19	99.8%	20.788	335.8	±	1.9
9	3.166E-15	±	4.1E-18	1.425E-16	±	1.1E-18	7.6E-19	±	6.7E-20	-1.9E-19	±	2.1E-19	1.9E-19	±	1.4E-19	98.2%	21.821	350.9	±	5.4
10	4.302E-15	±	5.8E-18	1.860E-16	±	7.5E-19	7.8E-19	±	5.8E-20	-3.6E-19	±	2.1E-19	-2.2E-20	±	-1.4E-19	100.2%	23.159	370.4	±	3.8

Laser muscovite data for this study, with corrections and presentation as in Appendix A.

WM-5(AU4.3F.mus)	328.6 Ma ± 1.1	J = 0.00984								
n	^{40}Ar(*+atm)	^{39}Ar(K)	^{38}Ar(Cl+atm)	^{37}Ar(Ca)	^{36}Ar(Atm)	%Rad	R	Age (Ma)		
1	6.685E-15 ± 1.9E-17	3.144E-16 ± 1.0E-18	8.8E-19 ± 3.0E-20	2.5E-19 ± 1.6E-19	8.9E-19 ± 1.0E-19	96%	20.422	330.4	±	2.2
2	4.044E-15 ± 3.8E-18	1.959E-16 ± 5.1E-19	5.4E-19 ± 4.3E-20	5.2E-20 ± 1.4E-19	3.4E-19 ± 1.3E-19	98%	20.133	326.1	±	3.3
3	7.834E-15 ± 1.4E-17	3.920E-16 ± 1.3E-18	9.1E-19 ± 2.9E-20	5.7E-19 ± 1.6E-19	4.2E-20 ± 1.0E-19	100%	19.952	323.4	±	1.8
4	4.659E-15 ± 1.9E-17	2.281E-16 ± 1.1E-18	5.7E-19 ± 3.0E-20	3.4E-19 ± 1.8E-19	1.3E-19 ± 1.2E-19	99%	20.265	328.0	±	3.3
5	6.947E-15 ± 1.0E-17	3.401E-16 ± 1.4E-18	1.0E-18 ± 3.8E-20	4.6E-19 ± 1.4E-19	9.9E-20 ± 1.5E-19	100%	20.338	329.1	±	2.5
6	8.985E-15 ± 9.8E-18	4.438E-16 ± 8.9E-19	1.4E-18 ± 4.5E-20	4.1E-19 ± 1.8E-19	7.9E-20 ± 1.1E-19	100%	20.193	327.0	±	1.4
7	2.182E-15 ± 2.0E-18	1.054E-16 ± 5.4E-19	6.8E-19 ± 8.0E-20	1.9E-19 ± 2.0E-19	2.7E-20 ± 1.1E-19	100%	20.621	333.3	±	5.2
8	8.232E-15 ± 1.1E-17	3.971E-16 ± 1.7E-18	1.1E-18 ± 4.2E-20	3.7E-19 ± 1.5E-19	1.3E-19 ± 1.3E-19	100%	20.629	333.4	±	2.2
9	9.365E-15 ± 1.3E-17	4.612E-16 ± 2.3E-18	8.6E-19 ± 2.6E-20	3.8E-19 ± 1.6E-19	2.3E-19 ± 1.2E-19	99%	20.156	326.4	±	2.1
10	7.880E-15 ± 9.8E-18	3.838E-16 ± 6.9E-19	8.1E-19 ± 3.7E-20	2.6E-19 ± 1.2E-19	2.4E-19 ± 1.2E-19	99%	20.346	329.2	±	1.7
WM-6(AU4.3G.mus)	**351.1 Ma ± 1.7**	**J = 0.00984**								
n	^{40}Ar(*+atm)	^{39}Ar(K)	^{38}Ar(Cl+atm)	^{37}Ar(Ca)	^{36}Ar(Atm)	%Rad	R	Age (Ma)		
1	6.012E-15 ± 4.5E-18	2.426E-16 ± 2.0E-18	1.2E-18 ± 6.3E-20	9.8E-20 ± 1.5E-19	2.6E-18 ± 1.0E-19	87%	21.663	348.6	±	3.9
2	6.752E-15 ± 7.7E-18	2.825E-16 ± 1.1E-18	9.8E-19 ± 4.2E-20	5.3E-21 ± 1.8E-19	2.2E-18 ± 9.7E-20	90%	21.559	347.1	±	2.3
3	7.424E-15 ± 7.9E-18	3.244E-16 ± 1.2E-18	9.4E-19 ± 5.2E-20	6.8E-20 ± 1.6E-19	1.4E-18 ± 1.1E-19	94%	21.611	347.9	±	2.1
4	6.923E-15 ± 8.8E-18	2.826E-16 ± 8.3E-19	1.4E-18 ± 6.4E-20	-1.0E-19 ± 1.4E-19	2.4E-18 ± 1.4E-19	90%	21.940	352.7	±	2.7
5	6.011E-15 ± 8.5E-18	2.504E-16 ± 8.9E-19	1.2E-18 ± 6.4E-20	2.3E-20 ± 1.5E-19	1.9E-18 ± 1.2E-19	91%	21.810	350.8	±	2.8
6	3.823E-15 ± 2.6E-18	1.648E-16 ± 8.8E-19	1.1E-18 ± 6.4E-20	1.3E-19 ± 1.8E-19	1.0E-18 ± 1.2E-19	92%	21.336	343.8	±	3.9
7	1.493E-14 ± 1.9E-17	6.125E-16 ± 3.4E-18	2.8E-18 ± 7.7E-20	1.5E-19 ± 2.0E-19	5.7E-18 ± 1.5E-19	89%	21.628	348.1	±	2.5
8	6.671E-15 ± 7.4E-18	2.727E-16 ± 7.8E-19	1.4E-18 ± 6.4E-20	1.7E-19 ± 2.1E-19	2.2E-18 ± 1.3E-19	90%	22.057	354.4	±	2.6
9	5.513E-15 ± 4.0E-18	2.230E-16 ± 9.3E-19	1.2E-18 ± 8.1E-20	9.3E-20 ± 1.7E-19	1.7E-18 ± 1.5E-19	91%	22.421	359.7	±	3.6
10	5.534E-15 ± 1.4E-17	2.283E-16 ± 9.5E-19	1.2E-18 ± 6.5E-20	1.1E-19 ± 1.4E-19	1.5E-18 ± 1.3E-19	92%	22.305	358.0	±	3.3
WM-7a(AU4.3H.mus)	**338.6 Ma ± 0.7**	**J = 0.00984**								
n	^{40}Ar(*+atm)	^{39}Ar(K)	^{38}Ar(Cl+atm)	^{37}Ar(Ca)	^{36}Ar(Atm)	%Rad	R	Age (Ma)		
1	3.580E-15 ± 8.2E-18	1.677E-16 ± 7.3E-19	4.4E-19 ± 2.9E-20	-3.9E-20 ± 2.0E-19	2.3E-19 ± 8.2E-20	98%	20.926	337.8	±	2.9
2	4.957E-15 ± 1.0E-17	2.336E-16 ± 9.3E-19	6.2E-19 ± 4.0E-20	6.6E-20 ± 1.9E-19	1.9E-19 ± 1.5E-19	99%	20.986	338.7	±	3.4
3	3.928E-15 ± 6.6E-18	1.813E-16 ± 1.1E-18	4.1E-19 ± 3.2E-20	3.4E-20 ± 2.0E-19	3.9E-19 ± 8.2E-20	97%	21.022	339.2	±	3.1
4	7.521E-15 ± 1.1E-17	3.552E-16 ± 8.5E-19	1.3E-18 ± 5.3E-20	5.5E-20 ± 1.5E-19	3.7E-19 ± 9.3E-20	99%	20.863	336.9	±	1.6
5	9.166E-15 ± 9.6E-18	4.291E-16 ± 1.3E-18	1.6E-18 ± 5.3E-20	-2.6E-19 ± 1.5E-19	7.1E-19 ± 1.3E-19	98%	20.876	337.1	±	1.8
6	3.987E-15 ± 5.6E-18	1.821E-16 ± 5.1E-19	7.8E-19 ± 5.3E-20	-4.5E-20 ± 1.6E-19	5.9E-19 ± 1.1E-19	96%	20.935	337.9	±	3.0
7	8.102E-15 ± 1.1E-17	3.671E-16 ± 1.6E-18	1.2E-18 ± 4.6E-20	1.2E-19 ± 1.6E-19	9.4E-19 ± 1.1E-19	97%	21.314	343.5	±	2.1
8	3.428E-15 ± 5.6E-18	1.574E-16 ± 9.0E-19	6.9E-19 ± 5.3E-20	-1.8E-19 ± 1.3E-19	3.9E-19 ± 1.0E-19	97%	21.041	339.5	±	3.7
9	2.921E-15 ± 3.5E-18	1.352E-16 ± 7.0E-19	5.4E-19 ± 3.6E-20	-1.5E-20 ± 1.4E-19	3.8E-19 ± 1.3E-19	96%	20.774	335.6	±	4.9
10	3.936E-15 ± 6.0E-18	1.836E-16 ± 7.8E-19	3.8E-19 ± 3.6E-20	-2.6E-19 ± 1.6E-19	2.2E-19 ± 9.8E-20	98%	21.086	340.1	±	3.0
WM-9a(AU4.4D.mus)	**360.6 Ma ± 1.5**	**J = 0.00938**								
n	^{40}Ar(*+atm)	^{39}Ar(K)	^{38}Ar(Cl+atm)	^{37}Ar(Ca)	^{36}Ar(Atm)	%Rad	R	Age (Ma)		
1	3.088E-14 ± 3.7E-17	1.266E-15 ± 2.2E-18	1.5E-17 ± 5.0E-19	1.3E-19 ± 1.3E-18	1.8E-18 ± 2.4E-19	98%	23.976	366.4	±	1.2
2	4.612E-14 ± 4.2E-17	1.936E-15 ± 5.2E-18	2.3E-17 ± 3.2E-19	-3.5E-19 ± -1.2E-18	5.8E-19 ± 2.6E-19	100%	23.740	363.1	±	1.2
3	3.579E-14 ± 7.8E-17	1.542E-15 ± 3.2E-18	1.7E-17 ± 4.9E-19	1.9E-18 ± 1.2E-18	3.7E-19 ± 2.3E-19	100%	23.138	354.7	±	1.3
4	7.307E-15 ± 8.0E-18	3.172E-16 ± 1.6E-18	2.8E-18 ± 3.8E-19	2.2E-18 ± 1.2E-18	-3.1E-19 ± -2.3E-19	101%	23.323	357.3	±	3.7
5	2.444E-14 ± 2.7E-17	1.044E-15 ± 3.2E-18	1.2E-17 ± 4.9E-19	-1.9E-20 ± -1.4E-18	5.7E-19 ± 2.4E-19	99%	23.248	356.3	±	1.6
6	1.194E-14 ± 2.0E-17	4.938E-16 ± 3.1E-18	6.2E-18 ± 3.4E-19	6.0E-19 ± 1.4E-18	2.9E-19 ± 2.1E-19	99%	23.998	366.7	±	3.1
7	2.248E-14 ± 2.5E-17	9.516E-16 ± 3.0E-18	1.1E-17 ± 3.5E-19	1.6E-18 ± 1.4E-18	9.3E-19 ± 2.0E-19	99%	23.339	357.5	±	1.5
8	1.528E-14 ± 2.2E-17	6.479E-16 ± 2.5E-18	7.9E-18 ± 4.7E-19	4.1E-19 ± 1.0E-18	1.2E-19 ± 2.5E-19	100%	23.533	360.2	±	2.3
9	3.182E-14 ± 3.6E-17	1.319E-15 ± 2.7E-18	1.5E-17 ± 3.5E-19	-2.3E-19 ± -9.3E-19	6.0E-19 ± 2.7E-19	99%	23.984	366.5	±	1.3
10	1.552E-14 ± 1.8E-17	6.589E-16 ± 2.1E-18	8.0E-18 ± 4.3E-19	-3.9E-19 ± -1.3E-18	5.2E-19 ± 2.9E-19	99%	23.313	357.2	±	2.3
Laser muscovite data for this study, with corrections and presentation as in Appendix A.										

WM-9b(AU4.4B.mus)				**389.5 Ma ± 10.7**			**J = 0.00938**													
n	$^{40}Ar(*+atm)$			$^{39}Ar(K)$			$^{38}Ar(Cl+atm)$			$^{37}Ar(Ca)$			$^{36}Ar(Atm)$			%Rad	R	Age (Ma)		
1	1.759E-14	±	2.5E-17	6.587E-16	±	2.1E-18	8.1E-18	±	3.9E-19	1.7E-18	±	1.4E-18	2.3E-18	±	1.9E-19	96%	25.690	389.9	±	1.9
2	5.961E-15	±	8.0E-18	2.249E-16	±	1.6E-18	2.7E-18	±	3.1E-19	-9.9E-19	±	-1.6E-18	1.0E-18	±	1.5E-19	95%	25.157	382.6	±	4.2
3	2.374E-14	±	1.3E-17	9.242E-16	±	3.1E-18	1.2E-17	±	2.6E-19	1.0E-18	±	1.6E-18	3.0E-18	±	1.6E-19	96%	24.735	376.8	±	1.5
4	5.144E-15	±	6.5E-18	2.023E-16	±	1.5E-18	2.6E-18	±	3.3E-19	-5.7E-19	±	-8.7E-19	3.4E-19	±	2.1E-19	98%	24.930	379.5	±	5.5
5	2.130E-14	±	1.7E-17	8.821E-16	±	1.5E-18	1.1E-17	±	2.1E-19	1.8E-18	±	1.0E-18	1.6E-18	±	2.1E-19	98%	23.622	361.4	±	1.3
6	1.059E-14	±	1.3E-17	3.149E-16	±	1.7E-18	4.3E-18	±	3.6E-19	5.5E-18	±	1.1E-18	1.2E-18	±	2.0E-19	97%	32.484	480.3	±	3.9
7	9.971E-15	±	1.3E-17	3.544E-16	±	3.1E-18	4.5E-18	±	3.3E-19	1.2E-18	±	1.1E-18	1.9E-18	±	1.4E-19	94%	26.533	401.4	±	4.2
8	6.023E-15	±	8.0E-18	2.413E-16	±	1.2E-18	3.3E-18	±	3.1E-19	-2.0E-19	±	-9.5E-19	6.4E-19	±	2.0E-19	97%	24.183	369.2	±	4.3
9	3.210E-14	±	4.0E-17	1.288E-15	±	3.5E-18	1.5E-17	±	2.5E-19	2.7E-18	±	1.1E-18	3.5E-18	±	2.4E-19	97%	24.105	368.1	±	1.4
10	3.478E-14	±	4.8E-17	1.323E-15	±	4.2E-18	1.7E-17	±	4.6E-19	4.8E-18	±	1.2E-18	4.1E-18	±	2.2E-19	97%	25.378	385.6	±	1.6
WM-9c(AU4.4E.mus)				**443.9 Ma ± 27.6**			**J = 0.00938**													
n	$^{40}Ar(*+atm)$			$^{39}Ar(K)$			$^{38}Ar(Cl+atm)$			$^{37}Ar(Ca)$			$^{36}Ar(Atm)$			%Rad	R	Age (Ma)		
1	1.624E-14	±	2.3E-17	5.840E-16	±	2.4E-18	6.6E-18	±	3.0E-19	-1.3E-18	±	-8.9E-19	1.6E-18	±	2.2E-19	97%	27.020	408.0	±	2.5
2	3.182E-14	±	4.1E-17	1.238E-15	±	2.0E-18	1.5E-17	±	4.1E-19	2.2E-18	±	8.9E-19	3.0E-18	±	2.6E-19	97%	24.987	380.3	±	1.2
3	3.434E-14	±	3.6E-17	6.972E-16	±	3.5E-18	8.5E-18	±	3.4E-19	3.3E-18	±	1.3E-18	3.8E-18	±	2.5E-19	97%	47.637	667.0	±	3.9
4	4.187E-14	±	7.2E-17	1.632E-15	±	4.4E-18	2.0E-17	±	5.0E-19	-5.0E-19	±	-1.1E-18	4.1E-18	±	2.7E-19	97%	24.924	379.4	±	1.4
5	3.287E-14	±	4.6E-17	1.181E-15	±	4.7E-18	1.4E-17	±	4.9E-19	2.5E-18	±	1.1E-18	2.8E-18	±	2.3E-19	98%	27.141	409.6	±	2.0
6	3.022E-14	±	4.1E-17	8.238E-16	±	3.8E-18	9.7E-18	±	5.2E-19	9.9E-19	±	1.1E-18	3.7E-18	±	2.6E-19	96%	35.345	517.1	±	2.9
7	1.745E-14	±	2.5E-17	6.434E-16	±	3.7E-18	8.2E-18	±	3.9E-19	-2.3E-19	±	-1.5E-18	1.0E-18	±	2.5E-19	98%	26.638	402.8	±	3.0
8	2.521E-14	±	4.3E-17	8.498E-16	±	2.9E-18	1.1E-17	±	4.0E-19	2.7E-19	±	1.2E-18	3.2E-18	±	3.2E-19	96%	28.547	428.5	±	2.4
9	1.141E-14	±	1.7E-17	3.925E-16	±	1.7E-18	4.7E-18	±	3.8E-19	-3.2E-18	±	-1.3E-18	4.8E-19	±	2.4E-19	99%	28.716	430.7	±	3.4
10	2.811E-14	±	1.3E-16	9.537E-16	±	7.4E-18	1.6E-17	±	1.0E-18	1.2E-17	±	3.0E-18	6.2E-18	±	2.6E-19	93%	27.559	415.2	±	4.2
WM-10(AU4.4C.mus)				**383.7 Ma ± 1.3**			**J = 0.00938**													
n	$^{40}Ar(*+atm)$			$^{39}Ar(K)$			$^{38}Ar(Cl+atm)$			$^{37}Ar(Ca)$			$^{36}Ar(Atm)$			%Rad	R	Age (Ma)		
1	4.106E-14	±	2.8E-17	1.598E-15	±	3.9E-18	1.9E-17	±	3.7E-19	4.3E-18	±	1.3E-18	2.0E-19	±	1.5E-19	100%	25.655	389.4	±	1.1
2	3.007E-14	±	3.5E-17	1.189E-15	±	1.8E-18	1.4E-17	±	3.6E-19	2.4E-18	±	1.3E-18	3.9E-19	±	1.7E-19	100%	25.195	383.1	±	1.0
3	5.955E-15	±	1.0E-17	2.312E-16	±	1.8E-18	3.4E-18	±	3.8E-19	4.4E-18	±	1.1E-18	4.5E-19	±	1.6E-19	98%	25.182	383.0	±	4.5
4	2.169E-14	±	1.9E-17	8.695E-16	±	2.7E-18	1.0E-17	±	4.1E-19	5.1E-18	±	9.0E-19	3.1E-19	±	1.2E-19	100%	24.840	378.3	±	1.4
5	5.657E-14	±	4.7E-17	2.241E-15	±	5.0E-18	2.7E-17	±	4.0E-19	3.4E-18	±	1.2E-18	1.1E-19	±	2.3E-19	100%	25.223	383.5	±	1.0
6	1.999E-14	±	2.1E-17	7.855E-16	±	2.9E-18	9.4E-18	±	3.8E-19	3.7E-18	±	1.1E-18	9.0E-19	±	1.6E-19	99%	25.106	381.9	±	1.7
7	3.308E-14	±	3.3E-17	1.290E-15	±	2.8E-18	1.5E-17	±	4.6E-19	3.4E-18	±	1.2E-18	8.4E-19	±	1.6E-19	99%	25.455	386.7	±	1.1
8	1.985E-14	±	2.8E-17	7.902E-16	±	2.3E-18	9.9E-18	±	3.4E-19	3.9E-18	±	1.2E-18	4.8E-19	±	1.3E-19	99%	24.947	379.7	±	1.4
9	7.359E-14	±	3.5E-17	2.847E-15	±	6.2E-18	3.3E-17	±	4.9E-19	3.0E-18	±	9.8E-19	7.1E-19	±	1.7E-19	100%	25.778	391.1	±	0.9
10	2.732E-14	±	2.3E-17	1.081E-15	±	2.9E-18	1.4E-17	±	3.8E-19	3.0E-17	±	2.0E-18	9.6E-19	±	1.7E-19	99%	25.008	380.6	±	1.3
BB-1(AU4.5E.mus)				**350.9 Ma ± 3.9**			**J = 0.00941**													
n	$^{40}Ar(*+atm)$			$^{39}Ar(K)$			$^{38}Ar(Cl+atm)$			$^{37}Ar(Ca)$			$^{36}Ar(Atm)$			%Rad	R	Age (Ma)		
1	3.117E-14	±	2.6E-17	1.273E-15	±	3.0E-18	1.5E-17	±	2.9E-19	1.3E-18	±	1.1E-18	5.5E-19	±	2.5E-19	99%	24.360	371.3	±	1.3
2	1.117E-14	±	1.5E-17	5.157E-16	±	2.0E-18	6.2E-18	±	3.4E-19	1.0E-18	±	1.3E-18	5.0E-19	±	2.3E-19	99%	21.379	329.7	±	2.5
3	3.774E-14	±	2.7E-17	1.645E-15	±	4.7E-18	2.0E-17	±	5.5E-19	9.5E-19	±	1.2E-18	8.2E-19	±	2.9E-19	99%	22.793	349.5	±	1.3
4	4.985E-14	±	5.5E-17	2.179E-15	±	5.8E-18	2.6E-17	±	6.1E-19	1.2E-18	±	1.2E-18	8.5E-19	±	2.6E-19	99%	22.758	349.1	±	1.2
5	7.080E-14	±	1.0E-16	3.008E-15	±	6.3E-18	3.5E-17	±	5.9E-19	1.2E-18	±	1.2E-18	9.6E-19	±	3.1E-19	100%	23.444	358.6	±	1.0
6	4.419E-14	±	6.8E-17	1.882E-15	±	2.7E-18	2.2E-17	±	4.0E-19	2.0E-18	±	1.5E-18	6.2E-19	±	2.7E-19	100%	23.377	357.7	±	1.0
7	2.895E-14	±	2.6E-17	1.247E-15	±	6.3E-18	1.4E-17	±	4.7E-19	-4.0E-18	±	-1.4E-18	1.4E-18	±	2.1E-19	99%	22.890	350.9	±	2.0
8	7.250E-14	±	1.1E-16	3.040E-15	±	8.4E-18	3.5E-17	±	6.2E-19	-2.5E-18	±	-1.1E-18	1.0E-18	±	2.3E-19	100%	23.751	362.9	±	1.2
9	2.584E-14	±	3.0E-17	1.171E-15	±	3.4E-18	1.4E-17	±	5.1E-19	2.2E-19	±	1.6E-18	9.8E-19	±	3.4E-19	99%	21.817	335.9	±	1.7
10	1.428E-14	±	2.6E-17	6.281E-16	±	3.4E-18	7.6E-18	±	3.8E-19	-1.9E-18	±	-1.2E-18	7.3E-19	±	2.8E-19	98%	22.395	344.0	±	2.8

Laser muscovite data for this study, with corrections and presentation as in Appendix A.

BB-2(AU4.5F.mus)	355.3 Ma ± 3.9			J = 0.00941																				
n	^{40}Ar(*+atm)			^{39}Ar(K)			^{38}Ar(Cl+atm)			^{37}Ar(Ca)			^{36}Ar(Atm)			%Rad	R	Age (Ma)		
1	7.667E-14	±	1.2E-16	3.279E-15	±	6.3E-18	4.0E-17	±	4.4E-19	5.5E-17	±	1.8E-18	5.3E-18	±	3.1E-19	98%	22.908	351.1	±	1.0
2	2.676E-14	±	2.2E-17	1.085E-15	±	2.5E-18	1.3E-17	±	4.1E-19	6.8E-17	±	2.1E-18	2.4E-18	±	2.8E-19	97%	24.013	366.5	±	1.5
3	6.732E-14	±	5.2E-17	2.920E-15	±	4.8E-18	3.5E-17	±	5.0E-19	3.2E-17	±	1.4E-18	1.1E-18	±	2.6E-19	100%	22.949	351.7	±	0.8
4	6.016E-14	±	4.4E-17	2.566E-15	±	5.3E-18	3.0E-17	±	5.4E-19	1.1E-17	±	1.3E-18	3.3E-18	±	3.9E-19	98%	23.066	353.4	±	1.0
5	6.865E-14	±	4.5E-17	2.999E-15	±	8.5E-18	3.5E-17	±	6.7E-19	3.8E-17	±	1.9E-18	2.2E-18	±	2.7E-19	99%	22.675	347.9	±	1.1
6	3.365E-14	±	3.1E-17	1.481E-15	±	4.6E-18	1.9E-17	±	5.8E-19	7.6E-17	±	2.1E-18	-1.5E-19	±	-4.2E-19	100%	22.754	349.0	±	1.7
7	3.227E-14	±	3.1E-17	1.318E-15	±	3.3E-18	1.6E-17	±	3.4E-19	3.5E-18	±	1.4E-18	1.8E-18	±	3.4E-19	98%	24.075	367.3	±	1.5
8	1.755E-14	±	2.0E-17	7.865E-16	±	3.7E-18	1.0E-17	±	3.8E-19	8.8E-17	±	3.0E-18	2.4E-19	±	3.5E-19	100%	22.229	341.7	±	2.6
9	2.809E-14	±	3.3E-17	1.251E-15	±	3.0E-18	1.6E-17	±	3.9E-19	6.0E-18	±	1.7E-18	3.4E-19	±	3.3E-19	100%	22.364	343.6	±	1.5
10	3.773E-14	±	4.5E-17	1.483E-15	±	4.6E-18	1.8E-17	±	4.5E-19	4.3E-18	±	1.5E-18	1.8E-18	±	3.7E-19	99%	25.076	381.1	±	1.7
MS-2(AU4.4F.mus)	**339.0 Ma ± 0.8**			**J = 0.00938**																				
n	^{40}Ar(*+atm)			^{39}Ar(K)			^{38}Ar(Cl+atm)			^{37}Ar(Ca)			^{36}Ar(Atm)			%Rad	R	Age (Ma)		
1	5.671E-14	±	3.9E-17	2.563E-15	±	4.5E-18	3.0E-17	±	4.8E-19	-2.3E-18	±	-1.4E-18	1.0E-18	±	2.2E-19	99%	22.010	339.0	±	0.8
2	4.509E-14	±	3.0E-17	2.036E-15	±	4.0E-18	2.6E-17	±	4.2E-19	2.2E-18	±	1.5E-18	8.6E-19	±	1.3E-19	99%	22.025	339.2	±	0.8
3	2.251E-14	±	2.6E-17	1.010E-15	±	3.4E-18	1.3E-17	±	4.7E-19	1.7E-18	±	1.4E-18	6.9E-19	±	2.0E-19	99%	22.089	340.1	±	1.5
4	3.562E-14	±	3.2E-17	1.626E-15	±	2.5E-18	2.0E-17	±	5.8E-19	1.8E-18	±	1.3E-18	3.5E-20	±	2.1E-19	100%	21.903	337.5	±	0.8
5	1.756E-14	±	1.6E-17	7.731E-16	±	2.2E-18	9.8E-18	±	4.9E-19	2.9E-18	±	1.4E-18	7.6E-19	±	1.5E-19	99%	22.418	344.7	±	1.4
6	3.406E-14	±	3.2E-17	1.542E-15	±	3.5E-18	1.7E-17	±	7.6E-19	-1.0E-18	±	-1.5E-18	1.2E-18	±	1.5E-19	99%	21.854	336.8	±	0.9
7	2.187E-14	±	3.2E-17	9.860E-16	±	2.9E-18	1.1E-17	±	6.7E-19	3.1E-19	±	1.1E-18	4.8E-19	±	1.7E-19	99%	22.034	339.3	±	1.3
8	3.712E-14	±	3.8E-17	1.685E-15	±	2.4E-18	2.0E-17	±	6.8E-19	-1.1E-18	±	-1.1E-18	7.3E-19	±	2.0E-19	99%	21.906	337.5	±	0.8
9	3.620E-14	±	2.6E-17	1.647E-15	±	5.8E-18	1.8E-17	±	8.7E-19	2.4E-18	±	1.2E-18	7.2E-19	±	1.6E-19	99%	21.851	336.7	±	1.3
MS-3(AU4.4G.mus)	**352.0 Ma ± 7.5**			**J = 0.00938**																				
n	^{40}Ar(*+atm)			^{39}Ar(K)			^{38}Ar(Cl+atm)			^{37}Ar(Ca)			^{36}Ar(Atm)			%Rad	R	Age (Ma)		
1	1.639E-14	±	3.2E-17	5.989E-16	±	2.4E-18	8.2E-18	±	5.0E-19	-8.4E-19	±	-1.1E-18	7.3E-19	±	1.2E-19	99%	27.005	407.8	±	2.1
2	2.881E-14	±	3.6E-17	1.306E-15	±	3.6E-18	1.6E-17	±	6.0E-19	-9.2E-19	±	-1.1E-18	7.6E-19	±	1.8E-19	99%	21.887	337.2	±	1.2
3	2.336E-14	±	3.2E-17	1.059E-15	±	2.8E-18	1.3E-17	±	5.3E-19	5.7E-18	±	1.6E-18	4.5E-19	±	1.3E-19	99%	21.929	337.8	±	1.2
4	1.279E-14	±	1.3E-17	5.589E-16	±	2.0E-18	6.8E-18	±	3.8E-19	-9.2E-19	±	-1.6E-18	-2.0E-19	±	-2.3E-19	100%	22.985	352.6	±	2.3
5	6.323E-14	±	6.1E-17	2.858E-15	±	5.9E-18	3.3E-17	±	8.3E-19	2.9E-18	±	1.7E-18	1.2E-18	±	2.3E-19	99%	21.993	338.7	±	0.9
6	5.940E-15	±	9.9E-18	2.676E-16	±	1.4E-18	4.0E-18	±	4.5E-19	-3.5E-20	±	-1.5E-18	3.3E-19	±	2.2E-19	98%	21.829	336.4	±	4.2
7	3.997E-14	±	4.0E-17	1.790E-15	±	5.2E-18	2.1E-17	±	6.2E-19	4.3E-18	±	1.5E-18	2.8E-19	±	2.1E-19	100%	22.280	342.7	±	1.2
8	4.055E-14	±	3.6E-17	1.813E-15	±	3.7E-18	2.1E-17	±	5.8E-19	-6.2E-19	±	-1.7E-18	6.1E-19	±	2.6E-19	100%	22.271	342.6	±	1.0
9	2.779E-14	±	3.3E-17	1.134E-15	±	2.1E-18	1.3E-17	±	5.8E-19	3.7E-18	±	1.3E-18	4.8E-19	±	2.7E-19	99%	24.379	371.9	±	1.4
MS-4b(AU4.4H.mus	**364.8 Ma ± 11.5**			**J = 0.00938**																				
n	^{40}Ar(*+atm)			^{39}Ar(K)			^{38}Ar(Cl+atm)			^{37}Ar(Ca)			^{36}Ar(Atm)			%Rad	R	Age (Ma)		
1	1.465E-14	±	1.0E-17	5.638E-16	±	2.2E-18	7.2E-18	±	3.0E-19	3.2E-18	±	1.5E-18	3.5E-18	±	2.7E-19	93%	24.130	368.0	±	2.7
2	1.270E-14	±	1.7E-17	3.905E-16	±	1.6E-18	5.1E-18	±	3.0E-19	8.1E-18	±	1.5E-18	1.8E-18	±	2.5E-19	96%	31.164	462.5	±	3.4
3	1.992E-14	±	2.4E-17	7.538E-16	±	2.3E-18	1.1E-17	±	3.9E-19	7.2E-18	±	1.1E-18	7.6E-18	±	3.3E-19	89%	23.433	358.4	±	2.4
4	1.875E-14	±	1.5E-17	7.775E-16	±	2.6E-18	9.9E-18	±	3.7E-19	8.5E-18	±	1.4E-18	3.1E-18	±	2.5E-19	95%	22.932	351.4	±	1.9
5	8.473E-15	±	1.0E-17	3.435E-16	±	2.2E-18	4.2E-18	±	2.8E-19	1.1E-18	±	9.5E-19	1.4E-18	±	3.0E-19	95%	23.435	358.4	±	4.6
6	1.169E-14	±	2.2E-17	4.550E-16	±	1.6E-18	6.3E-18	±	4.4E-19	2.1E-18	±	1.3E-18	1.6E-18	±	2.4E-19	96%	24.647	375.1	±	2.8
7	1.309E-14	±	2.1E-17	5.672E-16	±	2.4E-18	7.3E-18	±	2.6E-19	1.1E-18	±	1.1E-18	2.2E-18	±	2.8E-19	95%	21.926	337.4	±	2.8
8	1.065E-14	±	1.5E-17	4.105E-16	±	2.0E-18	5.6E-18	±	2.8E-19	2.0E-18	±	9.8E-19	4.8E-18	±	3.0E-19	87%	22.527	345.8	±	3.9
9	9.258E-15	±	1.0E-17	3.784E-16	±	1.9E-18	5.5E-18	±	2.3E-19	5.4E-18	±	1.1E-18	3.4E-18	±	3.0E-19	89%	21.815	335.8	±	4.1
10	1.216E-14	±	9.5E-18	4.303E-16	±	3.2E-18	6.6E-18	±	3.9E-19	7.6E-18	±	1.1E-18	7.3E-18	±	3.6E-19	82%	23.232	355.6	±	5.0

Laser muscovite data for this study, with corrections and presentation as in Appendix A.

MS-5(AU4.5A.mus)	352.9 Ma ± 12.7			J = 0.00941																	
n	^{40}Ar(*+atm)			^{39}Ar(K)			^{38}Ar(Cl+atm)			^{37}Ar(Ca)			^{36}Ar(Atm)			%Rad	R	Age (Ma)		
1	7.907E-15	±	2.1E-17	2.505E-16	±	2.3E-18	3.7E-18	±	4.3E-19	1.2E-16	±	2.1E-18	2.6E-19	±	2.7E-19	99%	31.307	464.5	±	6.6
2	1.567E-14	±	2.2E-17	7.114E-16	±	2.2E-18	9.5E-18	±	4.5E-19	8.1E-17	±	2.1E-18	9.0E-19	±	2.8E-19	98%	21.663	333.7	±	2.1
3	2.413E-14	±	4.3E-17	1.108E-15	±	3.6E-18	1.4E-17	±	4.9E-19	1.3E-16	±	3.9E-18	4.4E-19	±	2.0E-19	99%	21.680	334.0	±	1.5
4	1.464E-14	±	1.3E-17	6.116E-16	±	2.6E-18	7.7E-18	±	4.4E-19	1.9E-16	±	3.8E-18	1.2E-19	±	2.0E-19	100%	23.910	365.1	±	2.1
5	3.078E-14	±	4.8E-17	1.387E-15	±	6.7E-18	1.7E-17	±	4.9E-19	2.6E-16	±	3.5E-18	7.2E-19	±	2.2E-19	99%	22.052	339.2	±	1.9
6	2.039E-14	±	2.5E-17	9.294E-16	±	2.3E-18	1.2E-17	±	4.0E-19	8.7E-17	±	2.7E-18	6.0E-20	±	1.7E-19	100%	21.931	337.5	±	1.2
7	1.617E-14	±	1.9E-17	7.233E-16	±	3.8E-18	9.4E-18	±	3.6E-19	2.4E-16	±	2.6E-18	-2.1E-19	±	-4.4E-19	100%	22.473	345.1	±	3.3
8	1.904E-14	±	1.3E-17	8.729E-16	±	1.8E-18	1.1E-17	±	3.8E-19	6.6E-17	±	1.7E-18	1.4E-19	±	2.9E-19	100%	21.773	335.3	±	1.7
9	5.911E-15	±	1.3E-17	2.660E-16	±	2.2E-18	3.5E-18	±	3.6E-19	5.6E-18	±	1.4E-18	5.4E-20	±	2.6E-19	100%	22.161	340.7	±	5.4
10	1.992E-14	±	2.5E-17	9.134E-16	±	3.3E-18	1.1E-17	±	4.7E-19	5.5E-17	±	1.8E-18	3.6E-19	±	2.5E-19	99%	21.694	334.2	±	1.8
MS-6(AU4.5B.mus)	334.7 Ma ± 0.6			J = 0.00941																	
n	^{40}Ar(*+atm)			^{39}Ar(K)			^{38}Ar(Cl+atm)			^{37}Ar(Ca)			^{36}Ar(Atm)			%Rad	R	Age (Ma)		
1	1.984E-14	±	2.7E-17	9.199E-16	±	4.2E-18	1.1E-17	±	4.4E-19	1.8E-17	±	1.8E-18	-9.8E-20	±	-2.9E-19	100%	21.601	332.8	±	2.1
2	2.542E-14	±	6.0E-17	1.187E-15	±	3.4E-18	1.4E-17	±	4.8E-19	2.1E-17	±	1.2E-18	-1.3E-19	±	-2.7E-19	100%	21.450	330.7	±	1.6
3	3.732E-14	±	2.2E-17	1.720E-15	±	5.6E-18	2.0E-17	±	4.4E-19	3.1E-17	±	1.6E-18	-1.3E-19	±	-3.1E-19	100%	21.728	334.6	±	1.4
4	3.792E-14	±	4.3E-17	1.749E-15	±	3.6E-18	2.1E-17	±	6.2E-19	4.1E-17	±	1.8E-18	5.8E-20	±	2.4E-19	100%	21.674	333.9	±	1.0
5	1.713E-14	±	2.8E-17	7.882E-16	±	2.9E-18	9.7E-18	±	4.7E-19	5.2E-17	±	2.1E-18	-5.6E-19	±	-2.5E-19	101%	21.948	337.7	±	2.0
6	4.006E-14	±	3.1E-17	1.836E-15	±	6.4E-18	2.3E-17	±	4.1E-19	9.4E-17	±	2.4E-18	-2.0E-19	±	-2.8E-19	100%	21.853	336.4	±	1.4
7	2.520E-14	±	4.8E-17	1.154E-15	±	1.8E-18	1.4E-17	±	5.6E-19	3.0E-17	±	1.8E-18	1.1E-19	±	2.5E-19	100%	21.817	335.9	±	1.3
8	3.257E-14	±	2.6E-17	1.497E-15	±	3.7E-18	1.8E-17	±	4.7E-19	1.4E-17	±	1.5E-18	3.2E-20	±	2.1E-19	100%	21.752	335.0	±	1.1
9	4.075E-14	±	8.3E-17	1.870E-15	±	6.4E-18	2.2E-17	±	5.6E-19	1.5E-17	±	1.7E-18	5.4E-19	±	2.5E-19	100%	21.707	334.3	±	1.5
10	1.045E-14	±	2.1E-17	4.823E-16	±	2.1E-18	5.1E-18	±	3.7E-19	2.3E-18	±	1.3E-18	-2.2E-19	±	-2.2E-19	101%	21.803	335.7	±	2.7
MS-7(AU4.5C.mus)	342.1 Ma ± 5.3			J = 0.00941																	
n	^{40}Ar(*+atm)			^{39}Ar(K)			^{38}Ar(Cl+atm)			^{37}Ar(Ca)			^{36}Ar(Atm)			%Rad	R	Age (Ma)		
1	1.625E-14	±	1.2E-17	7.391E-16	±	1.8E-18	9.3E-18	±	4.6E-19	3.2E-17	±	1.9E-18	1.1E-18	±	2.8E-19	98%	21.551	332.2	±	1.9
2	1.003E-14	±	1.9E-17	4.511E-16	±	1.8E-18	5.9E-18	±	3.3E-19	4.4E-17	±	1.6E-18	1.2E-18	±	3.6E-19	96%	21.461	330.9	±	3.9
3	7.801E-15	±	1.4E-17	3.438E-16	±	1.3E-18	4.8E-18	±	3.3E-19	6.9E-17	±	1.9E-18	1.0E-18	±	2.9E-19	96%	21.853	336.4	±	4.1
4	1.346E-14	±	3.0E-17	6.159E-16	±	2.5E-18	7.5E-18	±	3.5E-19	3.5E-17	±	1.6E-18	1.3E-18	±	2.8E-19	97%	21.250	327.9	±	2.6
5	3.177E-14	±	8.1E-17	1.433E-15	±	4.3E-18	1.7E-17	±	4.5E-19	1.9E-16	±	3.7E-18	1.8E-18	±	2.7E-19	98%	21.830	336.1	±	1.6
6	1.251E-14	±	3.0E-17	5.424E-16	±	3.4E-18	6.7E-18	±	3.0E-19	9.6E-17	±	2.3E-18	1.6E-18	±	2.6E-19	96%	22.221	341.6	±	3.2
7	1.596E-14	±	3.5E-17	6.240E-16	±	2.9E-18	7.3E-18	±	3.5E-19	9.3E-17	±	2.3E-18	2.5E-19	±	2.8E-19	100%	25.481	386.6	±	2.9
8	8.135E-15	±	1.0E-17	3.564E-16	±	2.9E-18	4.7E-18	±	3.5E-19	5.6E-17	±	1.6E-18	5.0E-19	±	3.2E-19	98%	22.429	344.5	±	5.0
9	3.404E-14	±	4.3E-17	1.508E-15	±	3.1E-18	1.9E-17	±	6.1E-19	2.4E-16	±	2.3E-18	8.0E-19	±	3.4E-19	99%	22.428	344.4	±	1.3
10	2.238E-14	±	2.8E-17	9.944E-16	±	3.2E-18	1.2E-17	±	3.8E-19	5.7E-17	±	1.9E-18	1.3E-18	±	3.5E-19	98%	22.109	340.0	±	2.0
MS-8(AU4.5D.mus)	332.5 Ma ± 0.5			J = 0.00941																	
n	^{40}Ar(*+atm)			^{39}Ar(K)			^{38}Ar(Cl+atm)			^{37}Ar(Ca)			^{36}Ar(Atm)			%Rad	R	Age (Ma)		
1	3.410E-14	±	2.9E-17	1.555E-15	±	2.7E-18	1.9E-17	±	3.9E-19	-9.1E-19	±	-1.5E-18	1.3E-18	±	4.1E-19	99%	21.672	333.8	±	1.4
2	2.620E-14	±	3.9E-17	1.217E-15	±	3.7E-18	1.4E-17	±	5.2E-19	-1.5E-18	±	-1.5E-18	5.1E-19	±	3.2E-19	99%	21.395	329.9	±	1.6
3	1.617E-14	±	3.1E-17	7.446E-16	±	1.8E-18	8.2E-18	±	3.6E-19	-3.5E-18	±	-1.7E-18	3.9E-19	±	2.9E-19	99%	21.560	332.3	±	2.1
4	2.720E-14	±	2.6E-17	1.259E-15	±	3.3E-18	1.4E-17	±	4.0E-19	-4.6E-18	±	-1.4E-18	2.9E-19	±	3.1E-19	100%	21.535	331.9	±	1.5
5	2.096E-14	±	2.9E-17	9.535E-16	±	2.1E-18	1.1E-17	±	4.5E-19	-1.9E-18	±	-1.5E-18	1.6E-18	±	4.3E-19	98%	21.482	331.2	±	2.2
6	3.969E-14	±	4.2E-17	1.824E-15	±	2.6E-18	2.2E-17	±	4.4E-19	-3.6E-19	±	-1.2E-18	6.2E-19	±	3.2E-19	100%	21.656	333.6	±	1.0
7	3.864E-14	±	2.4E-17	1.785E-15	±	4.5E-18	2.1E-17	±	4.0E-19	3.9E-19	±	1.2E-18	2.6E-19	±	2.7E-19	100%	21.610	333.0	±	1.1
8	2.938E-14	±	3.0E-17	1.352E-15	±	1.8E-18	1.6E-17	±	3.2E-19	1.9E-18	±	1.5E-18	9.4E-19	±	3.0E-19	99%	21.525	331.8	±	1.1
9	5.268E-14	±	5.9E-17	2.415E-15	±	5.2E-18	2.9E-17	±	9.9E-19	3.8E-19	±	1.3E-18	6.9E-19	±	3.0E-19	100%	21.725	334.6	±	1.0

Laser muscovite data for this study, with corrections and presentation as in Appendix A.